CO_2/CH_4 SEPARATION USING EVA/SiO_2/PEG COMPOSITE MEMBRANES

PRACHYA WATASIT

A THESIS SUBMITTED IN PARTIAL FULFILLMENT OF THE REQUIREMENT FOR THE DEGREE OF DOCTOR OF PHILOSOPHY IN APPLIED CHEMISTRY

DEPARTMENT OF CHEMISTRY SCHOOL OF SCIENCE
KING MONGKUT'S INSTITUTE OF TECHNOLOGY LADKRABANG

2025
KMITL-2025-SC-D-012-041

Thesis Title	CO_2/CH_4 separation using EVA/SiO_2/PEG composite membranes
Student Name	Mr. Prachya Watasit
Student ID	62605114
Degree	Doctor of Philosophy (Applied Chemistry)
Department	Chemistry
Year	2025
Thesis Advisor	Asst.Prof.Dr. Chonlada Ritvirulh
Thesis Co-advisors	Prof.Dr. Tawan Sooknoi
	Asst.Prof.Dr. Suparat Rukchonlatee

Abstract

Gas separation using polymeric membranes has emerged as an effective strategy for removing CO_2 from household biogas. In this study, ethylene vinyl acetate copolymer (EVA) membranes were modified with silica (SiO_2) and polyethylene glycol (PEG) to enhance their performance in CO_2/CH_4 separation at atmospheric pressure. Flat-sheet membranes, fabricated via compression molding, were evaluated through single-gas permeation tests. Increasing the vinyl acetate (VA) content in EVA from 18 to 33 wt% resulted in higher CO_2 permeability (1.5–2.0 mL/m²·s), attributed to reduced crystallinity and enhanced quadrupole–dipole interactions between polar acetate groups and CO_2 molecules. Incorporation of SiO_2 (0.5–2.0 wt%) further enhanced membrane polarity due to the presence of silanol groups, increasing CO_2 flux up to 6.0 mL/m²·s. For mixed-gas separation (CO_2/CH_4; 40/60 v/v), an EVA blend (E28-18, 90:10) containing 28 wt% and 18 wt% VA was selected to facilitate lay-flat blown film reshaping into tubular membranes and improve CO_2/CH_4 selectivity. The addition of 0.5 wt% SiO_2 reduced CH_4 loss while enhancing gas selectivity. Moreover, PEG incorporation (0.5–1.0 wt%) increased membrane polarity, further improving CO_2/CH_4 selectivity from 3.9 to 5.3 by promoting CO_2 permeation and restricting CH_4 transport. These findings demonstrate the potential of EVA-based composite membranes for efficient CO_2 separation from household biogas, contributing to an increase in its heating value.

Keywords: biogas purification, CO_2/CH_4 separation, polymeric membrane, ethylene-vinyl acetate copolymer (EVA), silica (SiO_2) and polyethylene glycol (PEG)

Acknowledgements

I would like to express my sincere gratitude to my advisor, Asst.Prof.Dr. Chonlada Ritvirulh, and co-advisors, Professor Tawan Sooknoi and Asst.Prof.Dr. Suparat Rukchonlatee for their invaluable guidance, feedback, and support throughout my research. I am truly thankful to Assoc. Prof. Dr. Artit Ausavasukhi for his valuable guidance and for supporting the gas analysis instrument used in this research. I wish to acknowledge the generous financial support of Thailand Research Fund (RDG61D0001 and RDG62D0010), the Electricity Generating Authority of Thailand, the National Research Council of Thailand and School of Science, KMITL (RA/TA 2019). I would like to thank Rajabhat Rajanagarindra University for the scholarship. I would like to express thanks to my family for their understanding, patience, and backing during this PhD study.

Mr.Prachya Watasit

Table of contents

Table of contents (continued)

Table of contents (continued)

Table of contents (continued)

List of tables

List of figures

List of figures (continued)

List of figures (continued)

Chapter 1
Introduction

1.1 Research motivation

At present, the increasing energy demand is still the main problem of many countries in the world. Global demand for crude oil is continuing to rise while petroleum sources are limited [1]. To overcome this issue, various kinds of renewable energy have been developed, for example solar power, wind power, hydroelectricity, geothermal energy, biomass and biogas [2]. Among these, biogas have received wide interest in agricultural countries. This is because these countries have a large numerous raw materials to produce biogas [3]. Agricultural waste, manure, municipal waste, plant material, sewage, green waste, wastewater, and food waste can be used as natural resources for producing biogas through the anaerobic digestion process [4]. In this process microorganisms break down organic matter into small molecules. Typically, biogas products consist of 55-75% (v/v) methane (CH_4) and 25-45% (v/v) carbon dioxide (CO_2) along with other trace components such as water vapor and hydrogen sulfide (H_2S) [5]. The chemical composition of biogas varies with the nature of the organic waste, temperature and humidity inside the digester [6]. In developing countries such as Thailand, Vietnam, and India, household biogas has been utilized as fuel replacing liquefied petroleum gas (LPG) for cooking [7,8]. However, the presence of CO_2 in biogas results in a lower heating value which is an obstacle for usage [5]. Accordingly, the separation process of CO_2 is necessary to improve the quality of biogas.

There are several effective methods for removal CO_2, namely water absorption, chemical absorption, pressure swing absorption, cryogenic and membrane separation [9-11]. The absorption process requires chemical solvents to extract CO_2 leading to a negative environmental impact [12]. Whereas pressure swing and cryogenic processes consume high energy consumption to separate CO_2 [13]. In recent decades, polymeric membrane

has been widely investigated for gas separation due to its low energy consumption, ease of operation, and environmental friendliness [14,15].

Both porous and dense polymeric membranes have been studied for gas separation. For dense polymeric membranes, the transportation of gas through the membrane can be described by solution-diffusion mechanism. Firstly, gas molecules dissolve into the polymer matrix of the membrane. Then the molecules diffuse through the membrane. Finally, gas molecules are released on the downstream side of the membrane [16]. The efficiency of solution-diffusion can be influenced by the properties of both the polymer and the penetrant leading to variations in permeability and selectivity [17]. Typically, structure of CO_2 and CH_4 are symmetry resulting in a zero dipole moment. However, CO_2 is considered as a polar compound because of its quadrupole moment properties [18]. Accordingly, various polar polymeric membranes have been introduced to separate CO_2 molecules such as polysulfone [19], polycarbonate [20], polyimide [21], cellulose acetate [22], polyvinyl amine [23] and poly (ethylene-co-vinyl acetate) (EVA) [24]. Among these, EVA is relatively inexpensive and can be readily processed with low energy consumption. The acetate side group on EVA structure plays an important role in interacting with CO_2 molecules through the dipole-dipole force. This interaction can improve the permeation of CO_2 [25]. Wolinska-Grabczyk *et al.* [24] introduced the blended membrane of EVA for gas permeation. The results indicated that CO_2 permeability increased with increasing acetate content (from 25 to 46 wt%). Mousavi *et al.* [26] prepared EVA membranes using phase inversion method for O_2, N_2, CH_4, and CO_2 permeation. They found that the CO_2 permeability was evidently higher than those of the other gases. In addition, to improve the CO_2 permeability of EVA membranes, many types of inorganic fillers and/or organic additives with high polarity have been mixed to modify the EVA membranes. Recently, nano-SiO_2/EVA composite membrane for N_2, O_2, CO_2 and CH_4 single gas permeation was studied by Sadeghi *et al.* [27]. Adding silica from 5 to 10 wt% could enhance the amorphous regions of EVA membrane. This leads to an increase in CO_2 permeability and CO_2/CH_4 selectivity. Zamiri *et al.* [25] prepared a blended membrane EVA/polyethylene glycol (PEG) for CO_2/N_2 separation. They reported that incorporating PEG

into the EVA membrane can increase amorphous regions of EVA, resulting in an enhancement of CO_2 permeability and CO_2/N_2 selectivity.

In the past decade, hollow fiber membrane has been widely investigated for large-scale gas separation [28-30]. Although the hollow fiber membrane has a high surface area which is effective for CO_2 separation. This membrane has a high membrane thickness (100-400 μm), compared to thin film membrane, which requires high pressure (about 7-8 bar) for gas permeation [30,31]. Thus, it cannot apply to household biogas separation because of the rising operation cost. Therefore, gas separation membrane with concentration gradient process under atmospheric pressure is a good choice. To overcome this, thin film membrane module is a reasonable choice for using in the household biogas. However, this module also required the membrane with high surface area per volume. To solve this problem, the EVA membrane should be blown in a continuous-thin film tubular form to be usable with the designed plate-and-frame modules. From our knowledge, there are few reports studying gas separation at low pressure [32,33]. Accordingly, this is a challenging issue for this research.

In this work, CO_2/CH_4 separation was studied using EVA composite membrane at atmospheric pressure. The EVA composite membranes were fabricated both in a flat sheet membrane and a continuous-thin film tubular membrane. CO_2 and CH_4 permeability of the flat sheet membranes were investigated using the permeation cell with a single gas permeation system. Whereas the CO_2/CH_4 separation of the continuous-thin film tubular membranes were tested with a biogas model mixture containing 40 vol% CO_2 in CH_4 using plate-and-frame module. The effects of vinyl acetate contents (from 18 to 33 wt%) of EVA, SiO_2 loadings (from 0.5 to 2.0 wt%) and PEG contents (from 0.5 to 1.5 wt%) were evaluated for the CO_2 and CH_4 permeability and CO_2/CH_4 selectivity.

1.2 Objectives of the study

This research aims to increase the heating value of household biogas by employing polymeric membrane technology for the separation of CO_2 under atmospheric pressure. EVA and its composites were fabricated into a thin-flat membrane to evaluate their CO_2 and CH_4 permeability as well as CO_2/CH_4 selectivity through a single gas permeation

system. The effect of vinyl acetate content and SiO_2 loading on gas permeability and selectivity were investigated. For biogas-model mixed gas separation, EVA and its composites were shaped into continuous thin-film tubular membranes to enhance the surface area. The influence of SiO_2 loading and PEG content on CO_2 and CH_4 permeability as well as CO_2/CH_4 selectivity were highlighted.

1.3 Scopes of the study

Part 1: Single gas permeation in the permeation cell

1. Preparation of EVA membranes with various vinyl acetate contents of 18, 28 and 33 wt% using a compression molding technique
2. Preparation of EVA composite membranes with various SiO_2 loadings of 0.5, 1.0 and 2.0 wt% using a compression molding technique
3. Study of CO_2 and CH_4 permeation of EVA composite membranes through the permeation cell with a single gas permeation system
4. Analysis of the chemical and physical properties of the membranes by several techniques, such as Fourier transform infrared (FTIR) spectroscopy, Differential scanning calorimetry (DSC), Scanning electron microscopy (SEM), Contact angle and Tensile test

Part 2: Mixed gas separation in the tubular membrane module

1. Preparation and forming tubular EVA composite membranes with various SiO_2 loadings of 0.5, 0.75 and 1.0 wt% using blown film extrusion process
2. Preparation and forming tubular EVA composite membranes with various PEG contents of 0.5, 1.0 and 1.5 wt% using blown film extrusion process
3. Study of CO_2/CH_4 separation of tubular EVA composite membranes through the designed plate-and-frame module with a mixed gas CO_2/CH_4 (40/60 %v/v) permeation system
4. Analysis of the chemical and physical properties of the membranes by several techniques, such as FTIR, DSC, SEM, Dynamic mechanical thermal analysis (DMA), Contact angle, Melt flow index and Tensile test

1.4 Benefits of the study

The EVA/SiO_2/PEG composite membranes developed in this research demonstrated efficient CO_2 separation from a biogas model mixture, resulting in enhanced CH_4 purity. The investigation into the effects of vinyl acetate content, SiO_2 loading, and PEG content on CO_2 and CH_4 permeability provides valuable insights into understanding gas separation in composite membranes. These findings are useful for researchers working on polymeric membrane development for biogas upgrading. Furthermore, the thin-tubular EVA/SiO_2/PEG composite membranes show potential as a prototype gas separation module for biogas purification, leading to an enhancement in the heating value of household biogas.

Chapter 2

Theories and literature reviews

2.1 Background of Energy

The rising of world population and the expansion of industry causes the increasing demand of petroleum (Figure 2.1) [34]. These issues lead to an increase in petroleum prices. Meanwhile, the fossil fuel reserves are running out. To solve this problem, the development of renewable energy is a compelling option. The International Energy Agency (IEA) predicts that renewable energy capacity will increase by more than 5,500 gigawatts between 2024 and 2030 [35]. This fuel is applied in all economic sectors such as heating, lighting, industrial equipment, and transportation [5]. Additionally, using renewable energy can significantly reduce greenhouse gas emissions compared to fossil fuels. This is because renewable energy sources are naturally derived from continuous energy flows in our environment, such as the carbon cycle. The renewable energy sources and their applications are shown in Table 2.1 [36].

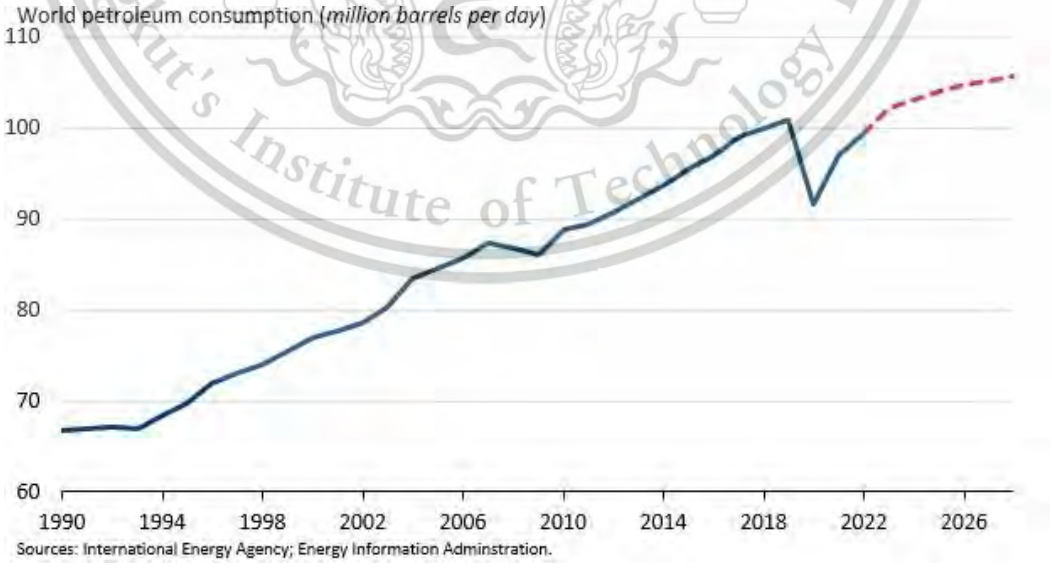

Figure 2.1 History and forecast world petroleum consumption [34]

Table 2.1 Renewable energy sources and their applications [36]

Energy sources	Applications
Hydropower	Power generation
Biomass	Power generation, gasification, digestion, heating
Geothermal	Urban heating, power generation, hydrothermal, hot dry rock
Solar	Solar home systems, solar dryers, solar cookers
Wind	Power generation, wind generators, windmills, water pump
Wave and tide	Numerous designs, barrage, tidal stream

2.2 Biogas

Biogas is a renewable energy that developed since the early 1980s [37]. This fuel has great potential for replacing energy from petroleum. It has been used for supporting many applications such as heating, power generation and transportation fuel after being upgraded to biomethane. In addition, household biogas has been directly used as fuel for cooking replacing liquefied petroleum gas (LPG) especially in the countryside of developing countries [5].

2.2.1 Biogas generation

Biogas is produced from the conversion of organic matter by microorganisms through a multiple metabolic stage namely hydrolysis, acidogenesis, acetogenesis and methanogenesis as shown in Figure 2.2 [38]. In the first stage, organic compounds like lipids, proteins, and carbohydrate are broken down into soluble monomers or oligomers such as long-chain fatty acids, amino acids, glycerol and sugars through hydrolysis process. This process is accelerated by fermentative bacteria. In the acidogenesis process, simple soluble compounds are fermented by acidogenic bacteria to obtain a mixture of alcohol, and low molecular weight volatile fatty acids (VFAs), for example, propionic and butyric acids. During acetogenesis, hydrogen-producing acetogenic bacteria anaerobically oxidizes volatile fatty acids (VFAs) and alcohols into acetate, hydrogen (H_2), and carbon dioxide (CO_2). Additionally, hydrogen-oxidizing acetogenic bacteria, known as homoacetogens, can

produce acetate from hydrogen (H_2) and carbon dioxide (CO_2). In acetotrophic methanogenesis process, acetate substrate is converted into CH_4 and CO_2. Hydrogenotrophic methanogens reduce CO_2 using H_2 as an electron donor in this process. Approximately 70% (v/v) of CH_4 products are generated through acetate decarboxylation, while the remaining CH_4 is mostly obtained from CO_2 reduction. Moreover, small amounts of CH_4 can be generated from organic substrates such as formic, propionic and butyric acids by methanogens [5].

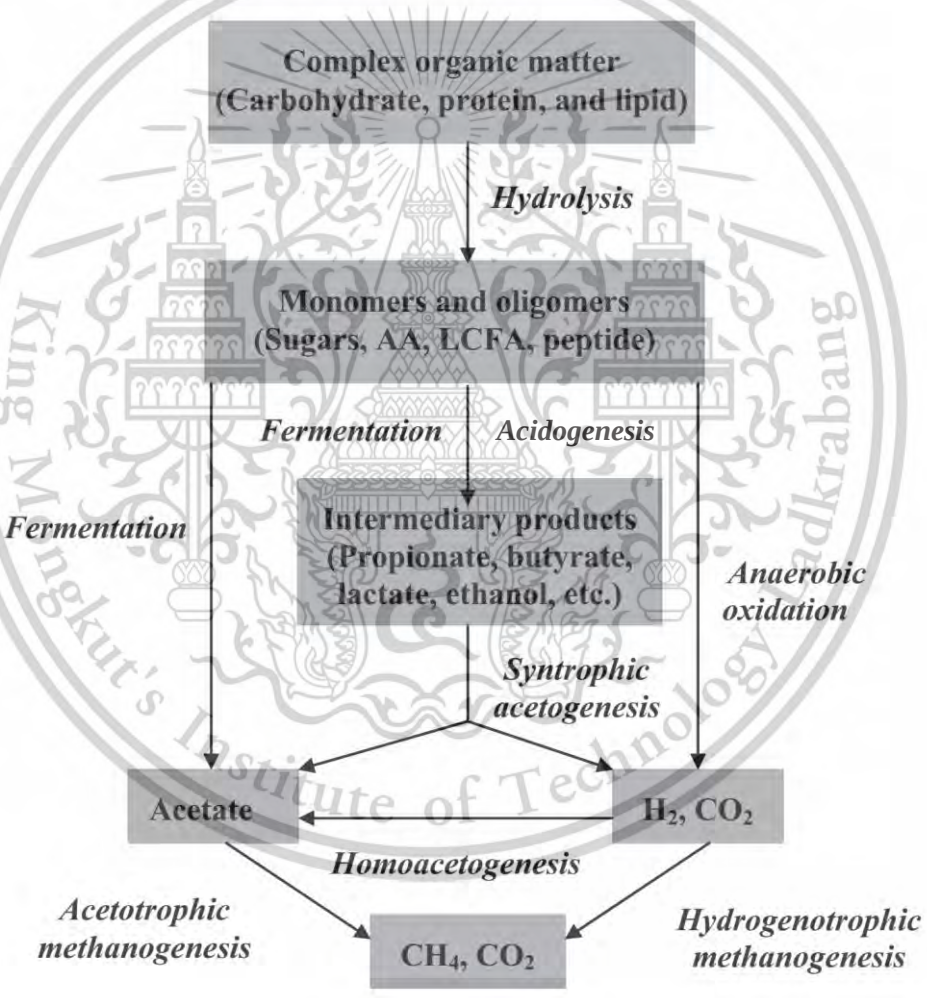

Figure 2.2 Stages of biogas production [38]

2.2.2 Biogas product

Generally, biogas products contain 55-75% (v/v) CH_4, 25-45% (v/v) CO_2, and small amounts of other gases, including ammonia (NH_3), hydrogen sulfide (H_2S) and vapor water [39]. The composition of biogas varies with types of feedstocks and the fermentation condition [40]. The composition of biogas and the properties of its components are summarized in Table 2.2 [39]. CH_4 is the primary energy-contributing component. On the other hand, the present of CO_2 reduces the heating value of biogas. For example, 1 m^3 of pure CH_4 at standard temperature and pressure has a heating value 35.8 MJ (9.94 kWh electricity equivalent) as compared to 21.5 MJ (5.97 kWh of electricity equivalent) of biogas containing 60% (v/v) CH_4 [5]. Accordingly, biogas purification step via removing CO_2 is necessary for upgrading the quality of biogas.

Table 2.2 Chemical composition of biogas and properties of components [39]

Components	Concentration	Properties
CH_4	55-75% (v/v)	Energy carrier
CO_2	25-45% (v/v)	Decrease heating value Corrosive, in the presence of moisture
H_2S	0-5000 ppm (v/v)	Corrosive SO_2 emission during combustion
NH_3	0-500 ppm (v/v)	NOx emission during combustion
N_2	0-5% (v/v)	Decrease heating value
Water vapor	1-5% (v/v)	Facilitate corrosion in the presence of CO_2 and SO_2

2.3 Gas purification technology

Currently, many technologies have been introduced for upgrading the quality of biogas including adsorption, absorption, cryogenic, and membrane separation [41]. These

technologies are classified and illustrated in Figure 2.3 [42]. In addition, a comparison and cost evaluation of various biogas purification technologies are presented in Table 2.3 [43].

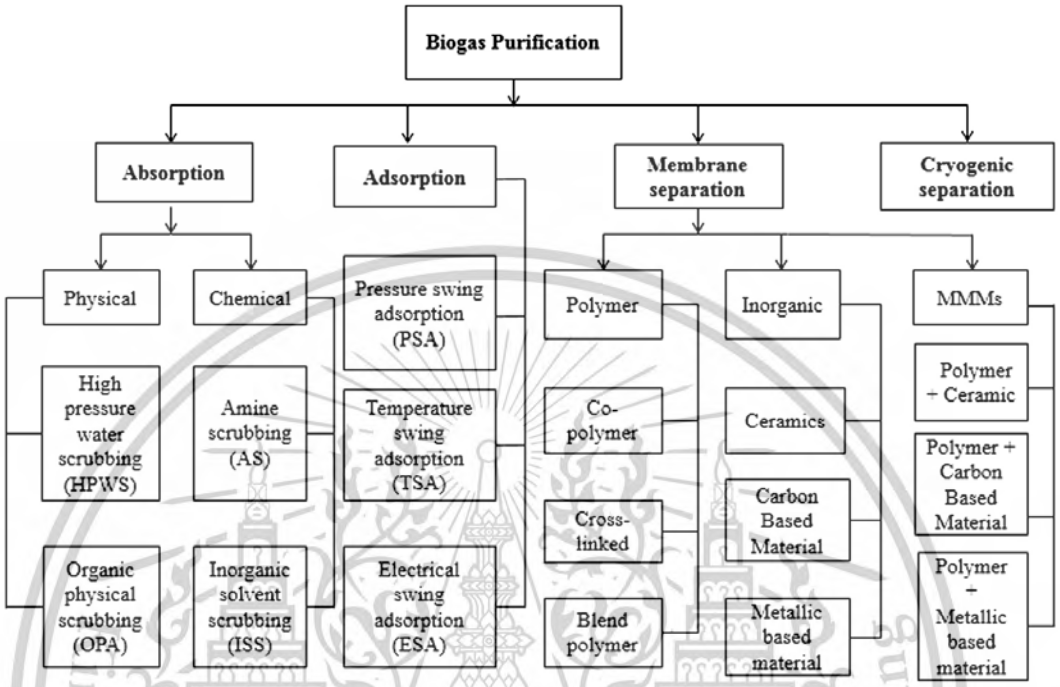

Figure 2.3 Classification of biogas upgrading technologies [42]

2.3.1 Absorption

CO_2 absorption using chemical solvents can be performed at a low temperature (40-65°C) [44]. The efficiency of this method depends on the solubility of CO_2 in the solvents. Typically, CO_2 is more soluble than CH_4 in polar solvent. This is because CO_2 is higher ability to interact with polar solvents through dipole–quadrupole interactions. The solvent absorption technique can be categorized into two types based on the nature of the interaction between gas molecules and the solvents. Organic physical scrubbing (OPS) and high pressure water scrubbing (HPWS) are considered as physical absorption, while inorganic solvent scrubbing (ISS) and amine scrubbing (AS) are classified as chemical absorption [43].

Table 2.3 Comparison and evaluation of the costs of different biogas upgrading technologies [43]

Parameter	Water scrubbing	Organic physical scrubbing	Amine scrubbing	PSA	Membrane technology
Typical content in biomethane [vol%]	95.0-99.0	95.0-99.0	>99.0	95.0-99.0	95.0-99.0
Methane recovery [%]	98.0	96.0	99.96	98.0	80-99.5
Typical delivery pressure [bar(g)]	4-8	4-8	0	4-7	4-7
Electric energy demand [kWhel/m^3biomethane]	0.46	0.49-0.67	0.27	0.46	0.25-0.43
Heating demand and temperature level	-	Medium 70-80°C	High 120-160°C	-	-
Desulphurization requirement	Process dependent	yes	yes	yes	yes
Consumables demand	Antifouling agent, drying aging	Organic solvent (non-hazardous)	Amine solution (hazardous)	Activated carbon (non-hazardous)	
Partial load rang [%]	50-100	50-100	50-100	85-115	50-105
Number of reference plants	High	low	medium	high	low
Typical investment costs [€/(m/h) biomethane					
For 100 m^3/h biomethane	10100	9500	9500	10400	7300-7600
For 250 m^3/h biomethane	5500	5000	5000	5400	4700-4900
For 500 m^3/h biomethane	3500	3500	3500	3700	3500-3700

2.3.2 Pressure swing adsorption (PSA)

In this technique, gas molecules in the gas stream are induced by surface of an adsorbent material via physical or Van der Waals forces. Under high pressure, selective gases in the mixture are preferentially adsorbed onto the surface of the adsorbent, while non-selective gases pass through adsorption column. Then the process swings to low pressure, the adsorbed gas molecules desorb from the adsorbent [45]. The PSA system

operates by alternating between high and low pressure to continuously separate and purify gases. This method is widely applied for separating CO_2 from biogas and is considered environmentally friendly. This is because the PSA does not use chemical solvents in the process.

2.3.3 Membrane separation (MS)

The membrane acts as a permeable barrier that allows specific compounds to pass through it. Selective molecules can diffuse through the membrane with applied driving forces such as the difference in concentration and pressure. Normally, two models are used to explain the membrane separation process namely solution-diffusion and pore-flow model. For solution-diffusion, gas molecules dissolve at the membrane surface and then diffuse through the membrane with a different concentration. This model is frequently used for explaining gas transportation in dense polymeric membranes. For pore-flow model, permeated gases are separated by pressure-driven convective flow through small pores [15,46].

2.3.4 Cryogenic separation (CS)

Cryogenic separation of biogas relies on the principle that gases such as CO_2 and H_2S can be liquefied at different pressures and temperatures. This technique is operated under high pressure (80 bar) and extremely low temperature (-170 °C) condition. At 1 atm pressure, the boiling point of CH_4 is -161.5 °C, which is lower than that of CO_2 (-78.2 °C). Thus, CO_2 can be removed from CH_4 by phase separation [47]. This technique requires a compressor and heat exchanger to maintain the operating conditions, leading to a rise in its capital and operational costs [48,49].

2.4 Gas permeation in polymeric membrane

Polymer materials can be used as a membrane for gas separation. This is because it provides the differences in affinity with gas molecules. The difference in affinity is based on either chemical or physical interactions. Polymers with a high affinity allow gas molecules to pass through their permeate side. Whereas non-permeated molecules flow

to the retentate side as depicted in Figure 2.4 [50]. To facilitate gas transport through the membrane, a driving force is required. The driving force for gas permeation is a difference in pressure or concentration of gas on each side of the membrane. The driving force gives the rise in a flux, which is the amount of gas molecules passing the membrane per unit area. The separation of two gases is evaluated using a gas selectivity, which is the ratio of the fluxes of the gases through the membrane [51]. To describe membrane gas separation processes, selectivity and permeability are equally important. Both quantities are influenced by the physical and chemical properties of gas molecules and polymeric membrane. Typically, there are three possible mechanisms to describe membrane separation such as knudsen diffusion, molecular sieving and solution-diffusion.

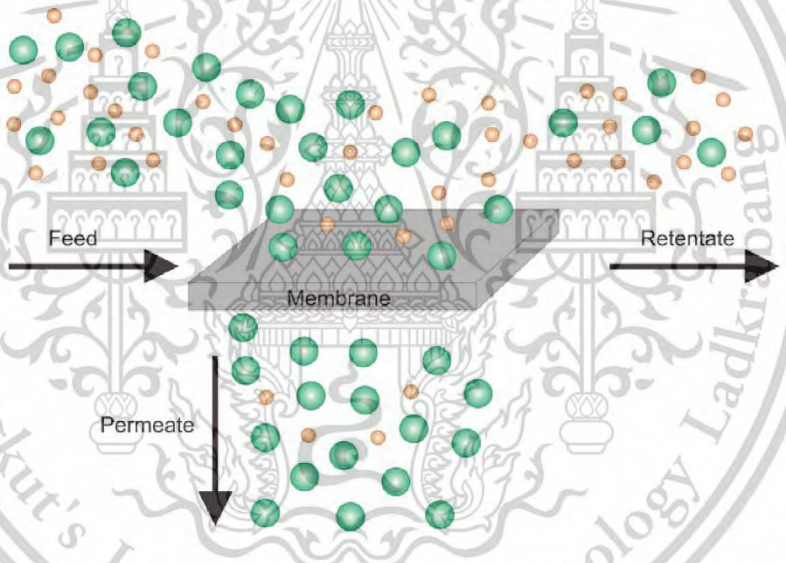

Figure 2.4 Permeation of gas molecules through membrane [50]

2.4.1 Knudsen diffusion

Knudsen diffusion of gas molecules occurs when the mean free path of the gas molecules is larger than the pore diameter of the medium through which they are diffusing. The separation mechanism relies on differences in the mean free path of gas molecules due to collisions with pore walls [52]. Gas separation is influenced by the

difference in molecular weights of the gases and the small pore size of the membrane, which causes lighter molecules to diffuse more rapidly than heavier ones (Figure 2.5a).

2.4.2 Molecular sieving

Molecular sieving method separates gas mixtures through size exclusion. Pore sizes within the membrane are the main factor in controlling the diffusion of gas molecules. Molecules smaller than the pores can diffuse through the membrane. Whereas gas molecules larger than the pores are blocked and cannot diffuse through the membrane (Figure 2.5b).

2.4.3 Solution-diffusion

Solution-diffusion is the primary mechanism in dense polymeric membranes. Gas molecules move through the free volume between the polymer chains. Each gas is separated based on their affinity and diffusivity through the membrane (Figure 2.5c). The affinity and diffusivity relate to the solubility and the diffusion coefficient, respectively [16].

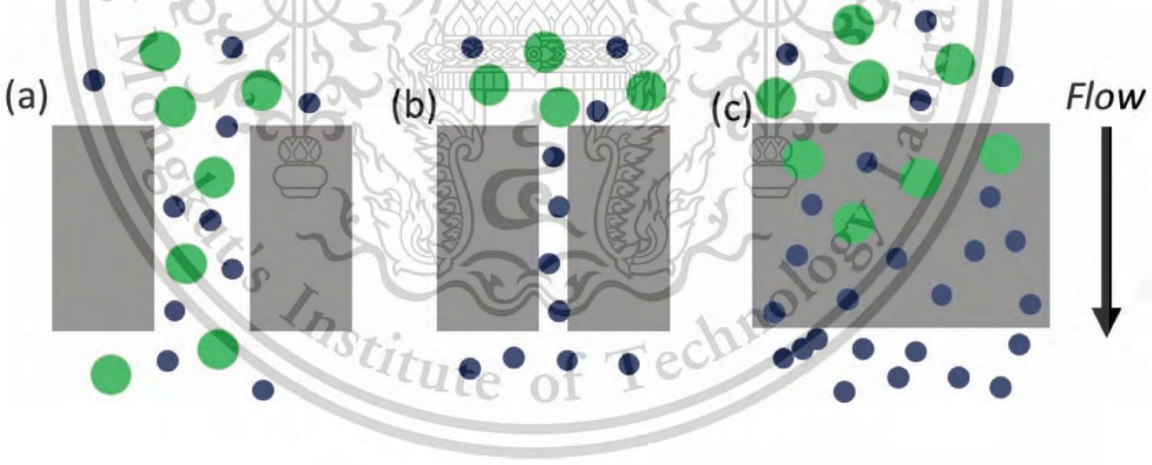

Figure 2.5 Transport mechanisms of gases through polymer membrane (a) Knudsen diffusion, (b) molecular sieving and (c) solution-diffusion [53]

In solution-diffusion processes, the primary mechanisms are typically defined by the following steps as illustrated in Figure 2.6 [54].

- Sorption (at the membrane interface)

- Diffusion (through the membrane)
- Desorption (at the membrane interface)

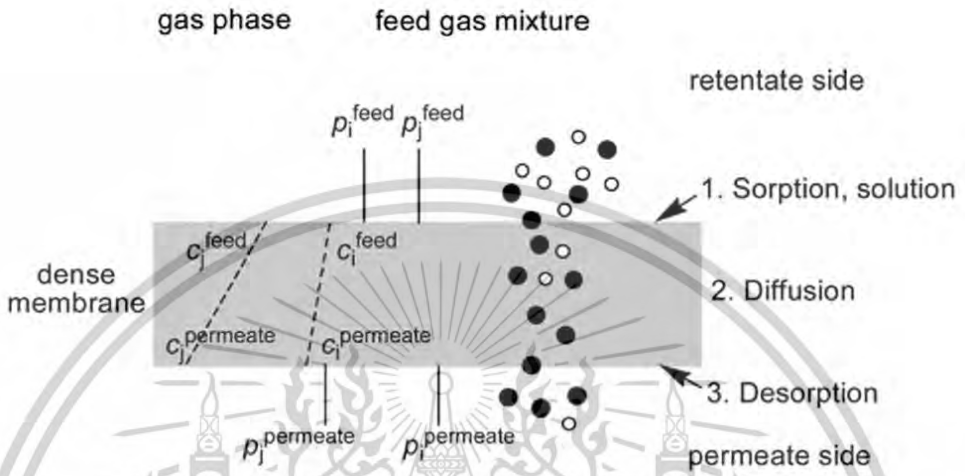

Figure 2.6 Sorption and diffusion mechanisms [54]

2.4.4 Gas permeability and selectivity calculation

Since sorption and desorption are opposing processes, an equation (adapted from Henry's Law) can be formulated to describe them as a function of CO_2 condensability in the membrane material [55]:

$$J_s = S_i(C_F - C_P) \tag{2.1}$$

where J_s is the molar flux of (de)sorption mechanisms. S_i is the condensability factor between the membrane material and the feed gas. C_F and C_P are the CO_2 concentration of the feed gas and the permeated gas. Furthermore, the diffusion process is governed by Fick's Law and is expressed as follows:

$$J_D = \frac{D_i}{\gamma}(C_F - C_P) \tag{2.2}$$

where J_D is the molar flux of diffusion. D_i is the diffusion coefficient of the membrane material. γ is the thickness of membrane. C_F and C_P are the CO_2 concentration of the feed gas and the permeated gas. Assuming both phenomena are independent, the total molar flux equation can be expressed as follows:

$$J_T = J_S + J_D \tag{2.3}$$

$$J_T = S_i(C_F - C_P) + \frac{D_i}{\gamma}(C_F - C_P) \tag{2.4}$$

$$J_T = \frac{S_i D_i}{\gamma}(C_F - C_P) \tag{2.5}$$

Multiplying both sides by the membrane area (A), the molar flow through the membrane (J_T) is obtained as follows:

$$J_T.A = F_T = \frac{A.S_i.D_i}{\gamma}(C_F - C_P) \tag{2.6}$$

Equations (2.5) and (2.6) clearly show the relation between the mass flow and (de)sorption and diffusion coefficients. Therefore, the total mass flux depends on both phenomena.

For single gas permeation system, the membrane's ability to separate two gases (i and j) are evaluated by membrane selectivity ($\alpha_{i/j}$), which is the ratio of the permeability of two gases. This parameter can be written as:

$$\alpha_{i/j} = \frac{P_i}{P_j} = \frac{D_i.S_i}{D_j.S_j} \tag{2.7}$$

The ratio D_i/D_j represents the diffusion coefficients of the two gases and serves as the mobility selectivity, reflecting the relative movement of individual molecules in each component. The selectivity is proportional to the ratio of the molecular kinetic size of the two permeants. The ratio S_i/S_j represents the sorption coefficients, indicating the relative concentration of the components i and j within the membrane material. Sorption selectivity is directly proportional to the relative condensability of components i and j. For the permeation of actual *i–j* mixtures, the mixed gas selectivity, also known as separation factor ($\alpha'_{i/j}$), can be determined from equation (2.8).

$$\alpha'_{i/j} = \frac{y_i/y_j}{x_i/x_j} \tag{2.8}$$

where y_i and y_j are the molar fractions of gas species *i* and *j* in the permeate side, x_i and x_j are the molar fractions of gas species *i* and *j* in the feed side.

The kinetic diameter and condensabilities of the gases are listed in Table 2.4. Generally, the small molecules such as water (Kinetic diameter of 2.65 Å) and CO_2 (Kinetic diameter of 3.30 Å) are more easily diffusion through the membrane over larger molecules such as CH_4 (Kinetic diameter of 3.80 Å) [56].

Table 2.4 Kinetic diameter and condensability temperature of gases [56]

Gas molecular	Kinetic diameter (Å)	Condensability temperature (K)
CO_2	3.30	195
N_2	3.64	71
CH_4	3.80	149
O_2	3.46	107
H_2O	2.65	373

2.5 Types of polymeric membranes

Polymer membranes have been widely used for gas separation [26,27]. Typically, the polymeric membranes can be divided into two general categories [57].

2.5.1 Rubbery polymer

Gas permeation in rubbery polymers is effectively described by the solution-diffusion model. Gas sorption in these materials follows the same principles as in low molecular weight liquids and generally obeys Henry's law. Thus, under a certain pressure, the permeation rate is governed by the diffusion step and can be accurately described by Fick's law [58]. In rubbery polymer, the polymer backbone segments can rotate freely due to its softness and high free volume. This leads to an easier for gases to diffuse through it.

Among the rubbery polymers, poly (ethylene oxide) (PEO)-based polymers have been widely studied to improve gas solubility [59-61]. PEO contains ether linkages that typically exhibit strong chemical interactions with CO_2, leading to a high solubility

coefficient. Additionally, polyether block amide (PEBAX) has also been studied owing to their high permeability and selectivity [62]. The structure of PEBAX consists of linear chains with rigid polyamide segments for mechanical strength and flexible polyether segments for high gas permeability. The polarity of both blocks enhances their chemical affinity for CO_2, enabling excellent CO_2/N_2 and CO_2/H_2 separation. Polyvinylamine (PVAm) membranes exhibited sorption selective permeability because of reversible reactions between the membrane components and CO_2. In a water swollen condition, the amine groups of PVAm can react with CO_2 in the form of HCO_3^- which promotes both permeability and selectivity of the membranes [63]. The chemical structures of the rubbery polymers as mentioned above are shown in Figure 2.7.

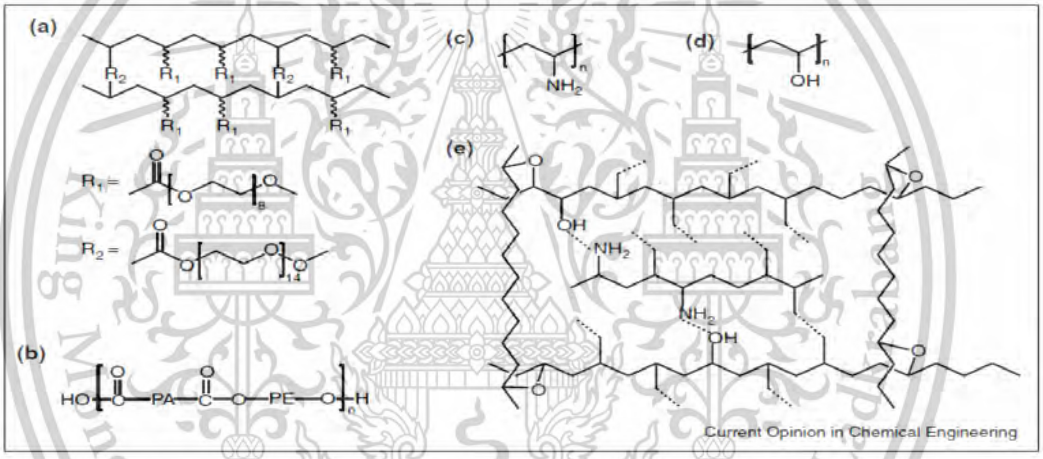

Figure 2.7 Chemical structure of rubbery polymers (a) Cross-linked amorphous poly(ethylene oxide), (b) Pebax®, (c) PVAm, (d) PVA and (e) PVAm/PVA blend [57]

2.5.2 Glassy polymer

In glassy polymer membranes, gas diffusivity and selectivity are governed by chain rigidity and the available free volume within the polymer structure. These polymer membranes are influenced by diffusion selective gas separation because gas diffusion occurs through the gap between polymer chains known as the free volume [64]. Glassy polymers with relatively small free volumes, such as polyimide (PI), cellulose acetate (CA), and polysulfone (PSU), have been extensively studied for gas separation over the past three decades. [19,21,22]. These membranes provide a low free volume, resulting in low

gas permeability. Recent research has aimed at developing glassy polymer membranes with enhanced free volume and higher diffusivity to improve gas permeability [57]. Examples of glassy membranes are illustrated in Figure 2.8. Moreover, the gas permeation and gas selectivity (CO_2/CH_4) of glassy membranes are summarized in Table 2.5.

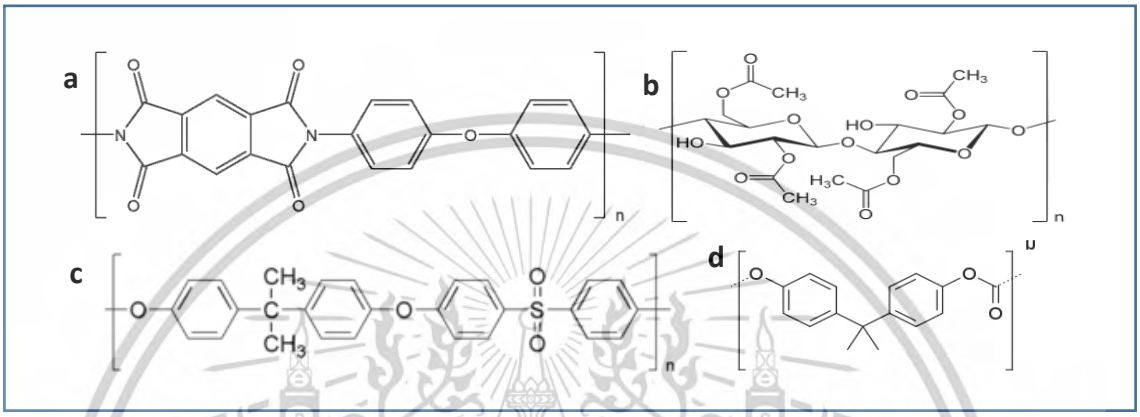

Figure 2.8 Chemical structures of glassy polymers (a) polyimide, (b) cellulose acetate, (c) polysulfone and (d) polycarbonate [19-22]

Table 2.5 Summarized gas permeation and gas selectivity of polymer membranes [65]

Membrane type	CO_2 permeance (Barrer)	CO_2 permeance (mol m^{-2} s^{-1} Pa^{-1})	α_{CO_2/CH_4} [a]
Film composite of PEBAX on PVDF ultra-porous substrate	0.12-1.7	4.0×10^{-11} – 5.7×10^{-10}	27-52
Sulfonated PC	1.5-6.3		27-75
Three different types of polyimide membranes (Matrimid, Katon, P84)	8.5-6.3	5.7×10^{-11} – 4.2×10^{-10}	18-85
Pure Matrimid, blends of Matrimid, CA, PEO (asymmetric hollow fibers)	-	3.0×10^{-9} – 4.0×10^{-9}	28-31
PC	230-560	8.4×10^{-10} – 1.0×10^{-9}	93-170
Matrimid 52218 chemically crosslinked at room temperature by PPG block PEG block PPG diamine	5.4-120	2.4×10^{-11} – 5.1×10^{-10}	17-36

[a] CO_2/CH_4 selectivity

Table 2.5 Summarized gas permeation and gas selectivity of polymer membranes [65] (continued)

Membrane type	CO_2 permeance (Barrer)	CO_2 permeance (mol m^{-2} s^{-1} Pa^{-1})	α_{CO_2/CH_4} [a]
Blends of Pebax MH 1657 and low molecular weight PEG	51	2.1×10^{-10}	15
PU and PVAc blends	26	8.9×10^{-11}	48
PEBAX with silver tetrafluoroborate on PVDF ultrafiltration substrate	-	4.1×10^{-9} – 1.1×10^{-8}	15-36
Fluorinated copolyimides synthesized with various diamine compositions by chemical imidization	40-550	-	23-57

[a] CO_2/CH_4 selectivity

2.6 Mixed matrix membrane

Mixed matrix membranes (MMMs) are typically composed of two or more materials with distinct properties. A polymer usually serves as the continuous phase, known as the matrix, while another material forms the dispersed phase, referred to the additive. These components are immiscible and exhibit different transport properties. Adding the additive into the matrix able to hinder the crystallization of polymer, leading to an escalation of gas permeability. CO_2 permeation and gas selectivity (CO_2/CH_4) of mixed matrix membranes are listed in Table 2.6.

Typically, additives are substants that can be added to polymeric membranes to improve their properties. It can be both organic and inorganic matters. The inorganic filler used in mixed-matrix membranes (MMMs) should possess: (1) strong affinity for the polymer, and (2) matching gas transport properties [66]. To achieve CO_2 separation, the filler should have a high interaction with CO_2 molecules. Inorganic fillers used in MMMs can be categorized into two types: solid (impermeable) fillers and porous (permeable) fillers. Impermeable fillers, such as ZnO and TiO_2, do not allow gas transport through their structure [67]. The permeable fillers include zeolite, carbon molecular sieve, carbon nanotube, montmorillonite, metal-organic framework, and graphene oxide [68]. Among these fillers, SiO_2 offers several advantages, including affordability, non-toxicity,

biocompatibility, high thermal resistance, and, most notably, its ability to enhance the mechanical properties of the polymer matrix [69]. In addition, the high hydrophilicity structure of SiO_2 surface can promote the permeation of CO_2.

Table 2.6 Gas permeability and selectivity of composited membranes [65]

Membrane type	CO_2 permeance (Barrer)	CO_2 permeance (mol m^{-2} s^{-1} Pa^{-1})	α_{CO_2/CH_4} [a]
Zeolite NaA and AgA dispersed in PES	1.0-2.7	5.2×10^{-12} - 1.4×10^{-11}	32-60
Organic-inorganic asymmetric hollow fiber, with HSSZ-13 zeolites dispersed in Ultem® 1000 PEI matrix		3.8×10^{-9} - 4.4×10^{-9}	36-40
Pure PC, PC/p-nitroaniline (pNA), PC/zeolite 4A and PC/pNA/zeolite 4A membranes	4.0-8.8	2.5×10^{-11} - 5.6×10^{-10}	24-53
PES-zeolite 4A hollow fiber membrane	1.9-5.6	2.2×10^{-9} - 6.8×10^{-9}	15-29
SSZ-13 zeolite dispersed in 3:2 6FDA-DAM-DABA chemically modified with 1,3-propane diol PES-zeolite NaA and PES-zeolite AgA	56-87		37-50
PES-zeolite NaA and PES-zeolite AgA	1.7-3.4	8.8×10^{-12} - 1.7×10^{-11}	30-39
End group-modified 6FDA-TAPOB hyperbranched polyimide-silica hybrid with tetramethoxysilane as precursor	7.4-2.6	1.2×10^{-10} - 4.4×10^{-10}	54-95
PES containing embedded nonporous fumed silica nanoparticles	6.3-2.0	3.0×10^{-11} - 9.4×10^{-11}	18.29
Polysulfone and functionalized single walled carbon nanotube mixed matrix	3.9-5.2	N/A	16-24
Microporous MOF (Cu-BPY-HFS) combined with polyimide (Matrimid) to form free-standing films	7.8-1.5		32-26
Polyimide (Matrimid) continuous phase embedded with MOF-5 nanocrystals	11-20	1.1×10^{-10}-1.9×10^{-10}	40-50

[a] CO_2/CH_4 selectivity

The mixing of organic additive as a third component can enhance the compatibility between the inorganic fillers and the polymer matrix. Examples of organic additives are

polyethylene glycol (PEG) and polyethyleneimine (PEI). Loloei *et al*. [70] studied the influence of PEG 200 additive on the gas separation properties of Matrimid®5218-ZSM-5 mixed matrix membranes. It was demonstrated that PEG can improve the compatibility between ZSM-5 and matrix polymers. Furthermore, ionic liquids (ILs) additives can be used as plasticizers for fillers and matrix polymer. Hudiono *et al*. [71,72] reported that ILs can act as wetting agents in polymer-zeolite mixed matrix membranes, enhancing the compatibility between the polymer and zeolite.

2.7 Ethylene-vinyl acetate copolymer

Ethylene-vinyl acetate (EVA) is a copolymer-based polyethylene. Its structure consists of nonpolar crystalline polyethylene and polar amorphous acetate segments. The physical and chemical properties of EVA copolymer depend on the vinyl acetate (VA) content. The chemical structural of EVA is displayed in Figure 2.9. Polar vinyl acetate segments can interact with CO_2 molecules, leading to increased CO_2 permeability.

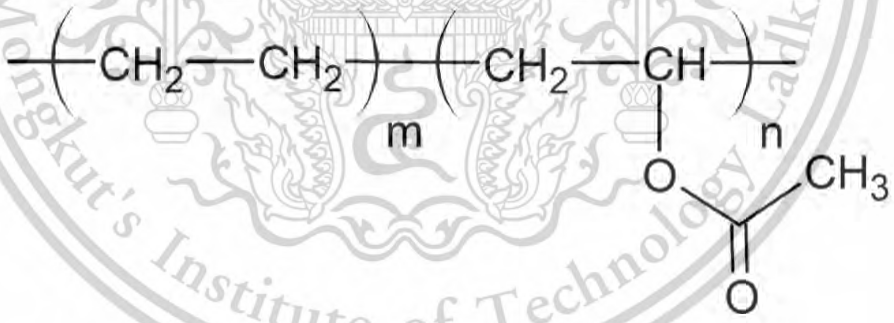

Figure 2.9 Chemical structure of EVA copolymer [73]

In the last decade, EVA membranes have been introduced for gas separation. Marais *et al*. [74] studied CO_2, H_2O and O_2 permeability using EVA membranes with different VA contents (19, 33, 50 and 70 wt%). The results indicated that the CO_2 permeability increased with the VA content in the membrane. This can be explained by the strong interaction between polar VA segments and CO_2. Mousavi *et al*. [26] prepared

EVA membranes using phase inversion method for gas separation. The results showed that the CO_2 permeability was evidently higher than O_2, N_2, and CH_4. This can be described by the lowest kinetic diameter (3.30 Å) and highest condensability (195 K) of CO_2 [56].

2.8 Silica

Silica or silicon dioxide (SiO_2) is a popular inorganic filler used to improve the performance of polymer membranes in gas separation applications. Adding SiO_2 particles increases the rigidity of the polymer matrix, enhancing the mechanical strength and thermal stability of the membrane. For gas separation membrane, the incorporation of SiO_2 can enlarge gas separation. The silanol (Si-OH) groups contained on the silica surface (Figure 2.10) [75] can interact with polar CO_2, resulting in an increasing gas solubility of the membranes [27]. Polyimide/silica has received considerable attention in gas permeation studies [76-78]. Other combinations such as PEBAX/silica [79], poly(4-methyl-2-pentyne) (PMP)/silica [80] and poly (1-trimethylsilyl-1-propyne) (PTMSP)/silica [81] have also been investigated to improve gas permeability and selectivity.

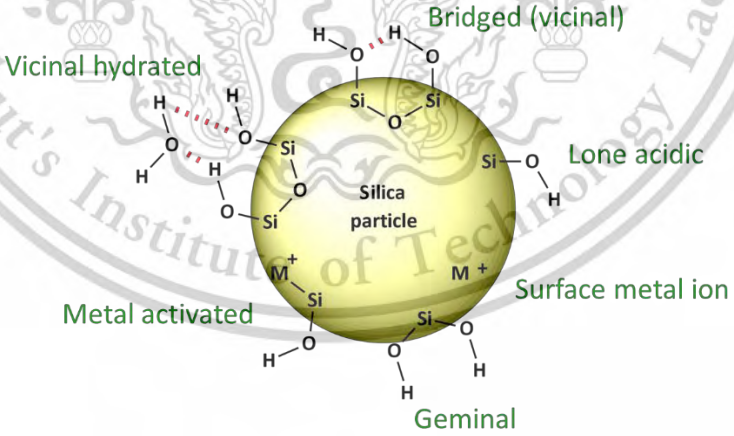

Figure 2.10 Silanol groups on the silica surface [75]

2.9 Polyethylene glycol

Polyethylene glycol (PEG) is widely used as plasticizer in polymer membrane fabrication due to its unique physicochemical properties. The chemical structure of PEG is shown in Figure 2.11. Incorporating PEG can increase the free volume within the membrane matrix. The increasing free volume can facilitate gas diffusion, especially for small molecules. PEG additives can enhance the membrane's ability to effectively separate CO_2. This is due to the strong interaction between the ether oxygen in PEG and CO_2 through quadrupole–dipole interactions. Zamiri *et al*. [25] prepared a mixing of ethylene vinyl acetate and PEG additive up to 20 wt.% for CO_2/N_2 separation. The results indicated that CO_2 permeability increases with higher PEG content in the membranes. The addition of PEG200 (molecular weight of 200) demonstrated efficient gas separation performance due to its effective providing amorphous regions in the membrane. PEBAX/PEG membranes for CO_2 separation have been reported by Taheri *et al*. [82]. Incorporating low molecular weight PEG (PEG600) into the matrix polymer enhanced chain mobility, resulting in increased gas permeability for N_2, O_2, CH_4, and CO_2. PEBAX with 20% PEG600 exhibited a CO_2 permeability of 63.12 Barrer and a CO_2/CH_4 selectivity of 23.6.

Figure 2.11 Chemical structure of polyethylene glycol (PEG) [83]

2.10 Membrane module

For applying polymeric membrane on a large scale, large membrane areas are required. Accordingly, the number of members should be packaged into modular units to form compact. Membrane modules for gas separation can be category into two types of membrane configurations such as flat and tubular [84]. The modules with flat membrane

are the plate-and-frame and spiral-wound modules while tube-like structures modules are tubular and hollow fiber (Figure 2.12) [85].

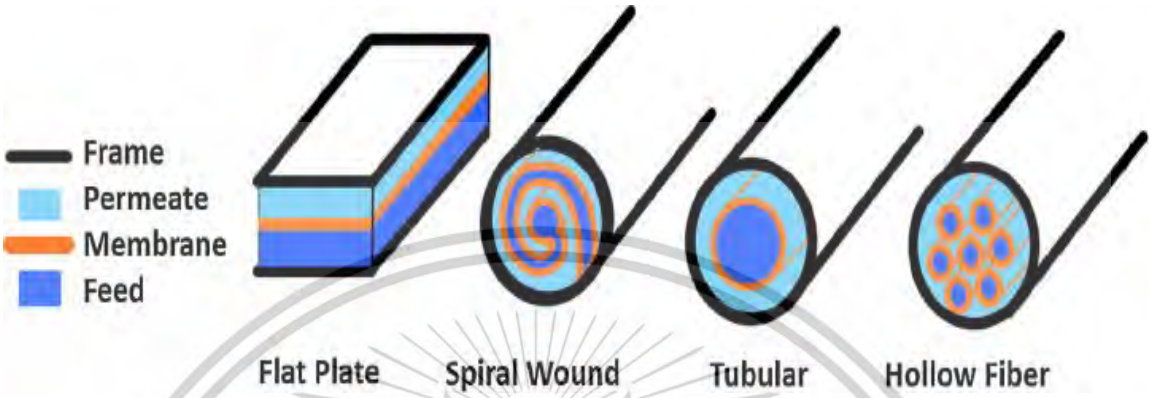

Figure 2.12 Types of modules for gas separation [85]

2.10.1 Plate and Frame

Plate-and-frame modules are similar to typical lab setups. Flat membranes can be arranged as plates, bags, or spiral-wound shapes. Each pair of membranes is separated by a spacer, and the layers are stacked together like a sandwich. These spacers are incorporated into frames, which simultaneously seal the module. The spacer plate separates the feed flow running alongside different membranes in the module. The module has a packing density of about 100-400 m^2/m^3 [86].

2.10.2 Spiral Wound

The spiral-wound module is a variation of the plate-and-frame design and is commonly used for gas separation. In this method, two flat sheet membranes are sealed together with a spacer placed both between them and on one external side. These layered sheets are then rolled into a spiral shape around a central permeate collection tube. The permeate flow moves across the feed flow rather than in a counter-current direction, making it less thermodynamically efficient. The feed gas travels through the spacer channels, while the membrane and its porous support form an envelope that wraps around a perforated central tube. This assembly is then placed inside an outer pressure shell. The feed moves axially through the channel across the membrane surface,

while the filtered gas flows along the permeate channel and is collected in the central perforated tube [87].

2.10.3 Tubular

Tubular membrane for gas separation is a type of membrane module designed in a tube-like shape, typically with a diameter greater than 10 mm. A module can contain between 4 and 8 tubes. The feed gas flows through the center of the tubes, while the permeated gases pass through the membrane from the inside to the outside. Then the permeated gases were collected and removed at the other side of module [88].

2.10.4 Hollow fiber

Hollow fiber modules are created by bundling multiple hollow fibers together to form a compact structure. These fibers, which have a thin selective membrane layer, are carefully arranged inside a stainless-steel tube. The ends of the fibers are securely sealed by gluing them to the tube openings, ensuring proper separation between the feed and permeate sides. This design allows for a high packing density, maximizing the membrane surface area within a small space, making hollow fiber modules highly efficient for gas separation applications. The mixed gas was fed into the side of the module. Then gas molecules diffused into the fiber bundle, and the permeated gas was collected at the end of the module (Figure 2.13) [84].

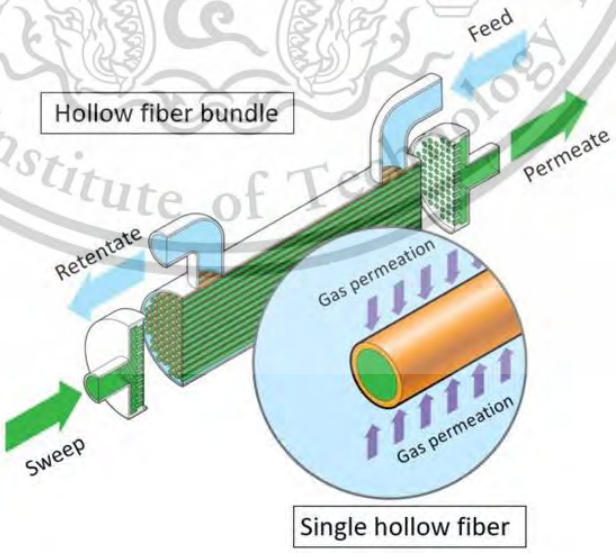

Figure 2.13 Hollow fiber modules [84]

2.11 Literature reviews

Wolinska-Grabczyk *et al*. [24] studied gas permeation of CO_2, He, O_2 and N_2 using EVA membranes. The EVA membranes and its blend were prepared using solution casting techniques. The samples were dissolved in xylene. Then the solutions were poured onto a Teflon plate. The effects of vinyl acetate (VA) contents varying from 25 to 70 wt% on gas permeation were investigated. It was found that gas permeability ranked in the following order: CO_2 > He > O_2 > N_2, aligning with the kinetic diameter of each gas (Figure 2.14). The acetate side group of EVA membrane can interact with the polar CO_2 molecules leading to a higher CO_2 permeability. In addition, EVA membrane with 46 wt% of VA content provided the highest CO_2 permeability compared to other gases. This can be explained by the highest fractional free volume (FFV) of this membrane. Generally, the membrane with higher FFV provides higher gas diffusivity, especially for smaller gas molecules.

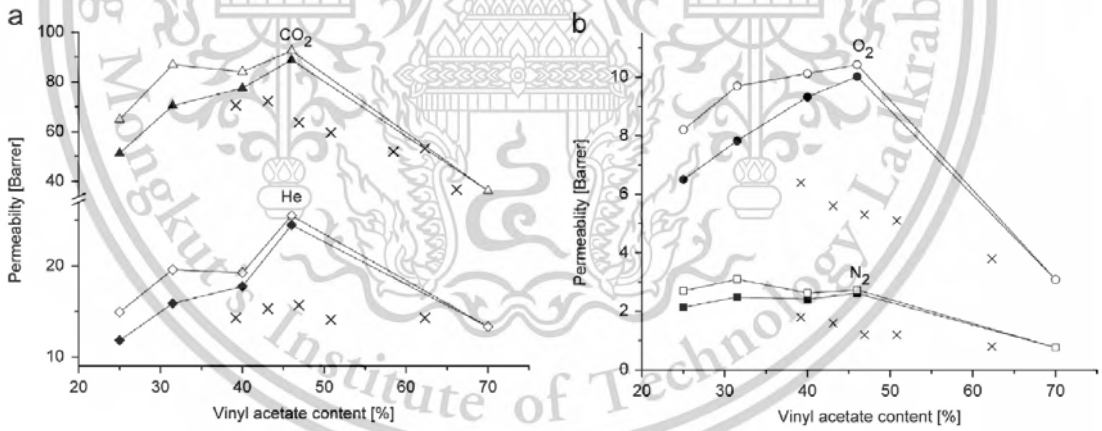

Figure 2.14 Permeability dependence on VA content of EVA membranes of (a) CO_2 and He (b) O_2 and N_2; filled points represent experimental results for EVA copolymers, empty points indicate the calculated permeability of the copolymer's amorphous phase, and crosses denote experimental data for blends [24]

Zamiri *et al.* [25] prepared blended membranes of EVA containing 28 wt% of VA (EVA28) and PEG (5, 10, 15 and 20 wt%) for CO_2/N_2 separation. Pure and blend membranes were fabricated using a solution casting technique. The samples were dissolved in chloroform casting solvent and casted on a glass plate with a doctor blade. The gas separation was performed using a constant pressure/variable volume method over the feed pressure of 2–8 bar. The results revealed that CO_2 permeability increased by increasing the PEG content as shown in Figure 2.15 (b). The ether groups of PEG play an important role in interacting with CO_2 molecules. An Increase in PEG loading (up to 10 wt%) to the membranes significantly improves CO_2/N_2 selectivity as illustrated in Figure 2.15 (c). Whereas, at higher PEG loading (15 to 20 wt%), CO_2/N_2 selectivity slightly increases. This can be explained by forming cavities inside the membrane leading to the enhancing diffusivities of CO_2 and N_2 gases. Furthermore, Increasing the feed pressure (2–8 bar) led to an increase in CO_2 permeability for pure and blend membranes.

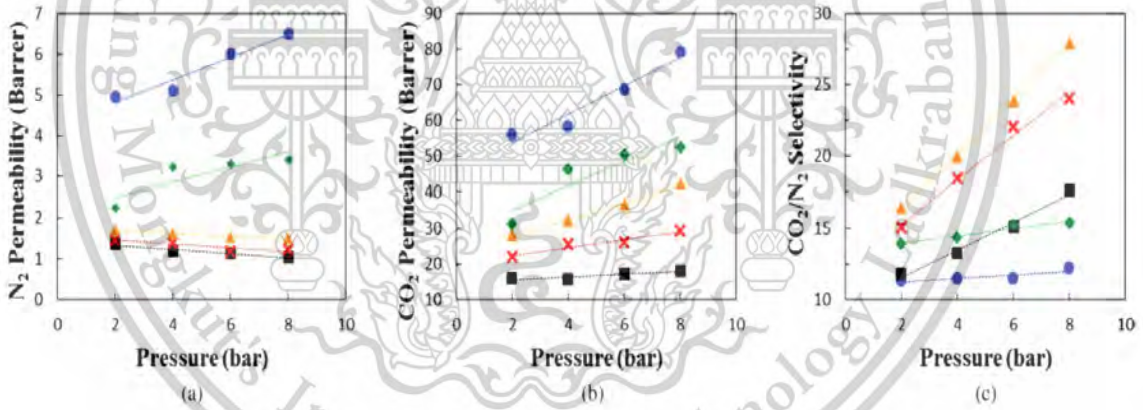

Figure 2.15 Effect of feed pressure on (a) N_2 permeability, (b) CO_2 permeability and (c) CO_2/N_2 selectivity ((■) EVA, (x) EVA/5%wt. PEG200, (▲) EVA/10%wt. PEG200, (♦)EVA/15%wt. PEG200 and (●) EVA/20%wt. PEG200 [25]

Adelnia *et al.* [89] fabricated mixed matrix membranes (MMMs) comprising EVA and fibrous sepiolite for gas permeation applications. The sepiolite fibers were modified by 3-aminopropyltrimethoxysilane (3-APTMS) before adding to the EVA matrix. The composite membranes were prepared by a solution casting technique. Microscopic images revealed

a uniform dispersion of sepiolite fibers within the EVA matrix. Permeabilities of single gas, namely N_2, O_2, CO_2 and CH_4 were significantly increased with increasing sepiolite loading as exhibited in Figure 2.16. This is because the incorporated sepiolite decreased crystallinity of the EVA membranes and hence enhanced gas permeation. It was observed that the composite membranes demonstrated a higher CO_2 permeability compared to N_2, O_2, and CH_4. It was due to the polar/polar interactions of CO_2/EVA.

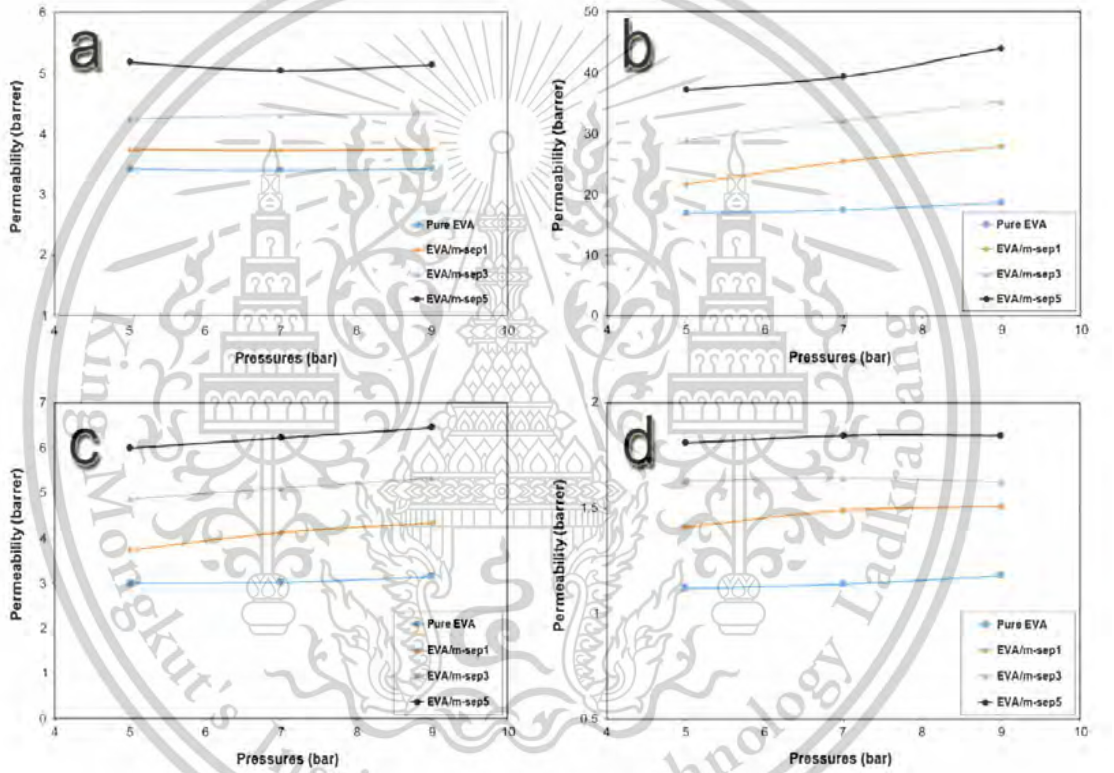

Figure 2.16 Gas permeability of (a) O_2, (b) CO_2, (c) CH_4, and (d) N_2 in EVA membrane and EVA/m-sepiolite membrane as a function of pressure [89]

Sadeghi *et al*. [27] studied the effect of silica nanoparticles incorporated in EVA containing 28 wt% of VA (EVA28) membrane on CO_2 and CH_4 permeability. Pure EVA and composite membranes were fabricated through the thermal phase inversion technique. The results showed that silica particles were uniformly dispersed in polymer matrix

(confirmed from SEM image as shown in Figure 2.17). The increase of silica content significantly enhanced amorphous regions of the membranes. This leads to an increase in CO_2 and CH_4 permeability as shown in Figure 2.18 (a) and (b). In addition, the strong affinity of residual OH groups on the silica for polar CO_2 molecules significantly enhances the interaction between CO_2 and the membrane matrix, resulting in greater solubility and, consequently, improved CO_2 permeability compared to CH_4. Accordingly, the CO_2/CH_4 selectivity was improved with increasing silica content.

Figure 2.17 SEM image of EVA–silica membrane [27]

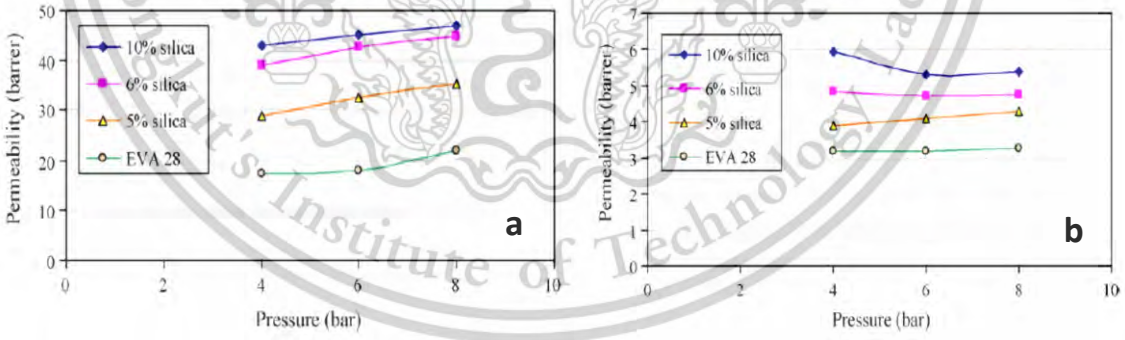

Figure 2.18 Permeability of (a) CO_2 and (b) CH_4 in EVA-silica hybrid membranes dependence on pressure [27]

Mousavi *et al.* [26] studied the gas permeation properties of O_2, N_2, CH_4, and CO_2 through EVA membranes with 18 and 28 wt% VA content. The EVA membranes were prepared using thermal and thermal/wet phase inversion techniques. The single gas

permeation was evaluated under varying feeding pressures from 2 to 11 bars. The findings revealed that CO_2 exhibited significantly higher permeability compared to the other gases as shown in Table 2.7. This can be explained by the highest condensability and lowest kinetic diameter of CO_2. The polar acetate groups in the main chain of EVA copolymers play a key role in influencing CO_2 solubility. Additionally, it was found that using tetrahydrofuran (THF) as the casting solvent improved gas permeability compared to chloroform. This is because the solvents with higher molar volumes, such as THF, can promote the formation of membranes with an increase in free volume, resulting in enhanced gas permeability. A significant increase in CO_2/N_2 and CO_2/CH_4 permselectivity was observed in the membrane with higher VA content, when using THF as solvent.

Table 2.7 Gas permeability and selectivity of EVA membranes [26]

Membrane	Permeability (Barrer)				Selectivity		
	O_2	N_2	CH_4	CO_2	O_2/N_2	CO_2/N_2	CO_2/CH_4
EVA28-THF	3.85	1.17	4.6	23.11	3.28	19.73	5.03
EVA18-THF	3.82	1.04	4.10	21.46	2.87	13.11	3.76
EVA28-Chloroform	2.88	1.04	4.31	17.07	2.78	16.47	3.96
EVA18-Chloroform	2.77	1.11	5.24	18.74	2.50	16.89	3.57

Hassanajili *et al.* [90] prepared polyesterurethane/silica and polyetherurethane /silica nanocomposite membranes for CO_2/CH_4 separation. The mixture of polymer and additive were dispersed in dimethylacetamide (DMAC). Then the mixtures were cast on Teflon-coated plate and dried. The pure gas permeation properties of the polyurethane/silica membranes were evaluated using the constant pressure method. The results suggest that nano silica additive can form hydrogen bonds with N-H groups of polyesterurethane matrix as confirmed from FTIR spectrum. The effect of nano silica content on gas separation was investigated. The results revealed that adding nano silica

to the membrane increases CO_2 permeability and CO_2/CH_4 selectivity as illustrated in Figure 2.19. This is because the silica particles disrupted the polymer chain packing leading to an enhancing in free volume of polymer matrix. Another reason is that the silanol groups on nano silica surfaces preferentially adsorb CO_2 molecules over CH_4. As a result, the CO_2/CH_4 selectivity increased with higher nano silica content.

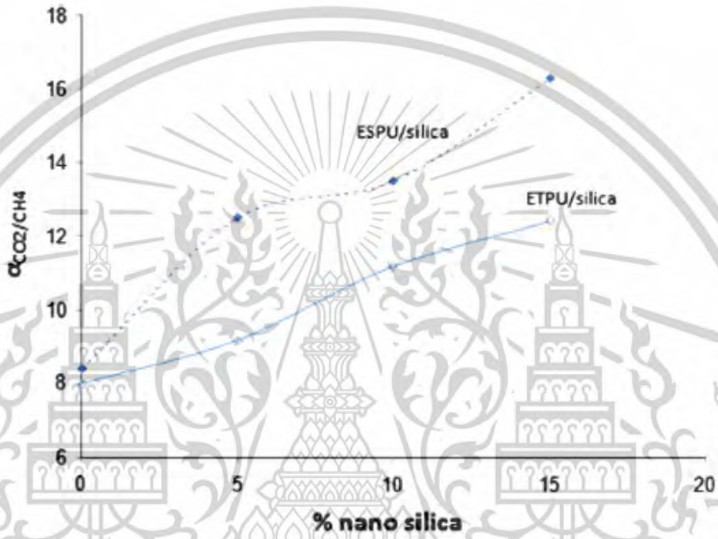

Figure 2.19 CO_2/CH_4 selectivity versus silica content of ETPU/silica and ESPU/silica nanocomposite membranes [90]

Ghadimi *et al.* [91] prepared poly(ether-block-amide)/silica (PEBAX/SiO_2) nanocomposite membranes for CO_2 separation. The nano SiO_2 was modified with cis-9-octadecenoic acid (OA) to prevent the agglomeration of the nano SiO_2. Then the modified SiO_2 and polymer were dispersed in mixture of ethanol/water and cast on Teflon flat-bottomed Petri dishes. Gas permeation experiments were conducted using the constant volume (CV) method. The results indicated that an incorporation of the modified nano SiO_2 into the polymer matrix enhanced CO_2/N_2, CO_2/CH_4 and CO_2/H_2 separation, as illustrated in Figure 2.20. This effect is attributed to the residual -OH groups on the surface of the modified SiO_2, which interact positively with polar CO_2 molecules. These

interactions enhance the solubility of CO_2 molecules within the polymer matrix. On the other hand, nano SiO_2 hindered the diffusion of non-polar gases (H_2, CH_4 and N_2). As a result, the selectivity for CO_2/N_2, CO_2/CH_4 and CO_2/H_2 increased with increasing nano SiO_2 content.

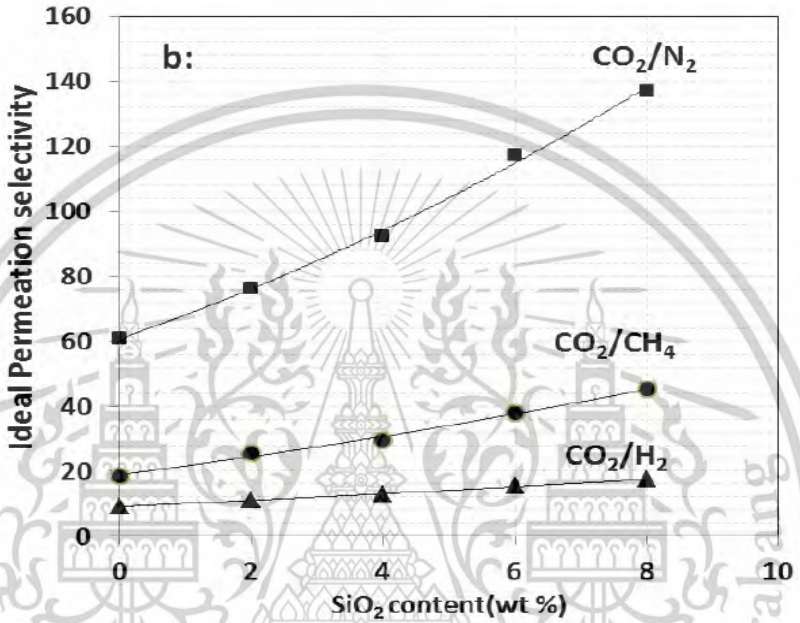

Figure 2.20 Ideal permeation selectivity of (■) CO_2/N_2, (●) CO_2/CH_4 and (▲) CO_2/H_2 [91]

Barooah *et al.* [92] prepared CO_2-selective membrane by incorporating SiO_2 nanoparticles into the poly (vinyl alcohol) (PVA)/poly(ethylene glycol) (PEG) via solution casting. The results of field emission scanning electron microscopy revealed the uniform dispersion of the SiO_2 filler within the polymer matrix. The overall membrane hydrophilicity was evaluated by the contact angle of water droplet. The results showed that the addition of 6.68 wt % silica, the contact angle decreased from 36.58° to 35.18°. This can be explained by the increase in surface hydrophilicity of the composite membrane because of the present of silanol groups of SiO_2. Compared to the pristine PVA/PEG membrane, the PVA/PEG/SiO_2 membrane with a 3.34 wt% SiO_2 loading demonstrated a remarkable enhancement in CO_2/N_2 separation performance. Specifically, the incorporation of SiO_2 nanoparticles led to a 78% increase in CO_2 permeability,

facilitating more efficient gas transport through the membrane. Additionally, CO_2/N_2 selectivity improved by 45% as observed in Figure 2.21.

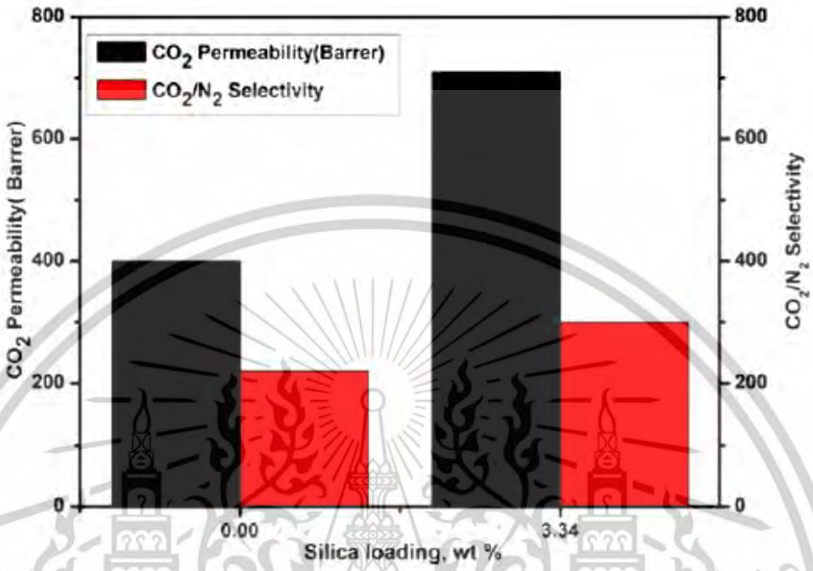

Figure 2.21 CO_2 permeability and CO_2/N_2 selectivity for pure PVA/PEG membrane and PVA/PEG-S3.34 membrane [92]

Muhammad *et al.* [93] prepared the composite membrane for gas separation. SiO_2 nanoparticles (0-20 wt%) were incorporated into PVA/PEG cross-linked membranes. The FTIR peak at 1088 cm^{-1} confirmed the successful cross-linking of the polymer matrix through C–O–C bond formation. Additionally, SEM analysis demonstrated the uniform dispersion of SiO_2 nanoparticles within the membrane. Thermal stability of the membranes was improved with the incorporation of SiO_2 nanoparticles as confirmed from TGA analysis. For the gas permeation experiment, it was found that permeability of all the gases (CO_2, N_2, and CH_4) increased with the increase of SiO_2 loading. This can be attributed to the increased free volume, resulting from the disruption of polymer chain packing. This structural modification facilitates gas transport through the membrane. Furthermore, the ideal selectivity of CO_2 over CH_4 improved with SiO_2 loading up to 10 wt.% as shown in Figure 2.22.

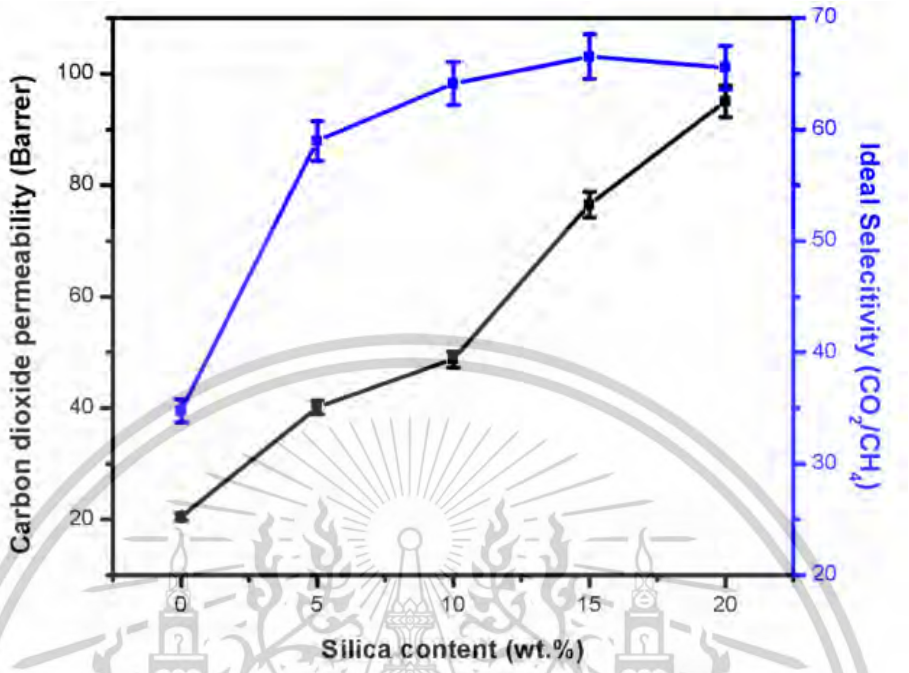

Figure 2.22 Effect of silica content on CO_2 permeability and CO_2/CH_4 selectivity [93]

Jinpeng *et al.* [94] prepared mixed matrix membranes (MMMs) with polyether-polyamide block copolymer (PEBAX) and SiO_2 nanosheets for gas permeation. The effect of different filler loadings on gas permeation was determined. The PEBAX/SiO_2 mixed matrix membranes (MMMs) exhibited outstanding CO_2 separation performance, achieving a CO_2 permeation coefficient of 313.24 Barrer and a CO_2/CH_4 selectivity of 31.26 at a SiO_2 loading of 1.0 wt% as shown in Figure 2.23. The superior performance of the PEBAX/SiO_2 MMMs is attributed to the horizontal alignment tendency of SiO_2 nanosheets within the membrane matrix, which enhances gas transport properties. However, at a higher SiO_2 nanosheet loading of 1.4 wt%, filler aggregation occurs within the membrane, leading to a decrease in both CO_2 permeability and CO_2/CH_4 selectivity due to reduced free volume and increased transport resistance.

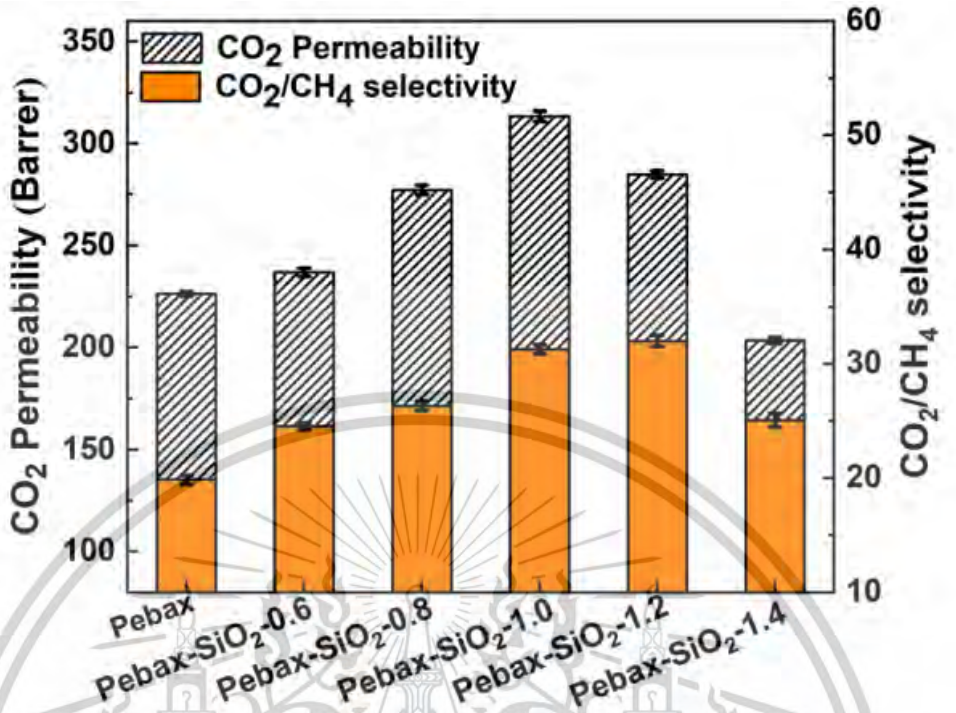

Figure 2.23 Effect of the SiO_2 loading on CO_2 permeability and CO_2/CH_4 selectivity [94]

Chapter 3
Research methodology

3.1 Chemicals and materials

1. LDPE, LD2426K, InnoPlus, PTT Polymer (Thailand)
2. EVA with VA 18 wt% (referred to as E18), POLENE® N8038F, TPI polene Company (Thailand)
3. EVA with VA 28 wt% (referred to as E28), Ultra UL 00728, Exxon Chemical (Belgium)
4. EVA with VA 33 wt% (referred to as E33), Ultra UL 04533, Exxon Chemical (Belgium)
5. SiO_2, Tokusil URT grade, Maruo calcium Company (China)
6. Polyethylene glycol (M.W. 6000), analytical grade, Kemaus (Australia)
7. CO_2 with 99.8% purity, United Industrial Gases (Thailand)
8. CH_4 with 99.99% purity, United Industrial Gases (Thailand)
9. CO_2/CH_4 mixed gas with 40/60 volume ratio, United Industrial Gases (Thailand)
10. He 99.9% purity, Praxair Company (Thailand)
11. Polyester resin, TM-189, Changzhou Tianma Group Co., Ltd.
12. Methyl ethyl ketone peroxide, 60% purity, Martect Products Co., Ltd.

Table 3.1 Specification of polymers

Property	Types of polymers			
	LDPE	E18	E28	E33
Vinyl acetate content (%)	-	18	28	33
Melt flow index (190 °C, 2.16 kg) (g/10 min)	4.0	2.8	7.0	43
Density (g/cm^3)	0.924	0.941	0.951	0.955
Melting point (°C)	110	86	73	58

3.2 Equipments

1. Permeation cell and permeation rig
2. Gas separation modules
3. Hot air oven, UN 500, Memmert GmbH Co., KG
4. Internal mixer, D-47055 Duisburg, Brabender® GmbH & Co., KG
5. Internal mixer, MX500-D75L90, CHAREON TUT Co., Ltd.
6. Compression molding machine, MGLF-2UAT, MACH GROUP Co., Ltd.
7. Plastic grinder, Bosco A600, Bosco Engineering Co., Ltd.
8. Blown film extrusion machine, LE2030/C & LF-250, LabTech Engineering Co., Ltd.
9. Universal testing machine, UTM QC-536M1, Comtech tasting machine Co., Ltd.
10. Thermal conductivity detector, Vici, Valco instrument Co., Inc.
11. Biogas analyzer, Biogas 5000, Entech industrial solution Co., Ltd.
12. Attenuated Total Reflectance Infrared Spectroscope, IRTracer-100, Shimadzu Corp., Ltd.
13. Differential Scanning Calorimeter, DSC 3+ STARe System, Mettler Toledo Co., Ltd.
14. Scanning Electron Microscope, SEM EVO® HD, Carl Zeiss Co., Ltd.
15. Contact angle analyzer, Contact angle OCA 20 model, DataPhysics Instruments Co., Ltd.
16. Melt Flow Index Tester, MF20 CEAST, Instron Co., Ltd.
17. Dynamical mechanical thermal analyzer, DMA 1 model, Mettler Toledo Co., Ltd.
18. Polyester sheets, Victor, Eastern Pioneer Sales and Service Co., Ltd.
19. Teflon sheet, Polytech Industry Co., Ltd.

3.3 Preparation of polymer blend and composites

3.3.1 Preparation of EVA/SiO_2 composites

SiO_2 powder and EVA containing 33 wt% VA (E33) were mixed using an internal mixer machine (D-47055 Duisburg) as shown in Figure 3.1. Each batch, 40 g of the matrix copolymer was filled in the mixing chamber with controlled temperature at 130 °C for 10 min. After the copolymer was completely melted, the desired amount of SiO_2 (0.5, 1.0

and 2.0 wt%) was gradually added in the mixing chamber. Mixing time and rotor speed were set as 30 min and 100 rpm, respectively. After finish mixing, the composites were let to cool at room temperature and grinded to small pieces using a grinder machine. The samples are referred to as E33Sx where x is the amount of SiO_2 loading (wt%).

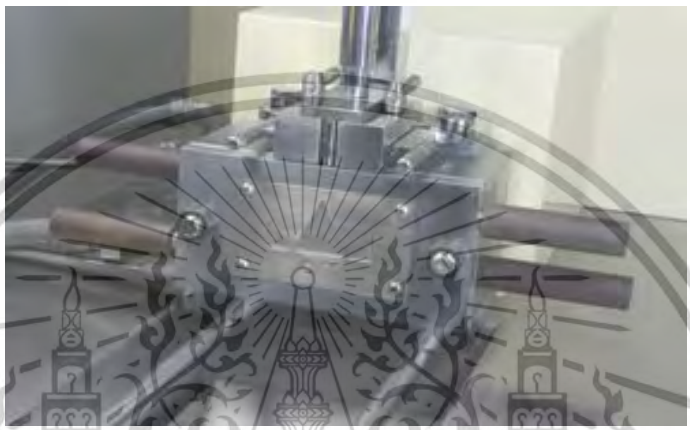

Figure 3.1 Internal mixer machine (D-47055 Duisburg)

3.3.2 Preparation of EVA/SiO_2/PEG composites

To improve the dispersion of SiO_2 within the EVA matrix, a master batch of E18 containing 5 wt% SiO_2 was compounded. The SiO_2 powder was gradually added into molten E18 using an internal mixer (MX500-D75L90) at 180°C with 100 rpm rotor speed for 30 min. Then the master batch was left to cool and then ground using a grinding machine. The obtained samples are referred to as E18S5. For the preparation of EVA blend, EVA/SiO_2, and EVA/SiO_2/PEG, the samples were prepared using an internal mixer under the same conditions as previously described. The weight ratios of the mixing components in each sample were controlled according to Table 3.2. The obtained samples are referred to as E28-18SxPy where E28 is EVA28, E18 is EVA18, x is the amount of SiO_2 loading (wt%) and y is the PEG content (wt%) in the composites.

Table 3.2 Weight ratio of components in the samples

Sample	Weight ratio of mixing components				
	EVA28	EVA18	E18S5	SiO_2	PEG
E28-18	90	10			
E28-18S0.5	90		10		
E28-18S0.75	89.75		10	0.25	
E28-18S1.0	89.5		10	0.50	
E28-18S0.5P0.5	89.5		10		0.5
E28-18S0.5P1.0	89		10		1.0
E28-18S0.5P1.5	88.5		10		1.5

3.3.3 Sample pellet preparation

All grounded compounds, composites or blends were prepared into pellet form using a single-screw extruder machine. Screw speed was set as 15 rpm. The temperature of zone 1 to 5 of the machine were controlled as 170, 170, 175, 175 and 180°C, respectively. The extruded samples were cooled down in the water bath and cut into 3-5 mm pellets using a pelletizing machine.

3.4 Membrane preparation

3.4.1 Thin-flat membrane preparation

Pure polymers (LDPE, E18, E28 and E33) and E33Sx composites were fabricated to a thin membrane using a compression molding machine (Figure 3.2). To control membrane thickness in a range from 40 to 50 μm, weight of each sample was fixed at 0.4 g. The sample was covered with polyester sheets and then placed between two flat steel molding plates. The temperature of the heating plates was set following each polymer type as shown in Table 3.3, while cooling plates were set equally around 12 °C. Before compression, the samples were preheated for 10 min at the desired temperature. Then the samples were compressed in the heating plates for 10 min. After that the samples were cooled for 10 min. Thereafter, the membrane was peeled from the polyester sheets.

Table 3.3 Compression temperature of the polymers

Polymer type	Compression Temperature (°C)
LDPE	210
E18	190
E28	170
E33	170
E33Sx	170

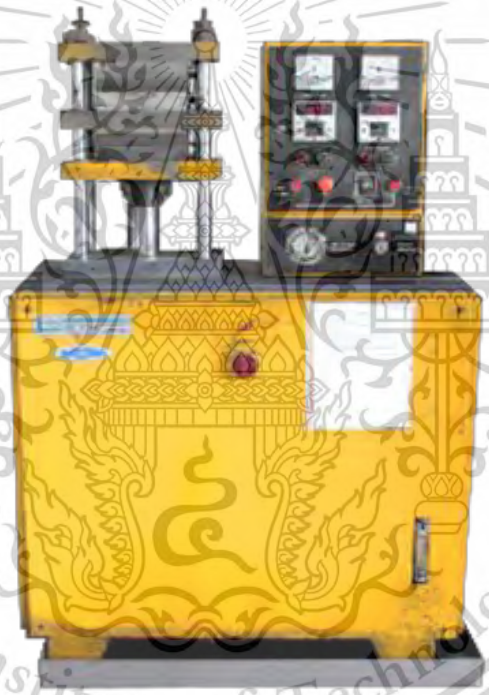

Figure 3.2 Compression molding machine

3.4.2 Thin-tubular membrane preparation

Pure polymers (E18 and E28) and the composites as listed in Table 3.2 were fabricated into thin-tubular membrane using a blown-film extruder machine (Figure 3.5). Screw speed was set as 70 rpm. The temperature of the machine for each zone was controlled as shown in Table 3.4. The nip roller speed was maintained at 2.4 rpm. The

blowing pressure was adjusted to obtain the thin-tubular membrane with a thickness around 60-80 μm.

Table 3.4 Temperature of the blown-film extruder machine

Position	Temperature (°C)
Feed zone	165
Compression zone	170
Metering zone	175
Screw speed	180
Blowing zone upper	180
Blowing zone lower	180

Figure 3.3 Blown-film extruder machine

3.5 Gas permeation of membranes

3.5.1 Gas permeation for a single gas system

Permeability of CO_2 and CH_4 through the membrane was tested using a single gas system as shown in Figure 3.3. A membrane sample (6x6 cm^2 size) with an active surface area of 25 cm^2 was equipped inside the permeation cell (Figure 3.4). At one side of permeation cell, feed gas (CO_2 or CH_4) was fed through the membrane cell with a flow rate of 30 mL/min under the membrane. On the other side, a carrier gas (He) was fed through the membrane cell with a flow rate of 30 mL/min at the top of the membrane (Figure 3.5). This carrier gas brought permeated gas to the thermal conductivity detector (TCD) to measure the amount of permeated gas. Upper and lower pressure of membrane were controlled as equal using a needle valve. Finally, the flux of permeated gas was calculated using the following equation 3.1.

$$Gas\ flux = \frac{(A_s/A_{std})\times F}{A\times 60} \tag{3.1}$$

where the unit of the flux is mL/m^2.s, A_s and A_{std} are peak areas of the sample and calibration gas, respectively, F is the feed gas flow rate (L/min), A is membrane area (m^2). The gas permeation selectivity (CO_2/CH_4) was defined as:

$$Selectivity = \frac{Flux_{CO_2}}{Flux_{CH_4}} \tag{3.2}$$

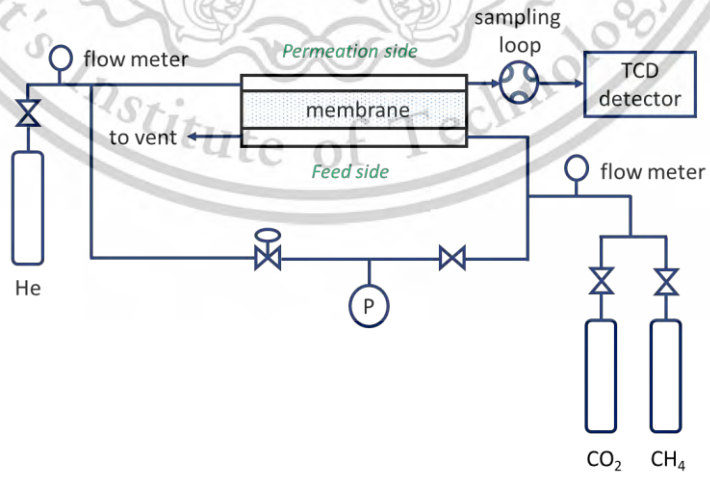

Figure 3.4 Schematic diagram of the gas permeation system

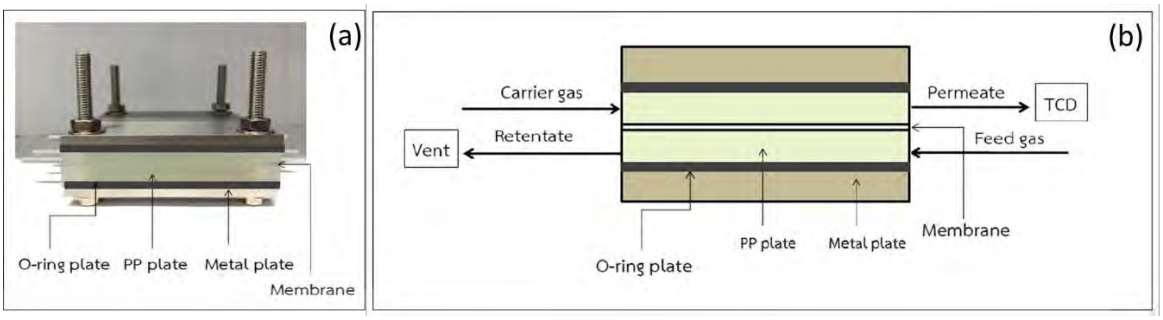

Figure 3.5 (a) Permeation cell and (b) gas flow direction of permeation cell

3.5.2 Gas permeation for mixed gas system

The designed module consists of small plastic fins placing together on the plastic base. Then lay-flat tubular membrane (0.12x5.0 m^2 size) was placed in the slits of the fin along the module length. After that, the membrane was pinned to the plastic fins using a small clothespin as depicted in Figure 3.6. Then the module was connected to the gas scheme separation system (Figure 3.6b). The mixed gas of CO_2/CH_4 (40:60) was fed into the membrane with the desired flow rates (200, 500, and 1000 mL/min). The composition of non-permeated gases and gas flow rate were measured by Biogas 5000 analyzer and bubble flow meter, respectively. The flux of permeated gas and gas selectivity were calculated by the following equations.

$$Flux\ of\ gas = \frac{F_1 - F_2}{A \times 60} \tag{3.3}$$

$$Selectivity = \frac{Flux_{CO_2}}{Flux_{CH_4}} \times \frac{CH_4\ conc.}{CO_2\ conc.} \tag{3.4}$$

where the flux unit is mL/m^2.s, F_1 and F_2 are flow rates of sample in/out the membrane (mL/min), respectively, and A is membrane area (m^2).

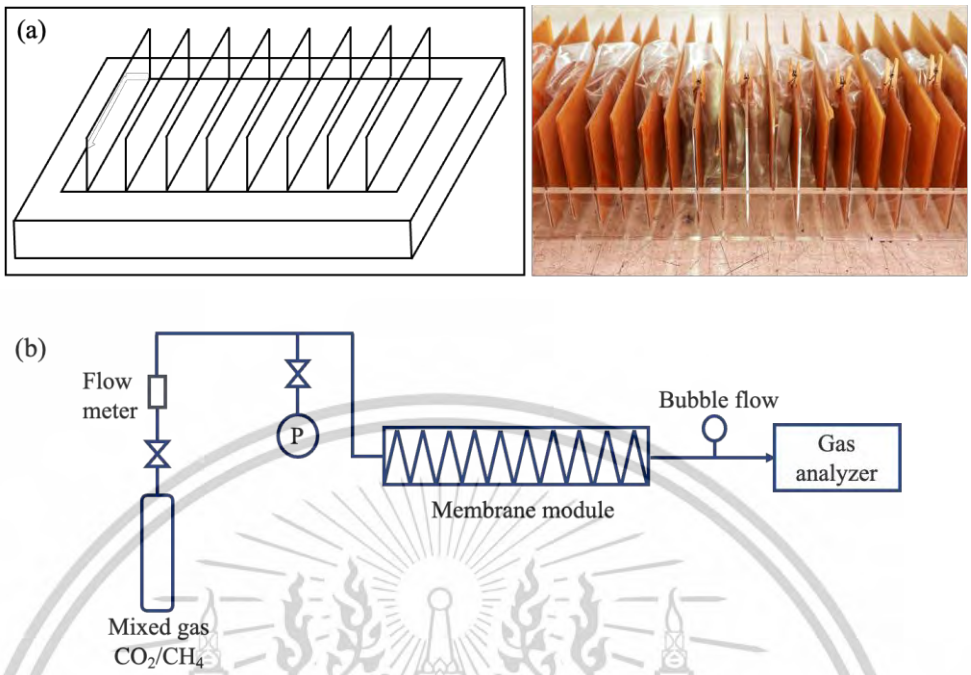

Figure 3.6 (a) Schematic diagram of the in-house tubular membrane module and (b) continuous gas separation process

3.6 Testing and Characterization

3.6.1 Functional group analysis

Functional groups of the membranes were analyzed by attenuated total reflectance infrared spectroscopy (IRTracer-100, Shimadzu). All the spectra were evaluated from 40 scans in the wavenumber range of 4000-650 cm^{-1}.

3.6.2 Thermal analysis

Thermal properties of the membranes were evaluated using differential scanning calorimetry (DSC 3+ STARe System, Mettler Toledo). About 10 mg of a sample was sealed in an aluminum pan and heated from -50 to 150°C at a heating rate of 10°C/min under nitrogen atmosphere.

3.6.3 Tensile testing

The tensile test of the membranes with the dimension of 15x80x0.1 mm^3 was investigated using universal testing machine (UTM model QC-536M1, Comtech) at room

temperature according to ASTM D882-10 [95]. The testing speed and load cell were 100 mm/min and 100 N, respectively. Gauge length was set at 25 mm. Each formula was measured 5 times and reported the average value.

3.6.4 Morphology analysis

Cross-sectional morphology of membranes was observed using scanning electron microscope (SEM model EVO® HD, Carl Zeiss) at accelerating voltage of 10 KV. The specimens with dimensions of 4x1 cm^2 were immersed in liquid nitrogen for 1 h and then cryogenic fractured under liquid N_2 to avoid yielding behavior. The samples were coated with a gold layer using a sputtering coater (108auto, CRESSINGTON) before investigation under SEM.

Specimen preparation

a) thin-flat membrane; the samples were prepared in sheet form using a compression molding machine. To obtain the membrane thickness of 2 mm, the Teflon sheet with thickness of 2 mm was used as a spacer. Compression temperature was controlled at 170°C. The preheating time, heating time and cooling time were set as 10 min.

b) thin-tubular membrane; the sample dimension (1x5 cm^2) was embedded in polyester resin containing 1 wt% methyl ethyl ketone peroxide. Furthermore, the samples were heated at 100°C for 2 h. Then the samples were fractured under liquid N_2.

3.6.5 Wettability testing

The wettability of the membrane was studied using a contact angle analyzer (Contact angle OCA 20, DATAPHYSICS). For thin-flat membrane, the samples were prepared in sheet form using a compression molding machine which the same condition described as in 3.6.4 (a). The samples were prepared by fracturing under liquid N_2. Thereafter, 2 µL of water was dropped on the cross-sectional area of the sample and then contact angle was measured. For thin-tubular membrane, a 2 µL droplet of water was dropped on the membrane surface, and the contact angle was subsequently measured.

3.6.6 Dynamic mechanical thermal analysis

Storage modulus and tan delta (tan δ) of the membrane were examined by a dynamical mechanical thermal analyzer (DMA 1, Mettler Toledo). All samples in thin film form (10x10 mm^2 size) were analyzed in tension mode with 1 Hz of frequency. The analytical temperature was controlled from -80 °C to 50 °C at a heating rate of 3°C/min.

3.6.7 Melt flow index testing

The melt flow index (MFI) of the samples were determined using a melt flow indexer (MF20 CEAST, Instron) according to ASTM D1238. The test was conducted at a temperature of 190 °C under a constant load of 2.16 kg. Approximately 5–7 grams of the samples were loaded into the instrument. The MFI was calculated and expressed in units of grams per 10 minutes (g/10 min).

Chapter 4

Results and Discussion

Part 1: Single gas permeation in the permeation cell

4.1 Chemical and physical properties of thin-flat membrane

4.1.1 Thermal properties of the membrane

Thermal properties of membrane samples were analyzed by a differential scanning calorimeter. The thermogram data with second run of the samples were evaluated for melting temperatures, fusion enthalpy and crystallinity percentage (X_c). The crystallinity percentage of the samples was calculated using the following equation

$$X_c = \frac{\Delta H_f}{\Delta H_f^*} \times 100\% \qquad (4.1)$$

where ΔH_f, and ΔH^*_f are the fusion enthalpy of the sample, and the fusion enthalpy of polyethylene with 100% crystallinity (293 J/g), respectively [96,97]. The results are illustrated in Table 4.1.

Table 4.1 Melting temperature and crystallinity of the membranes

Sample	Membrane	Melting temperature (°C)	Fusion enthalpy (J/g)	X_c (%)
1	LDPE	111	67	23
2	E18	86	49	17
3	E28	74	38	13
4	E33	69	17	6
5	E33S0.5	62	22	8
6	E33S1.0	60	23	8
7	E33S2.0	61	22	8

In this experiment, the LDPE membrane was used as reference for a membrane with containing VA as zero. This membrane provided the highest crystallinity as 23%. Compared to LDPE, the EVA membranes exhibited the lower crystallinity. This is because the acetate side groups on EVA structures hindering the chain packing of the copolymer. Furthermore, the acetate side groups also affected the decrease in melting temperatures (T_m) of EVA copolymer. The acetate side groups disrupted the ordered packing of chains, lowering the energy required in the melting stage [98,99] as shown in Table 4.1. Comparison of EVA membranes with different VA contents, it was observed that crystallinity percentage of EVA decreased with increasing VA content of copolymer. This is because VA unit can disrupt the regular packing of ethylene segments. As the VA content increases, the number of these disruptions increases, leading to less efficient packing and lower crystallinity. In addition, the increase in VA content able to interrupt the formation of ethylene crystalline structure, resulting in lower melting temperatures.

It was observed that adding silica to the E33 copolymer resulted in a slightly increased crystallinity of the composite membrane (from 6% to 8%), while the melting point decreased. This can be explained by the addition of small and rigid silica particles that can slightly induce a rapid crystallization of copolymer [100]. This can be confirmed by a shift to a higher onset crystallization temperature (T_c [onset]) as shown in Figure 4.1.

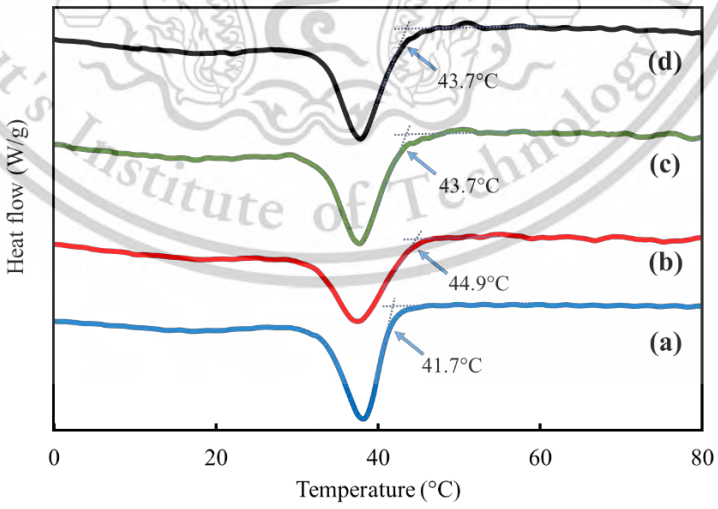

Figure 4.1 Crystallization temperature profiles of (a) E33, (b) E33S0.5, (c) E33S1.0 and (d) E33S2.0

However, the increasing of silica content (ranging from 0.5 to 2.0 wt%) does not influence the crystallinity of the composite membrane. This is because the higher adding of silica leads to a partial agglomeration of the silica particles. Hence, a larger particle size of dispersed phase was observed (confirmed from SEM in Figure 4.2).

4.1.2 Mechanical properties of the membranes

Mechanical properties of the membranes were determined from tensile strength, elongation at break and Young's modulus as shown in Table 4.2. It was found that the tensile strength of the membrane decreased with vinyl acetate content. This can be explained partly by the smaller crystallite size confirmed from the decreasing of the melting temperature (Table 4.1). Moreover, the membrane with a higher fraction of soft segments (18 to 33 wt% vinyl acetate) is more capable of extension. As a result, it provided a greater elongation at break (~900 to 1060%) and a reduction in Young's modulus (from 26 MPa to 3 MPa).

Table 4.2 Mechanical properties of the membranes

Sample	Membrane	Tensile strength (MPa)	Elongation at break (%)	Young's modulus (MPa)
1	LDPE	8.9 (±0.5)	772 (±105)	166.7 (±0.7)
2	E18	8.4 (±0.4)	902 (±37)	26.1 (±1.5)
3	E28	8.2 (±0.6)	992 (±47)	8.7 (±0.6)
4	E33	3.9 (±0.4)	1061 (±17)	3.3 (±0.1)
5	E33S0.5	4.2 (±0.8)	1310 (±102)	3.4 (±0.1)
6	E33S1.0	4.9 (±1.1)	1258 (±45)	3.0 (±0.3)
7	E33S2.0	3.8 (±0.1)	1060 (±23)	3.3 (±0.3)

When adding silica to the EVA copolymer, the tensile strength and Young's modulus of the composite membranes were quite similar, compared to the pure E33. This is because adding small amounts of silica (up to 2 wt%) cannot significantly reinforce the polymer matrix. However, elongation at break improved slightly with small SiO_2 loadings

(0.5 and 1.0 wt%). This improvement is attributed to the dispersion of silica particles (confirmed through SEM/EDS). which promotes rapid crystallization, resulting in a smaller crystallite size, as previously discussed. As a result, the deformation of the EVA matrix in the composite membrane enhances as compared to the parent membrane (E33). When adding more silica (2.0 wt%), elongation at break of the composite membrane dropped. This can be explained by the agglomeration of silica particles (confirmed from SEM/EDS).

4.1.3 Morphology of the membranes

Morphology of the composite membranes at cross-sectional region were determined using scanning electron microscopy. The elemental mapping of silicon element was also evaluated and illustrated in Figure 4.2. It was found that adding small amounts of SiO_2 (0.5 and 1.0 wt%) provided a good dispersion of silica in the EVA matrix (Figure 4.2 (a), (b)). However, the agglomeration of silica particles was observed when increasing SiO_2 loading at 2 wt% as shown in Figure 4.2 (c), (c'). In addition, it was observed that the size of SiO_2 particles is in the range of 2-7 μm.

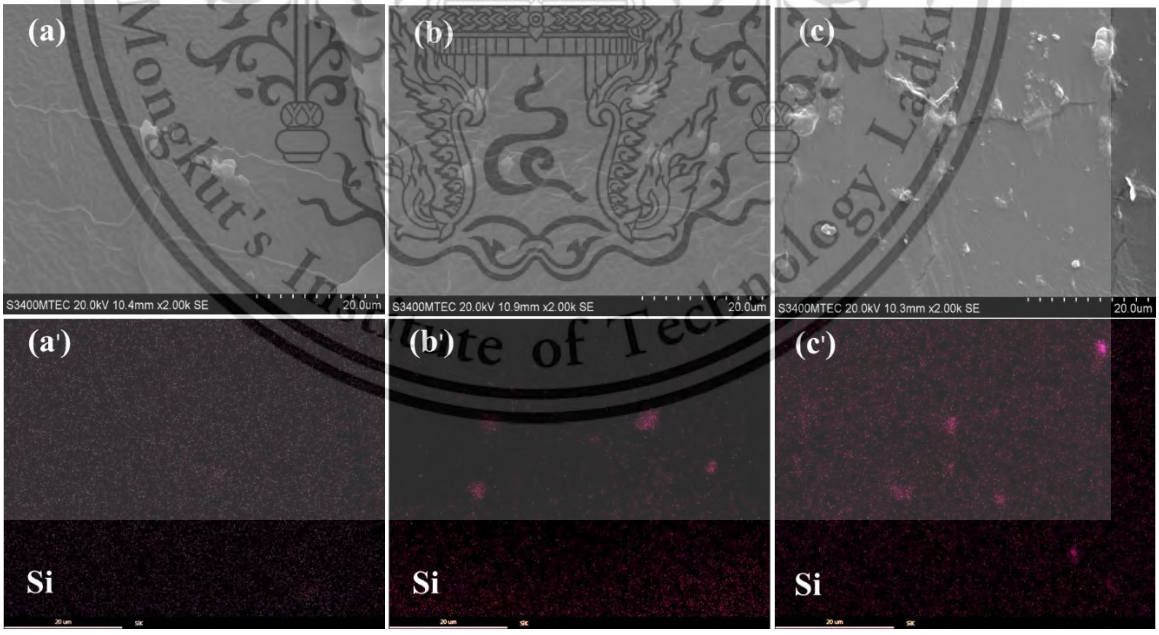

Figure 4.2 Cross-sectional SEM/EDS elemental mapping images of (a, a') E33S0.5, (b, b') E33S1.0 and (c, c') E33S2.0

4.1.4 Functional group of the membranes

Functional group of the membranes were analyzed using attenuated total reflection Fourier transform infrared spectroscopy (ATR-FTIR) technique. The infrared spectra of E18, E28 and E33 membranes are illustrated in Figure 4.3 (a)-(c). The band at 2846 and 2915 cm^{-1} can be attributed to the symmetric and asymmetric stretching of methylene. The bending and stretching of methylene groups are presented at 1460 and 1373 cm^{-1}. The rocking vibration of methylene is shown at 720 cm^{-1}. The band at 1734 cm^{-1} can be assigned to the C=O stretching of carbonyl groups which is a characteristics band of vinyl acetate (VA) in EVA membrane. In addition, the band at 1234 cm^{-1} is assigned for C-O-C stretching and the O-C=O out of plane bending is represented at 1018 cm^{-1} [25,26].

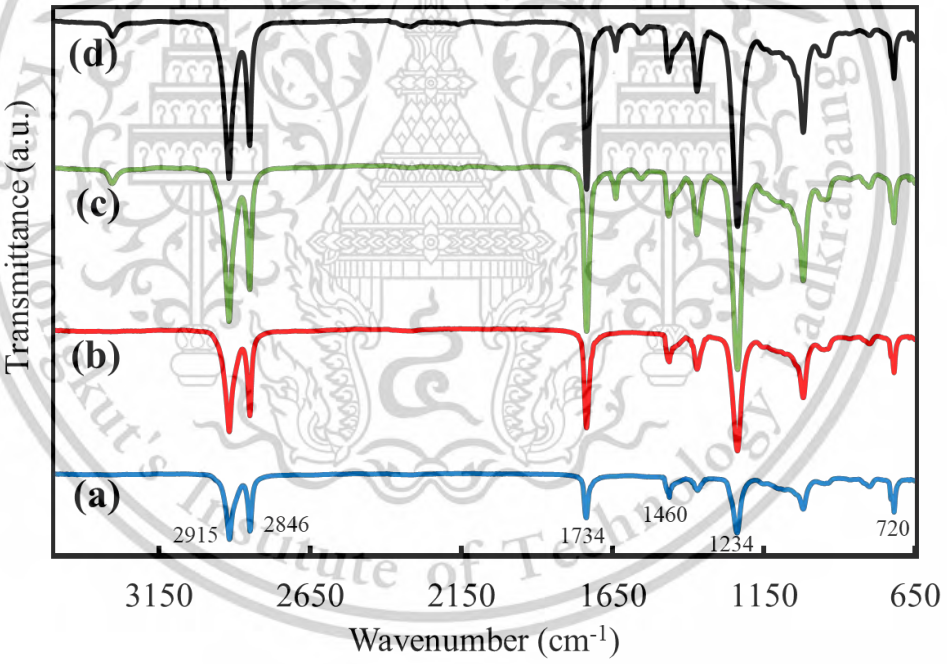

Figure 4.3 FTIR spectra of (a) E18, (b) E28, (c) E33 and (d) E33S2.0

From FTIR spectra, it was found that the intensity of the peak of C=O stretching at 1734 cm^{-1} increased with the increase in vinyl acetate content (Figure 4.3 (a)-(c)). To demonstrate the effect of vinyl acetate content, the carbonyl index (CI) was used to

evaluate. It can be calculated from the ratio of intensities at 1734 cm^{-1} and 1460 cm^{-1} [101-103]. The results showed that the ratio is proportionally enhanced with the vinyl acetate content of the membranes as shown in Figure 4.4. The carbonyl index indicates the number of carbonyl groups in the polymeric chains. Typically, this functional group provides a high polarity. The membrane with higher the carbonyl index, the higher the membrane polarity. Therefore, the sample with high vinyl acetate content such as E33 can interact with some moisture. It can be confirmed from the infrared absorption at 3304 and 1639 cm^{-1}, corresponding to the O-H stretching and O-H bending of H_2O [104-106] as shown in Figure 4.3 (c), (d). On the other hand, none of these bands can be observed for E18 and E28 membranes (Figure 4.3 (a), (b)).

Infrared absorption of composite membrane (E33S2.0) was also analyzed. It was found that the FTIR spectrum of the composite remains unchanged, as compared to that of the E33 copolymer (Figure 4.3 (c), (d)). Furthermore, no characteristic siloxane (Si-O-Si) vibrations were observed in the wavenumber range of 1000-1100 cm^{-1}. This can be suggested that the SiO_2 content is too low (2.0 wt%), its absorption bands cannot be detected. In addition, the infrared spectra of E33S0.5 and E33S1.0 are relatively close to the E33S2.0 membrane (the FTIR of all composite membranes are illustrated in appendix A).

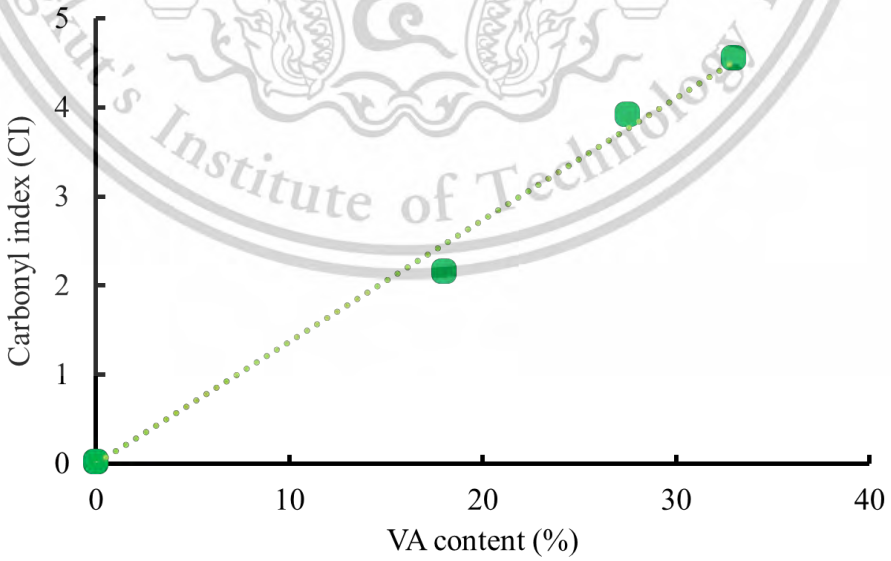

Figure 4.4 Effect of carbonyl index on vinyl acetate content

4.1.5 Wettability test of the membranes

Polarity of the composite membranes were estimated by wettability test. The contact angle of water on the cross-sectional membrane surface was determined using contact angle analyzer. The results were shown in Figure 4.5. It was found that the contact angle decreased with increasing SiO_2 loading (from 0.5 to 2.0 wt%). This result implies that the surface polarity increased. It can be explained by the effect of polar silanol group (Si-OH) on SiO_2 surface. This functional group strongly interacts with polar molecules such as H_2O, CO_2, NH_3, H_2S, etc. The stronger interactions between the water droplet and the composite membrane surface were obtained and hence a reduction in surface tension. This leads to a lower contact angle of the water droplet on the membrane [107]. The increased surface polarity is influenced not only by the VA content but also by the presence of silanol groups on the silica surface. Therefore, the increasing silica content in the membrane exhibited a lower contact angle, resulting in a higher membrane polarity.

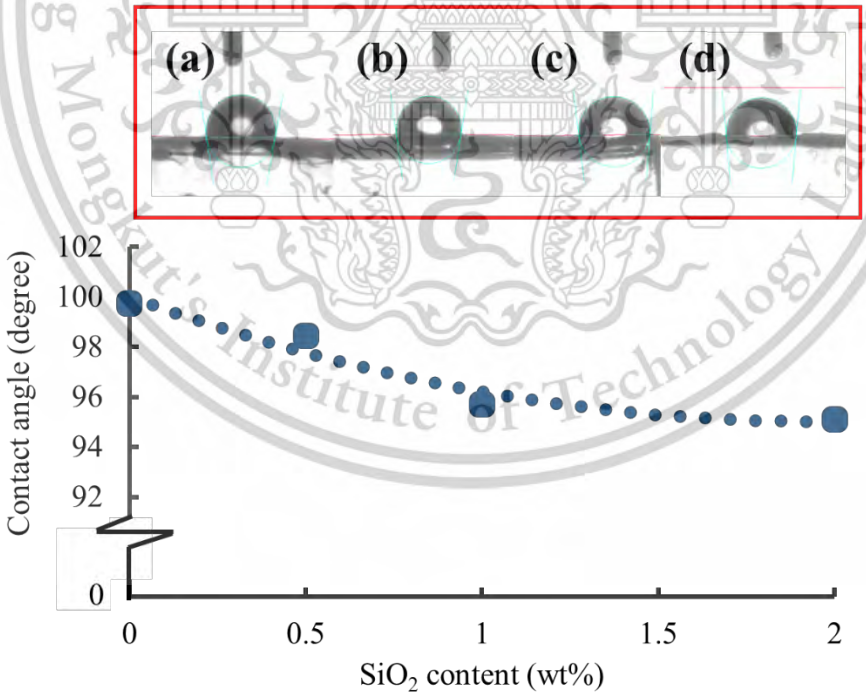

Figure 4.5 Effect of contact angle of composite membranes on silica content. Water droplet images of (a) E33, (b) E33S0.5, (c) E33S1.0 and (d) E33S2.0

4.2 Effect of vinyl acetate content on gas permeability and gas selectivity

Generally, gas molecules are easily diffused through the thinner membrane. Accordingly, the thickness of the membranes should be controlled. It was found that membrane thickness of the pure and composite membranes was in the range from 30 to 40 μm (Appendix I). Gas permeability and gas selectivity (CO_2/CH_4) of EVA membranes with different vinyl acetate contents were tested under single gas permeation system. The LDPE membrane (0 wt% of VA) was used as a control membrane. The results showed that flux of permeated CO_2 significantly increased with vinyl acetate content (Figure 4.6). These results corresponded to the decrease in crystallinity as illustrated in Table 4.1. Typically, gas molecules would not diffuse effectively through the crystalline regions of a polymer. Diffusion primarily occurs through the amorphous regions of a polymer. In addition, the rising permeated CO_2 was related to the increase in the membrane polarity as confirmed from the carbonyl index (Figure 4.4).

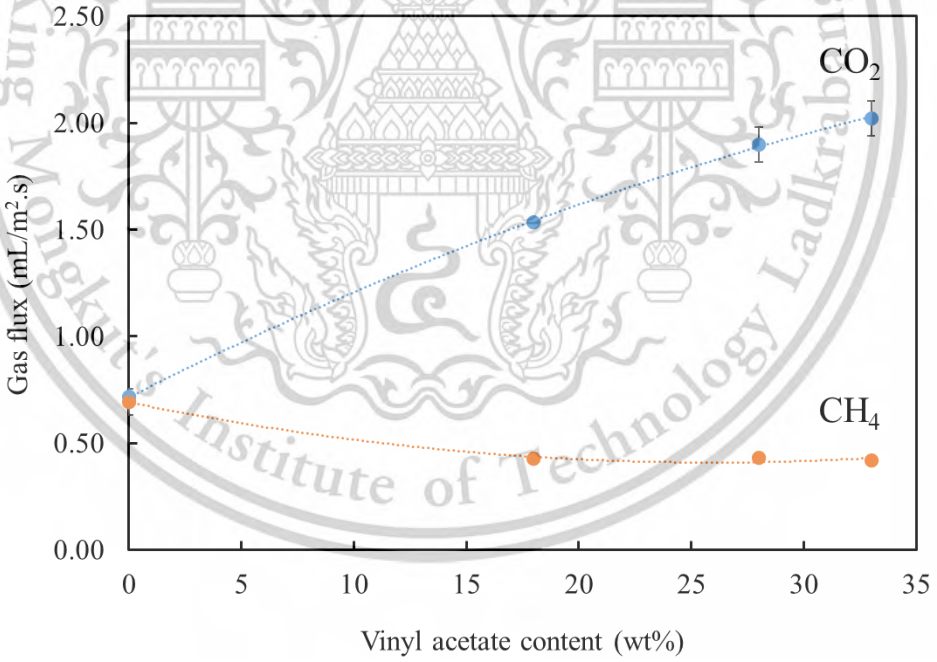

Figure 4.6 Effect of vinyl acetate content on gas flux

The experimental results can be explained by the interaction of the vinyl acetate groups of the copolymer and the CO_2 molecules. The polar carbonyl ester can promote the adsorption of polar CO_2 molecules via dipole-quadrupole interactions. In this process,

the CO_2 molecules favorably adsorb on the membrane surface. Subsequently, the adsorbed molecules diffuse through the membrane's free volume. There is no pressure drop across the membrane because the pressure of feed sides and permeate sides were adjusted equally. Thus, the process is driven by the concentration gradient of gases. Typically, gas diffusion occurs more easily in the amorphous region of the membrane, whereas the crystalline phase acts as a barrier for gas permeation. Accordingly, it can be suggested that a membrane with higher polarity and lower crystallinity (E33) demonstrates greater CO_2 permeability than a membrane with lower VA content.

For CH_4 permeation, it was found that the CH_4 flux slightly decreased for all EVA membranes (E18, E28 and E33) when compared to LDPE membrane. This is due to the difference in polarity of nonpolar CH_4 molecules and EVA membrane. This leads to the decreasing interaction between CH_4 and the membrane surface. Consequently, CH_4 exhibits low solubility in the EVA membrane, which limits its transport across the membrane. However, when considering only EVA membrane (E18, E28 and E33), it was observed that the CH_4 flux remained constant. This can be described by two effects; the increasing VA content of the membrane provided a higher free volume of the membrane facilitating gas diffusion. As VA content increases, it disrupts the ordered packing of ethylene segments, owing to high amorphous phase. Another effect is that nonpolar CH_4 molecules have a low interaction with the EVA membrane. This is because CH_4 is a nonpolar gas, while vinyl acetate groups are polar. The presence of VA moiety of the membrane can suppress the solubility of CH_4 in the polymer. The combination of these two effects results in no significant change in CH_4 flux. According to the above results, it can be suggested that gas permeation selectivity (CO_2/CH_4) was significantly enhanced with the VA content as illustrated in Figure 4.7. This implied that the EVA membrane is highly effective for CO_2/CH_4 separation, owing to its higher polarity and lower crystallinity (refer to Table 4.1 and Figure 4.4).

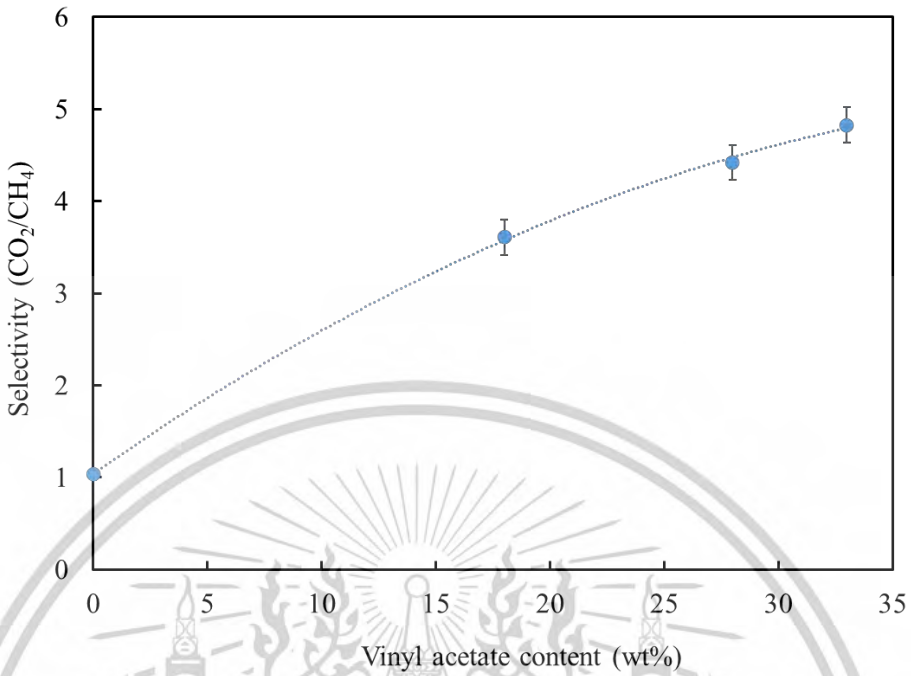

Figure 4.7 Effect of vinyl acetate content on selectivity (CO_2/CH_4)

4.3 Effect of SiO_2 loading on gas permeability and gas selectivity

The SiO_2 additive with different contents (0.5, 1.0 and 2.0 wt%) were incorporated into E33 matrix membrane to improve CO_2/CH_4 selectivity. The composite membranes were investigated for a single gas permeation system. The results of CO_2 and CH_4 permeation flux were demonstrated in Figure 4.8. The results revealed that flux of permeated CO_2 significantly increased with silica content as compared to the E33 membrane. This can be explained by the increased hydrophilicity of the composite membrane corresponding to the decrease in contact angle (Figure 4.5). Generally, the surface of SiO_2 particles is composed of numerous polar silanol (Si-OH) groups. This functional group can interact with polar gases, for example, CO_2, H_2O, and H_2S etc. This leads to an increase in the adsorption of CO_2 through the free volume of the membrane. Accordingly, the CO_2 permeation flux was improved.

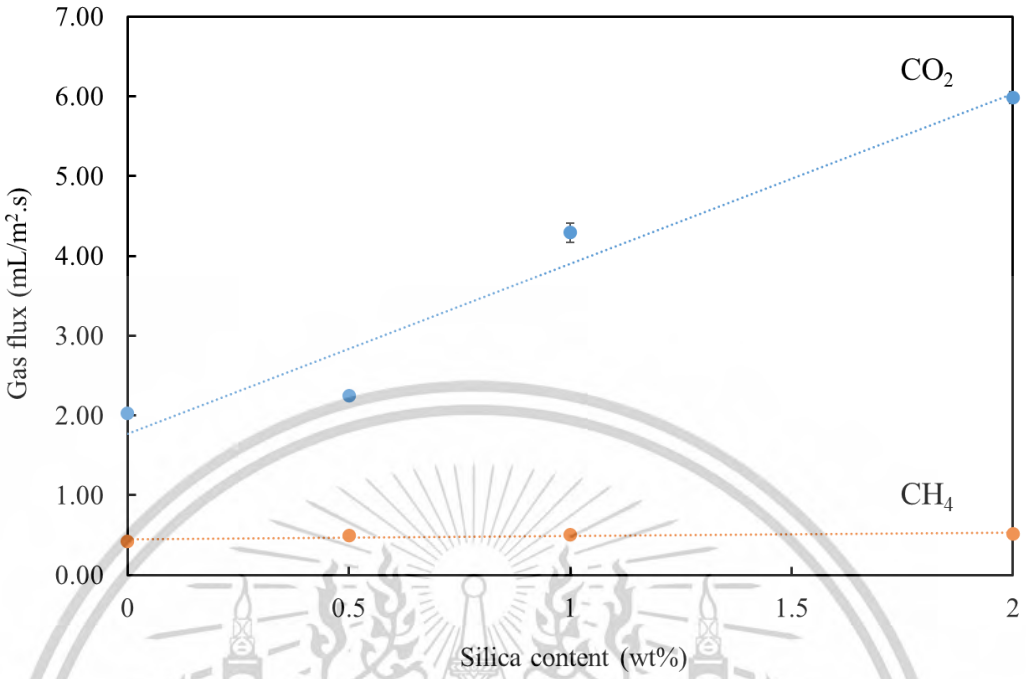

Figure 4.8 Effect of silica content on gas fluxes

From Figure 4.8, It was observed that permeation flux of CH_4 remained unchanged when silica content (from 0.5 to 2.0 wt%) was increased. Generally, CH_4 is a nonpolar gas, whereas SiO_2 is composed of numerous polar silanol groups. Consequently, the interaction between them is weak. In addition, the crystallinity of E33 membrane is insignificant when silica (0.5 to 2.0 wt%) was added (confirmed from DSC). Accordingly, the permeation flux of CH_4 remained unchanged.

CO_2/CH_4 selectivity was calculated from the ratio of CO_2 and CH_4 permeation flux as shown in Figure 4.9. It was indicated that CO_2/CH_4 selectivity increased with the silica content. The E33Si2.0 membrane exhibited CO_2/CH_4 selectivity up to 12, which is higher than the E33 membrane. This enhancement is attributed to the SiO_2 additive, which selectively promoted CO_2 flux, suggesting that the EVA/SiO_2 composite membrane is highly effective for separating CO_2 from CH_4. Therefore, the EVA/SiO_2 composite was selected as a membrane for a continuous mixed-gas separation.

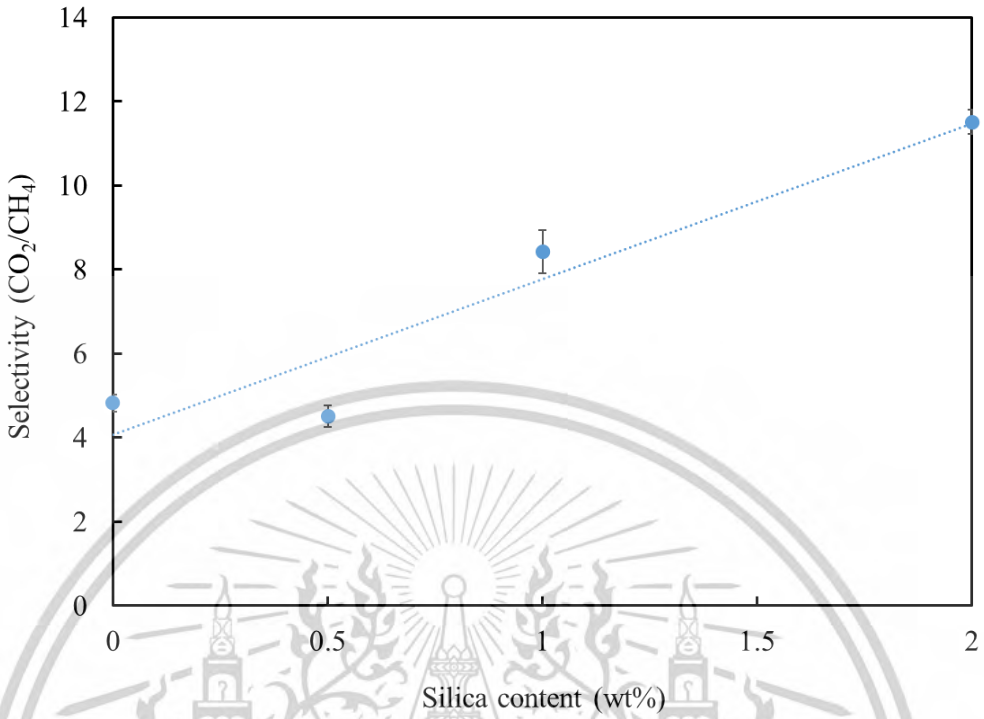

Figure 4.9 Effect of silica content on selectivity (CO_2/CH_4)

Part 2: CO_2/CH_4 separation in the tubular membrane module

The results from the experiment Part I confirm that the EVA copolymer and EVA/SiO_2 composite effectively separated CO_2 and CH_4 through a concentration gradient process. To practically use the membrane in household biogas, the membrane surface area should be enhanced. Accordingly, in this section, the EVA copolymer was shaped into the thin-tubular membrane for separating CO_2/CH_4 from biogas model mixed gases. Although the E33 membrane is effective for CO_2/CH_4 separation, this copolymer is difficult to fabricate into thin-tubular membranes due to its low melt strength. Thus, in this part of the experiment, the thin-tubular membranes of E18, E28 and its composite were tested for gas separation. The width and length of each tubular membrane was controlled as 0.12x5.0 m^2, while the membrane thickness was in the range of 70-80 μm (Appendix I).

4.4 Blending of EVA as matrix membrane

In this section, the E18 and E28 thin-tubular membranes were tested for gases separation under atmospheric pressure. Mixed gases (CO_2/CH_4) with a ratio of 40/60 %V/V were fed to the membrane module at a flow rate of 200 mL/min. The results indicate that the CO_2 permeation of E28 (0.30 mL/m²·s) is greater than that of E18 (0.21 mL/m²·s), as presented in Table 4.3. It can be explained by the higher VA content containing in E28 structure which promoted CO_2 absorption and hence increasing of CO_2 flux. This explanation can be confirmed by the higher peak height of C=O stretching (1737 cm^{-1}) [108] of E28 membrane as compared to E18 membrane (Figure 4.10).

Table 4.3 Gas flux, selectivity and peel strength of membranes

Membrane	CO_2 flux ($mL/m^2.s$)	CH_4 flux ($mL/m^2.s$)	CO_2/CH_4 selectivity	Peel strength (N/m^2)
E28	0.30 (±0.01)	0.20 (±0.02)	2.25 (±0.11)	0.32 (±0.02)
E18	0.21 (±0.01)	0.13 (±0.00)	2.42 (±0.02)	0.17 (±0.02)
E28-18	0.23 (±0.01)	0.12 (±0.01)	2.88 (±0.12)	0.20 (±0.02)

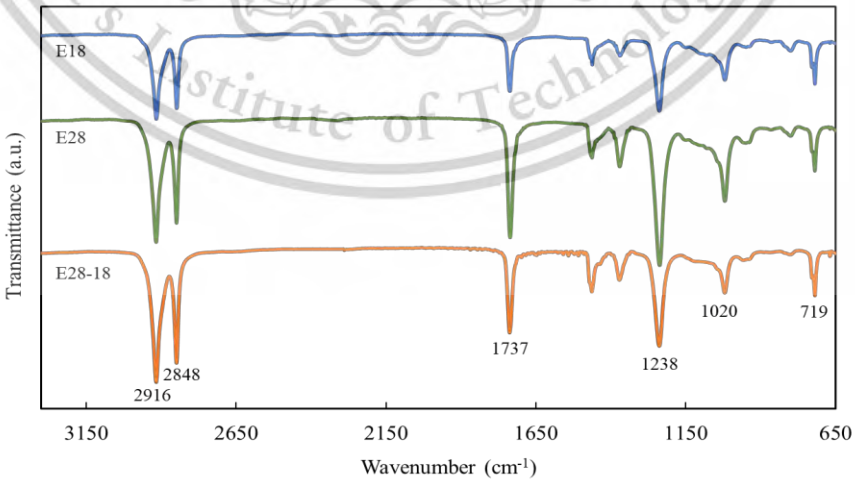

Figure 4.10 FTIR spectra of E18, E28 and E28-18 membranes

However, E28 membrane is difficult to reshape the lay-flat blown into the tubular membrane as compared to E18 membrane, corresponding to the higher membrane polarity, film softness and peel strength of E28 membrane. This leads to an increase in surface interaction, thereby enhancing the stickiness of the E28 film [109]. To enhance E28 film processability while maintaining effective CO_2 permeability, E28 copolymer would be blended with E18 copolymer (10 wt%), referred to as E28-18. The results suggest that the infrared spectrum of the E28-18 retains characteristics like its parent films (E28). In addition, it can be observed that the peel strength of the blend decreases to 0.20 N/m^2 as shown in Table 4.3. This result may facilitate the reshaping of the lay-flat blown E28-18 film into a tubular membrane.

Table 4.4 Thermal and mechanical properties of the E18, E28 and blend E28-18 membranes

Membrane	X_c (%)	T_m (°C)	Stress (max) (MPa)	Elongation at break (%)	Young's modulus (MPa)	MFI (g/10 min)
E28	3	74	6.5 (±1.2)	656 (±78)	14.0 (±0.4)	7.0
E18	17	86	10.8 (±1.9)	863 (±95)	28.2 (±1.1)	2.7
E28-18	6	74	10.4 (±1.7)	1017 (±92)	19.4 (±0.6)	6.8

When considering CO_2 permeation and CO_2/CH_4 selectivity of the blend membrane, it was found that E28-18 membrane provided a lower CO_2 permeation (0.23 mL/m^2.s) as compared to E28 (0.30 mL/m^2.s). However, E28-18 membrane gave a higher CO_2/CH_4 selectivity (~2.9) than E28 (~2.3) and E18 (~2.4). This can be described by the decrease in CH_4 permeation flux of the blend membrane. This is due to the high stiffness properties of the E28-18 membrane, as evidenced by the increased storage modulus as shown in Figure 4.11. Compared to E28 membrane, it was observed that E28-18 membrane exhibited a higher storage modulus throughout the range of testing temperature. In contrast, the storage modulus of the E28-18 membrane is quite close to that of E18

membrane although it contained only 10 wt% of E18 (Figure 4.11). This may be implied from the formation of elongated E18 microstructure in the matrix membrane (E28) [110]. This is because of the difference in viscosity between the two components, with E18 having a higher viscosity (MFI ~2.7) compared to E28 (MFI ~7.0, Table 4.4). Accordingly, the E18 domain was separated from the E28 matrix during the melt mixing step. When applying tensile force in the blown film extrusion process, the E18 domain may well be elongated. This domain serves as a reinforcing microstructure for the E28-18 blend. In addition, it was observed that the MFI of the blend membrane showed a slight reduction as compared to the E28 matrix. This is due to the addition of a small amount of E18.

Melting temperature and crystallinity of pure and blend membranes are presented in Table 4.4. It was observed that melting temperature and crystallinity of the blend remain unchanged as compared to the parent E28. It was indicated that adding small amount of E18 does not interfere with the crystallization behavior of E28. In addition, DSC thermograms of the blend membranes showed two melting peaks at 76 and 100 °C (Appendix B). This may be attributed to EVA and LDPE, respectively. However, the presence of small LDPE melting peak was occurred due to the cleaning of the blown-film extruder.

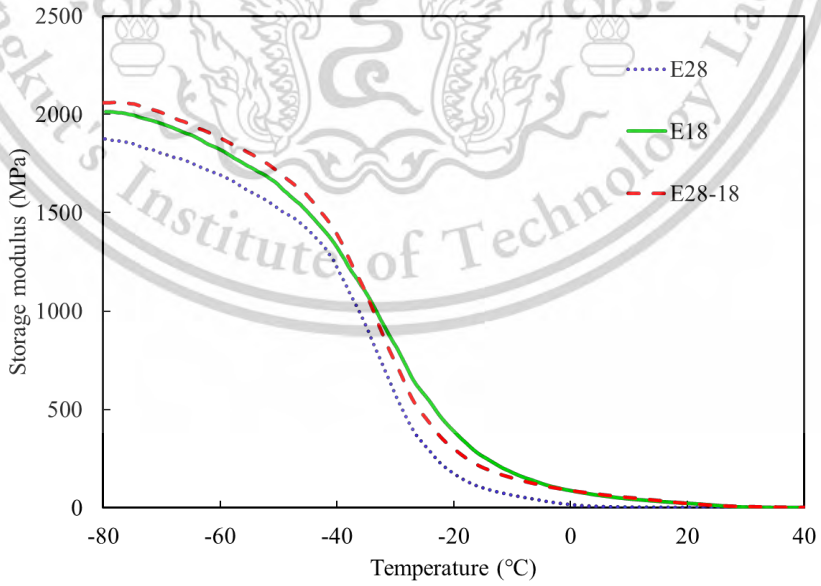

Figure 4.11 Storage modulus of the membranes as a function of temperature

Mechanical properties of the EVA copolymer and the blend EVA membrane were illustrated in Table 4.4. It was observed that the presence of an elongated E18 domain could enhance the mechanical properties of the blend membrane. This can be explained by the strong interaction between the elongated E18 domain and the E28 matrix that facilitates efficient force transfer between them. In addition, the elongated E18 domain served more rigid properties causing to withstand the deformation. This leads to a hindering the molecular motion of the polymer chain in the E28-18 blend. A similar reinforcing effect has been reported experimentally in the blending of syndiotactic polybutadiene with butadiene elastomers [110].

In addition, it was observed that tan delta (δ) of E28-18 exhibits a broad T_g demonstrating the characteristic glass transition temperature of both E28 membrane (Tg ~ -26 °C) and E18 membrane (broad Tg ~ -22 °C), as shown in Figure 4.12. The contribution from the existing components (E28 and E18) indicates that E28-18 is an immiscible blend. It can be confirmed that this membrane possesses an elongated domain (E18) as a dispersed phase in the matrix membrane (E28).

From the reinforcing effect above, mixing only 10 wt% of E18 into E28 matrix can improve a blend membrane with satisfying mechanical properties for further investigation.

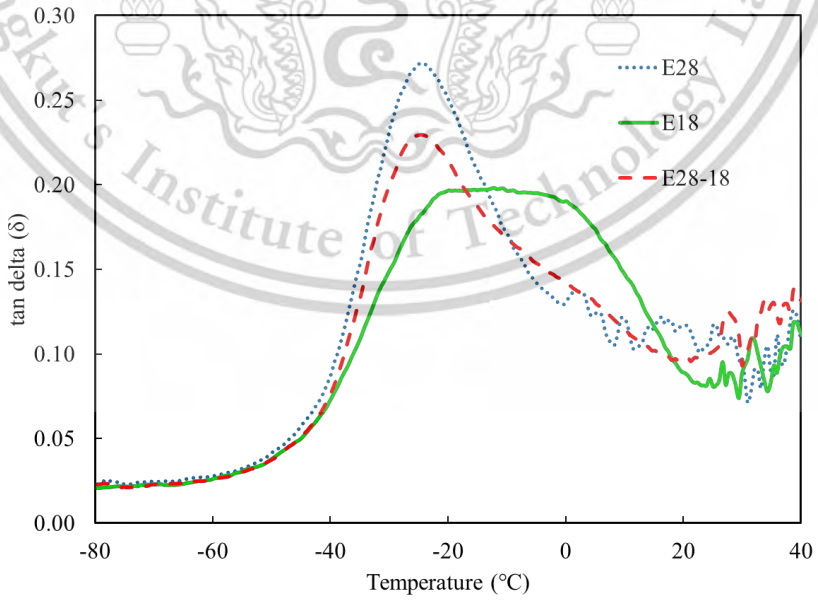

Figure 4.12 Tan Delta (δ) of the membranes as a function of temperature

4.5 Effect of SiO_2 loading on gas separation

Based on the previous study in Part 1, adding SiO_2 to the EVA membrane can enhance both CO_2 permeation flux and CO_2/CH_4 selectivity. Thus, SiO_2 additives (from 0.5 to 1.0 wt%) were added to the E28-18 matrix membrane for separating CO_2/CH_4 from biogas model mixed gases. Permeation flux of CO_2 and CH_4 is shown in Figure 4.13. It was found that the composite membrane with 0.5 wt% SiO_2 (E28-18S0.5) reduced both CO_2 and CH_4 permeation flux, compared to E28-18 membrane. This suggests that the incorporation of a small amount of SiO_2 (0.5 wt%) enhanced the membrane stiffness, thereby hindering the diffusion of CO_2 and CH_4. These results related to the increase in Young's modulus of the E28-18S0.5 membrane, as compared to the E28-18 matrix membrane as illustrated in Table 4.4 and 4.5. In addition, it can be confirmed by a dispersion of SiO_2 particles within the membrane, as evidenced by the SEM/EDS elemental mapping images as shown in Figure 4.14 (a, a', a''). This leads to a stronger interaction between the silanol group of the SiO_2 particles and the acetate groups of the EVA matrix. From SEM/EDS, it was indicated that a small amount of SiO_2 (0.5 wt%) serves as a reinforcing filler for the E28-18 matrix. This can reduce the membrane's free volume and consequently lower total gas permeation.

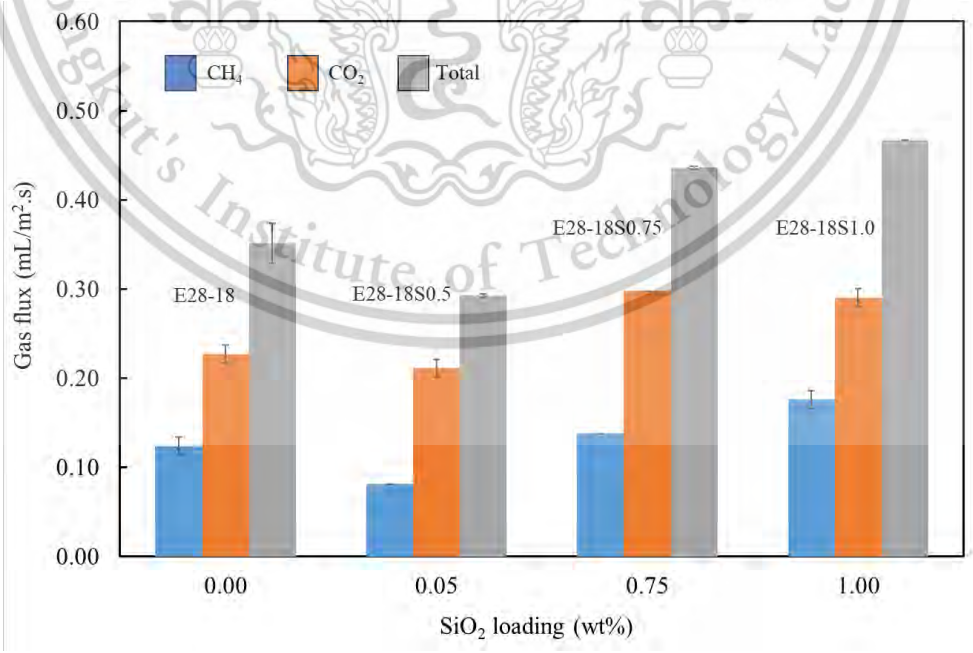

Figure 4.13 CH_4 and CO_2 permeation flux as a function of SiO_2 loading

Table 4.5 Thermal and mechanical properties of the composite membrane modified with SiO_2

Membrane	X_c (%)	T_m (°C)	Stress (max) (MPa)	Elongation at break (%)	Young's modulus (MPa)
E28-18S0.5	7	74	11.7(±1.2)	902(±34)	30.8(±3.4)
E28-18S0.75	7	74	10.1(±1.3)	943(±55)	25.1(±2.1)
E28-18S1.0	7	74	10.6(±0.5)	903(±29)	20.6(±0.9)

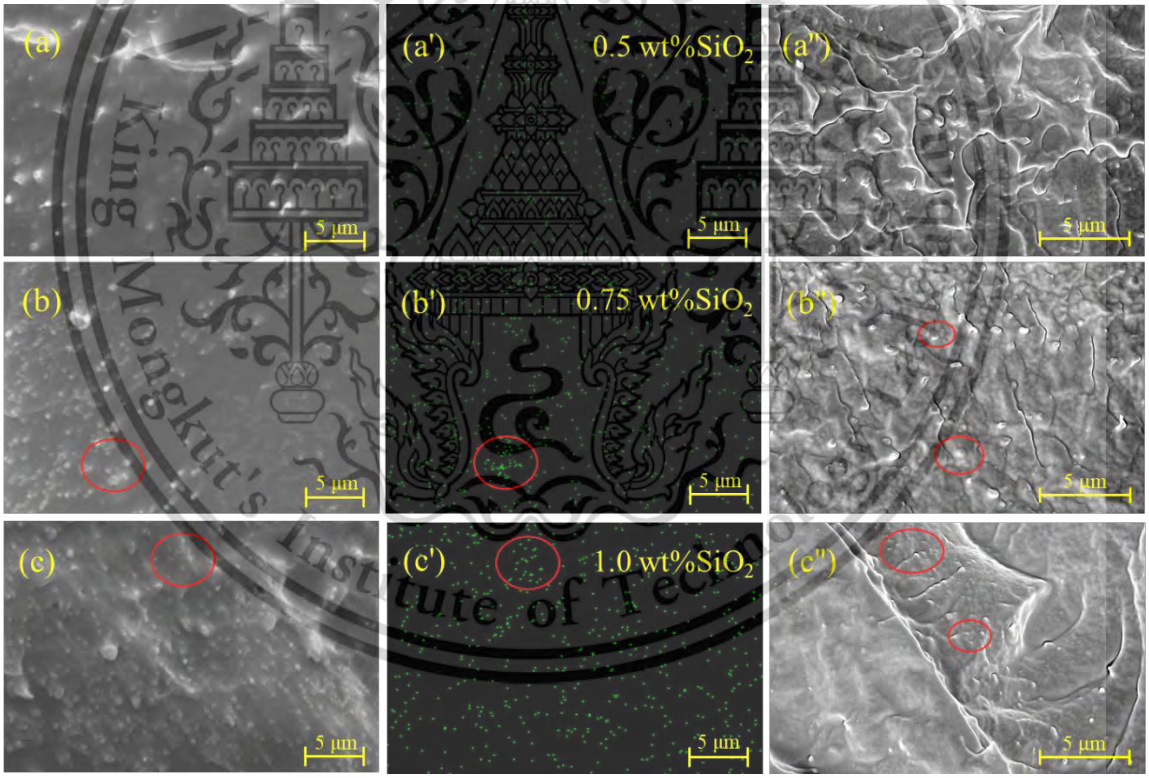

Figure 4.14 Cross-sectional SEM/EDS elemental mapping images of (a, a', a") E28-18S0.5, (b, b', b") E28-18S0.75, and (c, c', c") E28-18S1.0

The lower of both CO_2 and CH_4 permeation flux was observed in E28-18S0.5 membrane. However, the addition of 0.5 wt% SiO_2 enhanced the CO_2/CH_4 selectivity as shown in Figure 4.15. This is due to the enhancement of the membrane's polarity [111,112], as evidenced by the decrease in water contact angle with increasing SiO_2 loading as shown in Figure 4.16. This can be implied to a weak interaction between the composite membrane and CH_4, as non-polar gas. Hence, the CH_4 permeation was reduced. Subsequently, CO_2/CH_4 selectivity increased from ~2.9 to 3.9, compared to E28-18 matrix.

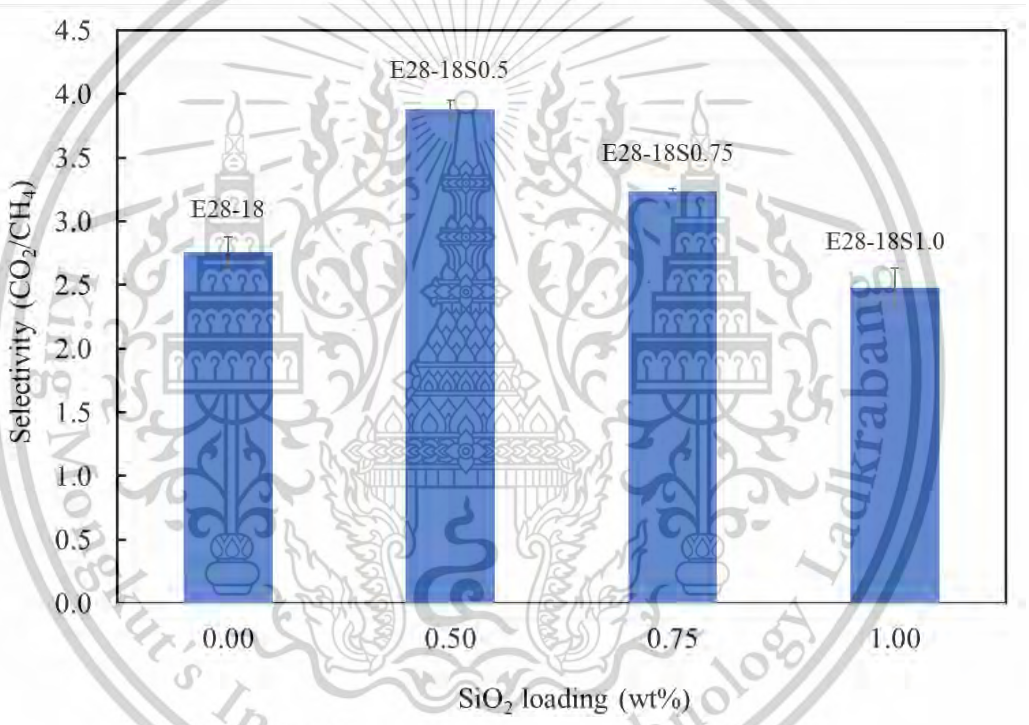

Figure 4.15 CO_2/CH_4 selectivity as a function of SiO_2 loading

When increasing SiO_2 content (0.75 to 1.0 wt%) to the matrix membrane, it was found that both CO_2 and CH_4 permeation flux were increased (Figure 4.13). This suggests that high SiO_2 loadings (0.75 and 1.0 wt%) lead to increased interparticle voids of SiO_2. The partially degraded was observed from SEM images under a high-energy electron beam as shown in Figure 4.14 (a", b", c"). The higher SiO_2 loadings may cause particle agglomeration (indicated by red circles in Figure 4.14). This agglomeration can lead to the formation of interparticle voids in the composite membranes. These voids act as non-selective

pathways for gas molecules, resulting in an increasing the permeation flux of CH_4. As this result, the permeation flux of CH_4, a non-selective gas, significantly increases to 0.14 mL/m²·s (E28-18S0.75) and 0.18 mL/m²·s (E28-18S1.0). Meanwhile, the permeation flux of CO_2 remains constant at ~0.3 mL/m²·s for both E28-18S0.75 and E28-18S1.0, owning to low CO_2/CH_4 selectivity of two composite membranes.

In addition, the higher interparticle void of E28-18S0.75 and E28-18S1.0 membranes resulted in a decreasing maximum stress and Young's modulus, compared to the E28-18S0.5 membrane (Table 4.5). Therefore, the E28-18S0.5 membrane, which exhibits relatively high CO_2/CH_4 selectivity and favorable mechanical properties, was chosen for further experiment.

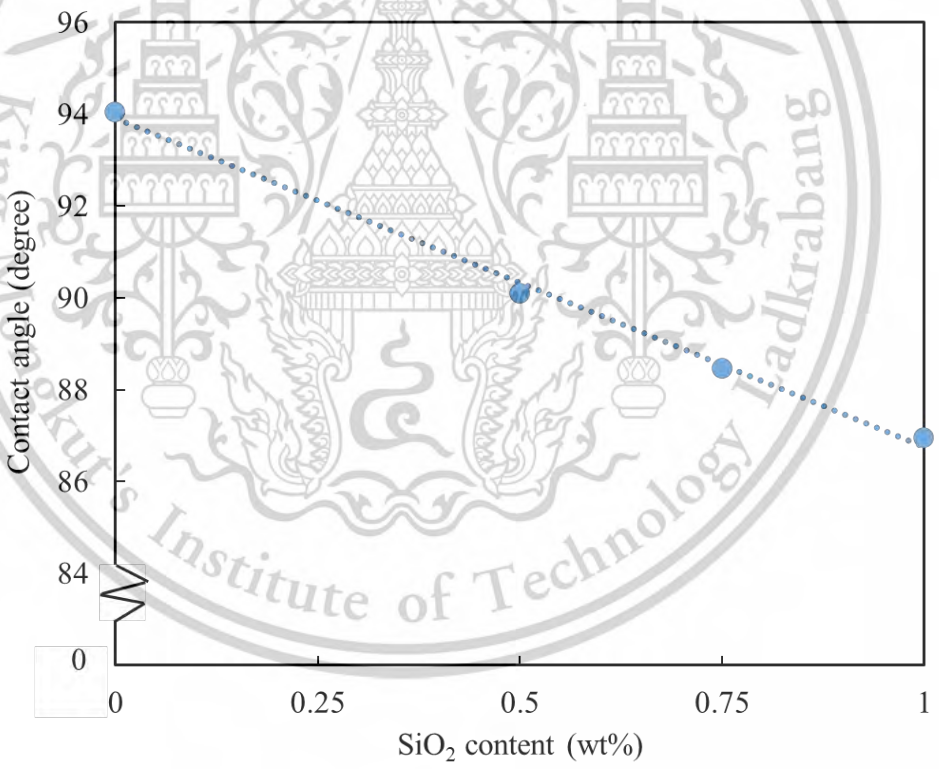

Figure 4.16 Dependence of contact angle on SiO_2 content of composite membranes

4.6 Effect of PEG content on gas separation

Although the E28-18S0.5 membrane exhibited high CO_2/CH_4 selectivity, its CO_2 permeation flux remained low. To improve the CO_2 permeability, the PEG additive was introduced into the composite membrane. Many publications suggested that the polar ether groups of PEG can promote the interaction between the composite membrane and CO_2 molecules [25,82]. The PEG with different ratios (0.5, 1.0 and 1.5 wt%) were mixed with matrix polymer and tested for CO_2/CH_4 separation. The gas permeation flux results were illustrated in Figure 4.17. It was observed that adding PEG additives can improve the CO_2 permeation flux of the E28-18S0.5 membrane.

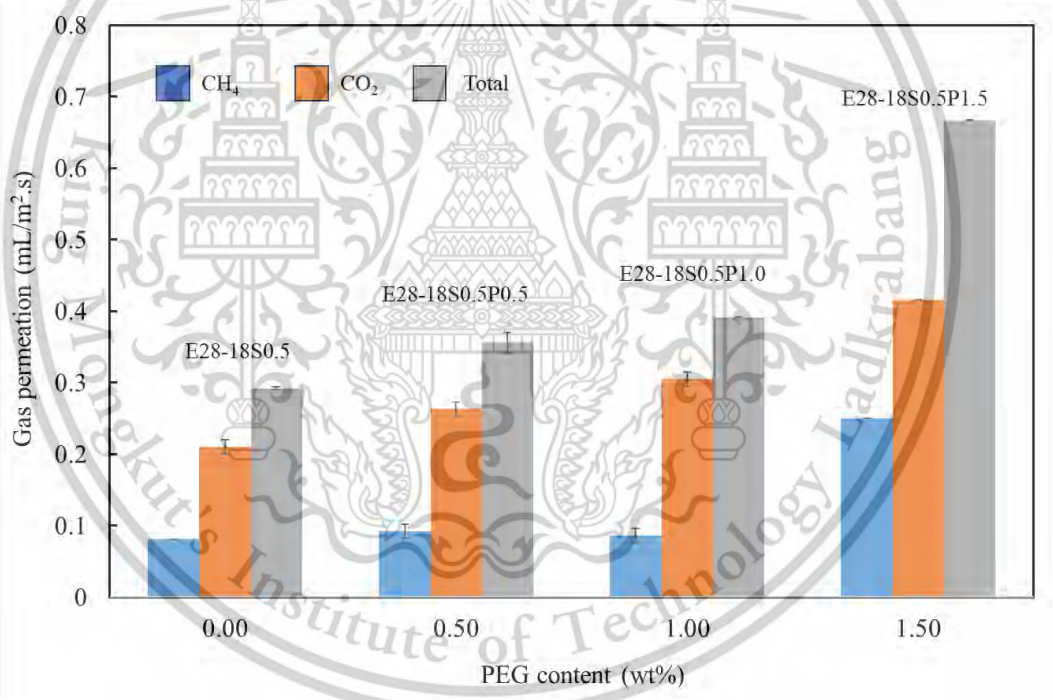

Figure 4.17 CH_4 and CO_2 permeation flux as a function of PEG content

Generally, PEG additive acts as plasticizer, this plasticizer can diffuse into EVA chains, especially in the amorphous region. As a result, the membrane's free volume increases [113,114]. However, its crystallinity remains unchanged (Table 4.5 vs Table 4.6). Accordingly, the polar CO_2 can readily diffuse through the membrane. This is attributed to the increased membrane polarity with high PEG content (from 0.5 to 1.5 wt%). The increased membrane polarity can be estimated by the reduction in water contact angle, as shown in Figure 4.18. It can be observed that the water contact angle of the composite membrane decreases in proportion to the enhancing PEG content (0 to 1.5 wt%) [115]. This is because PEG contains polar functional groups, specifically hydroxyl and ether groups, which strongly interact with water through hydrogen bonding at the membrane/water interface [82]. Consequently, the surface tension of water decreased, resulting in a lower contact angle of the water droplet on the membrane surface.

Table 4.6 Thermal and mechanical properties of the composite membrane modified with PEG

Membrane	X_c (%)	T_m (°C)	Stress (max) (MPa)	Elongation at break (%)	Young's modulus (MPa)
E28-18S0.5P0.5	7	74	11.8(±1.1)	996(±48)	20.1(±1.4)
E28-18S0.5P1.0	8	73	11.2(±1.1)	909(±36)	17.9(±0.7)
E28-18S0.5P1.5	8	72	12.2(±1.9)	839(±50)	16.7(±2.0)

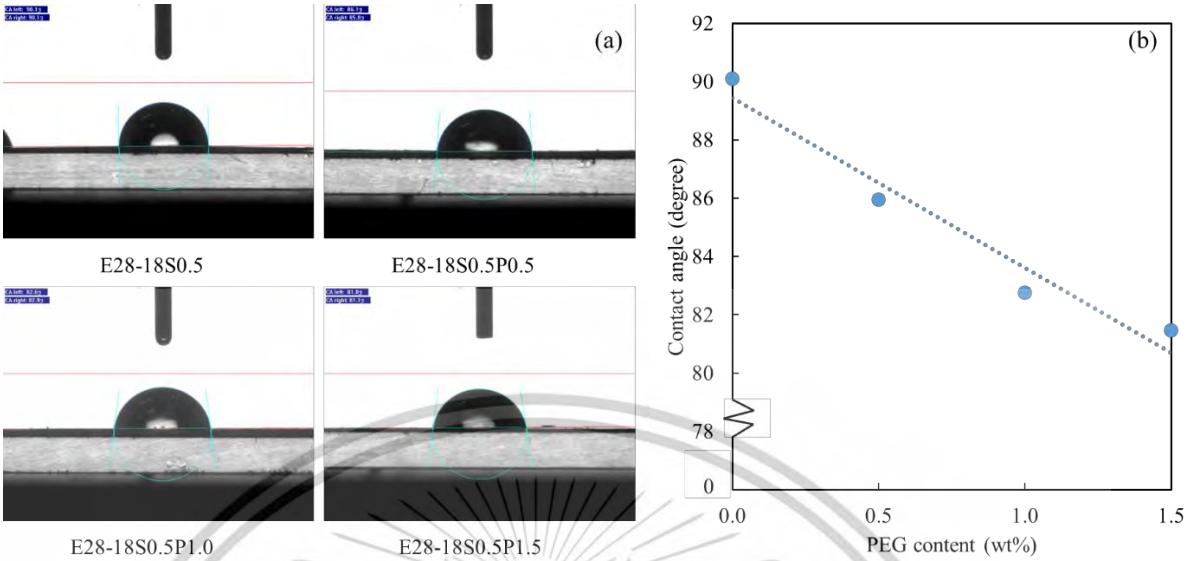

Figure 4.18 (a) Water droplet images of composite membranes and (b) Dependence of PEG content on contact angle of composite membranes

Furthermore, the enhanced polarity of the membrane can be confirmed by ATR-FTIR techniques. It was observed that the intensity of carbonyl group at 1737 cm^{-1} in the composite membranes increased with higher PEG content as shown in Figure 4.19 (a). Although the EVA content in composite membrane remained relatively constant, the incorporation of PEG facilitated interactions between the carbonyl groups and the polar moieties within the matrix. This interaction enhanced the polarization of the carbonyl groups, leading to an increase in the carbonyl index as shown in Figure 4.19 (b). In addition, the absorption of C–O stretching at 1116 cm^{-1}, associated with the ether linkage, dramatically enhances as PEG loading increases [116,117].

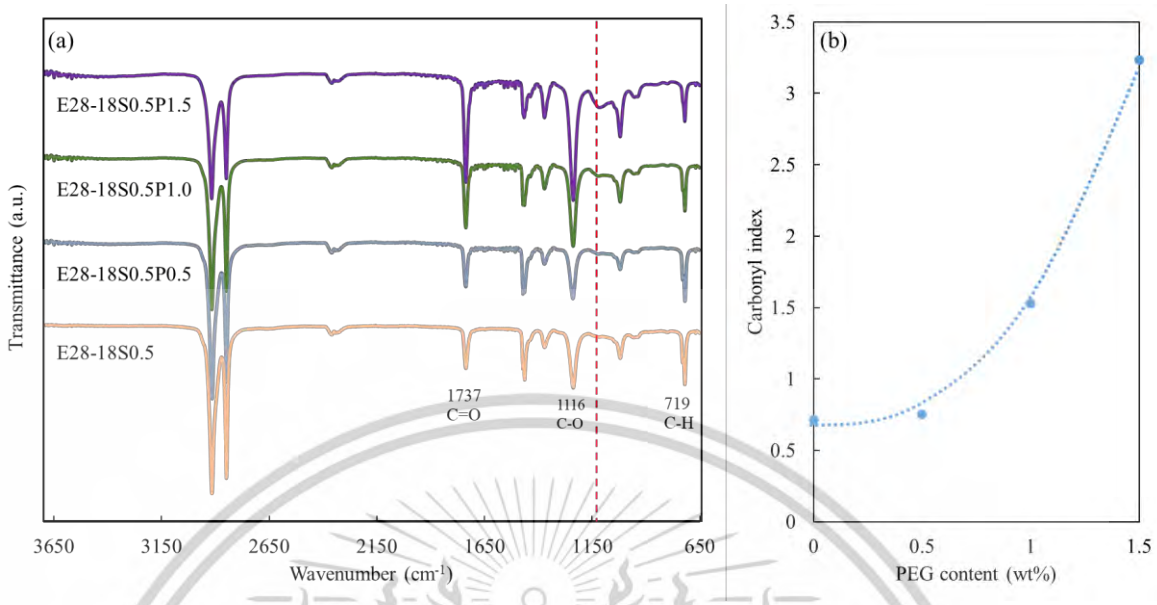

Figure 4.19 (a) FTIR spectra of membranes modified with PEG and (b) Dependence of PEG content on carbonyl index

Compared to CO_2 permeation, the CH_4 permeation flux of the membranes modified with 0.5 wt% and 1.0 wt% PEG (E28-18S0.5P0.5 and E28-18S0.5P1.0) remains similar to that of the unmodified membrane (E28-18S0.5) as illustrated in Figure 4.17. The results revealed that the CH_4 flux is relatively stable, indicating that the incorporation of PEG at these concentrations does not significantly impact CH_4 permeability. This is due to CH_4 being a non-polar molecule that does not interact with the membrane containing PEG. Since the CH_4 permeation flux remained unchanged, the CO_2/CH_4 selectivity increased from approximately 3.9 to 5.3 as the PEG content was raised from 0 to 1.0 wt% (Figure 4.20).

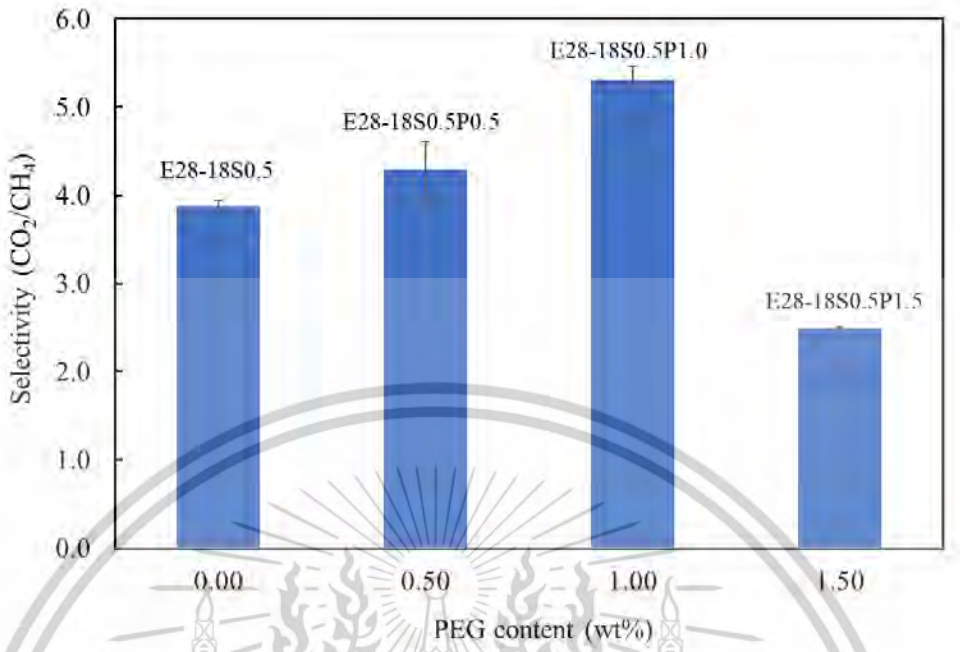

Figure 4.20 CO_2/CH_4 selectivity as a function of PEG content

However, the CH_4 permeation increased significantly when increasing PEG content up to 1.5 wt%. It can be explained by an excessive amount of polar PEG enhances adhesion between SiO_2 particles instead of lubricating the interface of SiO_2 and EVA. Generally, PEG acts as a plasticizer that can reduce shear viscosity of the composite by enhancing polymer chain mobility and decreasing internal friction. This leads to a lower of mixing shear force causing an agglomeration of the SiO_2 particles in the composite membrane as presented from SEM image in Figure 4.21(c). The poor mixing of the composite results in enhanced interfacial voids within the agglomerated SiO_2. These results can be confirmed from the moderate decrease in Young's modulus (rigidity) of this membrane as illustrated in Table 4.6, which is consistent with the findings reported by Sudirman *et al.* [118]. Both CO_2 (polar molecule) and CH_4 (a non-polar molecule) can easily diffuse through the interface of the agglomerated SiO_2 of E28-18S0.5P1.5 membrane. The enrichment of CH_4 permeation of this membrane leads to the decreasing of CO_2/CH_4 selectivity as compared to that of the E28-18S0.5P1.0 membrane. Thus, the E28-

18S0.5P1.0 membrane achieves optimal CO_2/CH_4 selectivity while maintaining permeation stability through the testing times (120 min), as illustrated in Figure 4.22.

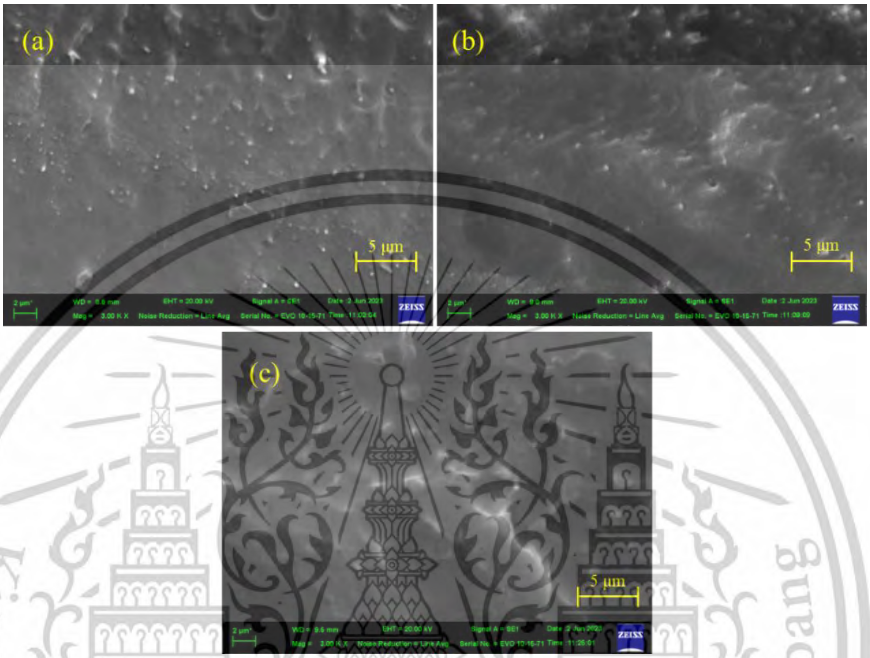

Figure 4.21 Cross-sectional SEM images of (a) E28-18S0.5P0.5, (b) E28-18S0.5P1.0, and (c) E28-18S0.5P1.5

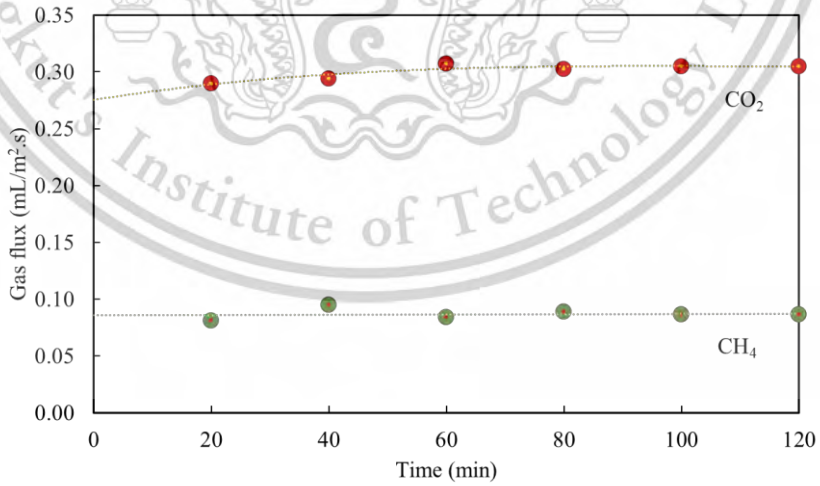

Figure 4.22 CO_2 and CH_4 permeation flux of E28-18S0.5P1.0

From the above results, it was noticed that atmospheric pressure, the permeation flux and CO_2/CH_4 selectivity of this soft membrane would be lower than those of rigid membranes, such as hollow fiber membranes. This can be explained by permeation of gases is driven by concentration gradient. Therefore, gas permeation selectivity is influenced by both interaction and concentration. Whereas the diffusion of gases in rigid membrane is pushed by pressure gradient [30,31]. The gas selectivity primarily depends on the interaction between CO_2 and the membrane. Although the CO_2/CH_4 selectivity and permeation flux obtained in this study are relatively low compared to other works (Table 4.7). However, the separation of CO_2 from CH_4 in this research can be operated under atmospheric pressure. Accordingly, this method would be particularly useful for enhancing the heat value of household biogas by selectively removing CO_2, which increases the methane concentration.

Table 4.7 Comparison of gas permeability and selectivity with other flat sheet membranes

Entry	Membrane	Gas separation system	Pressure difference (cmHg)	CO_2 flux ($mL/min.m^2$)	CO_2 permeability (Barrer)	CO_2/CH_4 selectivity	Ref.
1	Hydrogel chitosan-PEG/PVTMS	Single gas	76	92	153	23	[32]
2	Zeolite/ionic liquid chitosan/PES	Mixed gas	224	1397	779	20	[119]
3	Polylactic acid	Single gas	825	1283	70	285	[120]
4	SiO_2/Pebax®1657	Single gas	300	127	54	19	[121]
5	EVA/SiO_2/PEG	Mixed gas	1.8	18	-	5.3	This work

Chapter 5
Conclusions

5.1 Conclusions

In this study, the effects of vinyl acetate content, silica loading and PEG content of EVA composite membranes on CO_2 and CH_4 permeability and CO_2/CH_4 selectivity were investigated. Increasing vinyl acetate groups to the membrane can enhance polarity of the membrane, leading to a rising interaction with CO_2. Additionally, these polar groups disrupted the crystallization of the EVA copolymer, resulting in higher CO_2 permeation fluxes. The blending E28 matrix with 10 wt% of E18 can improve membrane processibility for shaping a thin-film tubular membrane. In addition, the blend membrane also decreased the CH_4 permeation flux during the gas separation. Adding small amounts of SiO_2 improved mechanical properties of the composite membranes and hindered the CH_4 permeability. This leads to an enhancement of CO_2/CH_4 selectivity. However, the agglomeration of SiO_2 particles in the membranes were observed at higher SiO_2 loading, resulting in a non-selective permeation and hence a lower CO_2/CH_4 selectivity. Mixing PEG into the composite membranes can increase the membrane polarity. This leads to facilitating CO_2 permeation flux and retaining CH_4 diffusion. The E28-18S0.5P1.0 thin-film tubular membrane provided the highest CO_2/CH_4 selectivity as 5.3 for mixed gas separation.

5.2 Suggestions for future works

Future work could explore the long-term stability and performance of the optimized E28-18S0.5P1.0 composite membrane. The membrane gas separation process could be scaled up by integrating multiple membrane modules to improve CH_4 purity. Further investigation of surface modification of various additives can reduce agglomeration of SiO_2 at higher loadings, potentially enhancing CO_2 permeability and CO_2/CH_4 selectivity.

References

1. Statista Research Department. 2024. **Demand for crude oil worldwide from 2005 to 2024, with a forecast for 2025.** [Online]. Available : https://www.statista.com/statistics/271823/global-crude-oil-demand/.
2. Owusu, P.A. and Asumadu-Sarkodie, S. 2016. "A review of renewable energy sources, sustainability issues and climate change mitigation." *Cogent Engineering*. 3 : 1167990.
3. Afridi, Z.U.R. Ullah, K. Mustafa, M.F. Saleem, H. Shaker, B. Ashraf, N. and Aslam, S. 2023. "Biogas as sustainable approach for social uplift in South East Asian Region." *Energy Reports*. 10 : 4808-4818.
4. Jeon, Y.-W. and Lee, D.-H. 2015. "Gas Membranes for CO_2/CH_4 (Biogas) Separation: A Review." *Environmental Engineering Science*. 32 : 71-85.
5. Surendra, K.C. Takara, D. Hashimoto, A.G. and Khanal, S.K. 2014. "Biogas as a sustainable energy source for developing countries: Opportunities and challenges." *Renewable and Sustainable Energy Reviews*. 31 : 846-859.
6. Triviño-Pineda, J.-S. Sanchez-Rodriguez, A. and Peláez, N.P. 2024. "Biogas production from organic solid waste through anaerobic digestion: A meta-analysis." *Case Studies in Chemical and Environmental Engineering*. 9 : 100618.
7. Ni, J.-Q. 2024. "A review of household and industrial anaerobic digestion in Asia: Biogas development and safety incidents." *Renewable and Sustainable Energy Reviews*. 197 : 114371.
8. Tolessa, A. 2024. "Current Status and Future Prospects of Small-Scale Household Biodigesters in Sub-Saharan Africa." *Journal of Energy*. 2024 : 5596028.
9. Yousef, A.M.I. Eldrainy, Y.A. El-Maghlany, W.M. and Attia, A. 2016. "Upgrading biogas by a low-temperature CO_2 removal technique." *Alexandria Engineering Journal*. 55 : 1143-1150.
10. Das, J. Ravishankar, H. and Lens, P.N.L. 2022. "Biological biogas purification: Recent developments, challenges and future prospects." *Journal of Environmental Management*. 304 : 114198.
11. Baena-Moreno, F.M. Rodríguez-Galán, M. Vega, F. Vilches, L.F. and Navarrete, B. 2019. "Review: recent advances in biogas purifying technologies." *International Journal of Green Energy*. 16 : 401-412.

12. Abdeen, F.R.H. Mel, M. Jami, M.S. Ihsan, S.I. and Ismail, A.F. 2016. "A review of chemical absorption of carbon dioxide for biogas upgrading." *Chinese Journal of Chemical Engineering*. 24 : 693-702.
13. Naquash, A. Qyyum, M.A. Haider, J. Bokhari, A. Lim, H. and Lee, M. 2022. "State-of-the-art assessment of cryogenic technologies for biogas upgrading: Energy, economic, and environmental perspectives." *Renewable and Sustainable Energy Reviews*. 154 : 111826.
14. Robeson, L.M. 1999. "Polymer membranes for gas separation." *Current Opinion in Solid State and Materials Science*. 4 : 549-552.
15. Liang, C.Z. Chung, T.-S. and Lai, J.-Y. 2019. "A review of polymeric composite membranes for gas separation and energy production." *Progress in Polymer Science*. 97 : 101141.
16. Ma, C. Wang, M. Wang, Z. Gao, M. and Wang, J. 2020. "Recent progress on thin film composite membranes for CO_2 separation." *Journal of CO_2 Utilization*. 42 : 101296.
17. Oh, H.J. and Phillip, W.A. 2024. "Polymer Physics of Separation Membranes." *Macromolecules*. 57 : 9489-9497.
18. Raveendran, P. Ikushima, Y. and Wallen, S.L. 2005. "Polar Attributes of Supercritical Carbon Dioxide." *Accounts of Chemical Research*. 38 : 478-485.
19. Mohamad, M.B. Fong, Y.Y. and Shariff, A. 2016. "Gas Separation of Carbon Dioxide from Methane Using Polysulfone Membrane Incorporated with Zeolite-T." *Procedia Engineering*. 148 : 621-629.
20. Şen, D. Kalıpçılar, H. and Yilmaz, L. 2007. "Development of polycarbonate based zeolite 4A filled mixed matrix gas separation membranes." *Journal of Membrane Science*. 303 : 194-203.
21. Sridhar, S. Veerapur, R.S. Patil, M.B. Gudasi, K.B. and Aminabhavi, T.M. 2007. "Matrimid polyimide membranes for the separation of carbon dioxide from methane." *Journal of Applied Polymer Science*. 106 : 1585-1594.
22. Raza, A. Farrukh, S. Hussain, A. Khan, I. Othman, M.H. and Ahsan, M. 2021. "Performance Analysis of Blended Membranes of Cellulose Acetate with Variable Degree of Acetylation for CO_2/CH_4 Separation." *Membranes*. 11 : 245.
23. Shen, Y. Wang, H. Liu, J. and Zhang, Y. 2015. "Enhanced Performance of a Novel Polyvinyl Amine/Chitosan/Graphene Oxide Mixed Matrix Membrane for CO_2 Capture." *ACS Sustainable Chemistry & Engineering*. 3 : 1819-1829.

24. Wolinska-Grabczyk, A. Kubica, P. and Jankowski, A. 2013. “Effect of the acetate group content on gas permeation through membranes based on poly(ethylene-co-vinyl acetate) and its blends.” *Journal of Membrane Science*. 443 : 227-236.
25. Zamiri, M.A. Kargari, A. and Sanaeepur, H. 2015. “Ethylene vinyl acetate/poly(ethylene glycol) blend membranes for CO_2/N_2 separation.” *Greenhouse Gases: Science and Technology*. 5 : 668-681.
26. Mousavi, S.A. Sadeghi, M. Motamed-Hashemi, M.M.Y. Pourafshari Chenar, M. Roosta-Azad, R. and Sadeghi, M. 2008. “Study of gas separation properties of ethylene vinyl acetate (EVA) copolymer membranes prepared via phase inversion method.” *Separation and Purification Technology*. 62 : 642-647.
27. Sadeghi, M. Khanbabaei, G. Dehaghani, A.H.S. Sadeghi, M. Aravand, M.A. Akbarzade, M. and Khatti, S. 2008. “Gas permeation properties of ethylene vinyl acetate–silica nanocomposite membranes.” *Journal of Membrane Science*. 322 : 423-428.
28. Seong, M.S. Kong, C.I. Park, B.R. Lee, Y. Na, B.K. and Kim, J.H. 2020. “Optimization of pilot-scale 3-stage membrane process using asymmetric polysulfone hollow fiber membranes for production of high-purity CH_4 and CO_2 from crude biogas.” *Chemical Engineering Journal*. 384 : 123342.
29. Esposito, E. Clarizia, G. Bernardo, P. Jansen, J.C. Sedláková, Z. Izák, P. Curcio, S. Cindio, B.d. and Tasselli, F. 2015. “Pebax®/PAN hollow fiber membranes for CO_2/CH_4 separation.” *Chemical Engineering and Processing - Process Intensification*. 94 : 53-61.
30. Jeon, Y.-W. and Shin, M.-S. 2017. “Separation of biogas using newly prepared cellulose acetate hollow fiber membranes.” *Energy Procedia*. 136 : 219-224.
31. Karousos, D.S. Lei, L. Lindbråthen, A. Sapalidis, A.A. Kouvelos, E.P. He, X. and Favvas, E.P. 2020. “Cellulose-based carbon hollow fiber membranes for high-pressure mixed gas separations of CO_2/CH_4 and CO_2/N_2.” *Separation and Purification Technology*. 253 : 117473.
32. Kunalan, S. Palanivelu, K. Sachin, E.K. Syrtsova, D.A. and Teplyakov, V.V. 2022. “Thin-film hydrogel polymer layered polyvinyltrimethylsilane dual-layer flat-bed composite membrane for CO gas separation.” *Journal of Applied Polymer Science*. 139 : 52024.

33. Zhou, Y. Jia, M. Zhang, X. and Yao, J. 2020. “Etched ZIF-8 as a Filler in Mixed-Matrix Membranes for Enhanced CO_2/N_2 Separation.” *Chemistry – A European Journal*. 26 : 7918-7922.

34. Green, M. 2023. **About Peak Oil Demand.** [Online]. Available : https://www.api.org/news-policy-and-issues/blog/2023/06/21/about-peak-oil-demand.

35. International Energy Agency. 2024. **Growth in demand in 2024 and 2025 is forecast to be among the highest levels in the past two decades.** [Online]. Available : https://www.google.com/search?q=IEA+is&rlz=1C1GCEU_thTH1161TH1161&oq=IEA+is&gs_lcrp=EgZjaHJvbWUyBggAEEUYOTIGCAEQRRg8MgYIAhBFGDzSAQgyMzUwajBqN6gCALACAA&sourceid=chrome&ie=UTF-8.

36. Panwar, N.L. Kaushik, S.C. and Kothari, S. 2011. “Role of renewable energy sources in environmental protection: A review.” *Renewable and Sustainable Energy Reviews*. 15 : 1513-1524.

37. Kabeyi, M.J.B. and Olanrewaju, O.A. 2022. “Biogas Production and Applications in the Sustainable Energy Transition.” *Journal of Energy*. 2022 : 8750221.

38. Khanal, S.K. 2008. **Anaerobic Biotechnology for Bioenergy Production: Principles and Applications Book.** New York : John Wiley & Sons.

39. Braun, R. 2007. **In Improvement of Crop Plants for Industrial End Uses Book.** Dordrecht : Springer.

40. Czekała, W. Nowak, M. and Bojarski, W. 2023. “Characteristics of Substrates Used for Biogas Production in Terms of Water Content.” *Fermentation*. 9050449.

41. Aguilloso, G. Arpia, K. Khan, M. Sapico, Z.A. and Lopez, E.C. 2024. “Recent Advances in Membrane Technologies for Biogas Upgrading.” *Engineering Proceedings*. 2024067057.

42. Ullah Khan, I. Hafiz Dzarfan Othman, M. Hashim, H. Matsuura, T. Ismail, A.F. Rezaei-DashtArzhandi, M. and Wan Azelee, I. 2017. “Biogas as a renewable energy fuel-A review of biogas upgrading, utilisation and storage.” *Energy Conversion and Management*. 150 : 277-294.

43. Chen, X.Y. Vinh-Thang, H. Ramirez, A.A. Rodrigue, D. and Kaliaguine, S. 2015. “Membrane gas separation technologies for biogas upgrading.” *RSC Advances*. 5 : 24399-24448.

44. Karali, D. Peloriadi, K. Margaritis, N. and Grammelis, P. 2023. "CO_2 Absorption Using Potassium Carbonate as Solvent." *Engineering Proceedings*. 10.3390/ASEC2022-13824.

45. Grande, C.A. 2012. "Advances in Pressure Swing Adsorption for Gas Separation." *International Scholarly Research Notices*. 2012 : 982934.

46. Fahim, I.S. Mamdouh, W. and Salem, H.G. 2015. "Chitosan nanocomposite mesoporous membranes: mechanical and barrier properties as a function of temperature." *Journal of Materials Science Research*. 4 : 1.

47. Lins, L.P. Martinez, D.G. Furtado, A.C. and Padilha, J.C. 2023. "Biomethane generation and CO_2 recovery through biogas production using brewers' spent Grains." *Biocatalysis and Agricultural Biotechnology*. 48 : 102579.

48. Font-Palma, C. Cann, D. and Udemu, C. 2021. "Review of Cryogenic Carbon Capture Innovations and Their Potential Applications." *C*. 10.3390/c7030058

49. Erdöl, H.B. Şahin, F.İ. and Acaralı, N. 2024. "Novel Study on Cryogenic Distillation Process and Application by Using CHEMCAD Simulation." *ACS Omega*. 9 : 15165-15174.

50. Hunger, K. Schmeling, N. Jeazet, H.B.T. Janiak, C. Staudt, C. and Kleinermanns, K. 2012. "Investigation of Cross-Linked and Additive Containing Polymer Materials for Membranes with Improved Performance in Pervaporation and Gas Separation." *Membranes*. 2040727.

51. Freeman, B.D. 1999. "Basis of Permeability/Selectivity Tradeoff Relations in Polymeric Gas Separation Membranes." *Macromolecules*. 32 : 375-380.

52. Zalc, J.M. Reyes, S.C. and Iglesia, E. 2004. "The effects of diffusion mechanism and void structure on transport rates and tortuosity factors in complex porous structures." *Chemical Engineering Science*. 59 : 2947-2960.

53. Lova, P. Manfredi, G. and Comoretto, D. 2018. "Advances in Functional Solution Processed Planar 1D Photonic Crystals." *Advanced Optical Materials*. 6 : 1800730.

54. Mohsenpour Tehrani, M. and Chehrazi, E. 2024. "Metal–Organic-Frameworks Based Mixed-Matrix Membranes for CO_2 Separation: An Applicable-Conceptual Approach." *ACS Applied Materials & Interfaces*. 16 : 32906-32929.

55. Baker, R.W. and Lokhandwala, K. 2008. "Natural Gas Processing with Membranes: An Overview." *Industrial & Engineering Chemistry Research*. 47 : 2109-2121.

56. Ahmadizadegan, H. 2020. “Polyester/SiO_2 Nanocomposites: Gas Permeation, Mechanical, Thermal and Morphological Study of Membranes.” *Iranian Journal of Chemistry and Chemical Engineering*. 39 : 33-47.

57. Kim, S. and Lee, Y.M. 2013. “High performance polymer membranes for CO_2 separation.” *Current Opinion in Chemical Engineering*. 2 : 238-244.

58. Siracusa, V. 2012. “Food Packaging Permeability Behaviour: A Report.” *International Journal of Polymer Science*. 2012 : 302029.

59. Bernardo, P. Drioli, E. and Golemme, G. 2009. “Membrane Gas Separation: A Review/State of the Art.” *Industrial & Engineering Chemistry Research*. 48 : 4638-4663.

60. Zhao, H.-Y. Cao, Y.-M. Ding, X.-L. Zhou, M.-Q. Liu, J.-H. and Yuan, Q. 2008. “Poly(ethylene oxide) induced cross-linking modification of Matrimid membranes for selective separation of CO_2.” *Journal of Membrane Science*. 320 : 179-184.

61. Sanchez, J. Charmette, C. and Gramain, P. 2002. “Poly(ethylene oxide-co-epichlorohydrin) membranes for carbon dioxide separation.” *Journal of Membrane Science*. 205 : 259-263.

62. Bondar, V.I. Freeman, B.D. and Pinnau, I. 2000. “Gas transport properties of poly(ether-b-amide) segmented block copolymers.” *Journal of Polymer Science Part B: Polymer Physics*. 38 : 2051-2062.

63. Kim, T.-J. Li, B. and Hägg, M.-B. 2004. “Novel fixed-site–carrier polyvinylamine membrane for carbon dioxide capture.” *Journal of Polymer Science Part B: Polymer Physics*. 42 : 4326-4336.

64. Thornton, A.W. Nairn, K.M. Hill, A.J. and Hill, J.M. 2009. “New relation between diffusion and free volume: I. Predicting gas diffusion.” *Journal of Membrane Science*. 338 : 29-37.

65. Iarikov, D.D. and Ted Oyama, S. 2011. **Membrane Science and Technology.** Amsterdam : Elsevier B.V.

66. Aasadi, H. Alizadeh, O. Ramazani, A. and Dorosti, F. 2022. “A review on the effects of fillers on gas separation Mixed Matrix Membranes.” *Iranian Journal of Chemical Engineering*. 19 : 3-28.

67. Azizi, N. Isanejad, M. Mohammadi, T. and Behbahani, R.M. 2019. “Effect of TiO_2 loading on the morphology and CO_2/CH_4 separation performance of PEBAX-based membranes.” *Frontiers of Chemical Science and Engineering*. 13 : 517-530.

68. Vinoba, M. Bhagiyalakshmi, M. Alqaheem, Y. Alomair, A.A. Pérez, A. and Rana, M.S. 2017. "Recent progress of fillers in mixed matrix membranes for CO_2 separation: A review." *Separation and Purification Technology*. 188 : 431-450.

69. Wang, X. Wang, L. Su, Q. and Zheng, J. 2013. "Use of unmodified SiO_2 as nanofiller to improve mechanical properties of polymer-based nanocomposites." *Composites Science and Technology*. 89 : 52-60.

70. Loloei, M. Omidkhah, M. Moghadassi, A. and Amooghin, A.E. 2015. "Preparation and characterization of Matrimid® 5218 based binary and ternary mixed matrix membranes for CO_2 separation." *International Journal of Greenhouse Gas Control*. 39 : 225-235.

71. Hudiono, Y.C. Carlisle, T.K. Bara, J.E. Zhang, Y. Gin, D.L. and Noble, R.D. 2010. "A three-component mixed-matrix membrane with enhanced CO_2 separation properties based on zeolites and ionic liquid materials." *Journal of Membrane Science*. 350 : 117-123.

72. Hudiono, Y.C. Carlisle, T.K. LaFrate, A.L. Gin, D.L. and Noble, R.D. 2011. "Novel mixed matrix membranes based on polymerizable room-temperature ionic liquids and SAPO-34 particles to improve CO_2 separation." *Journal of Membrane Science*. 370 : 141-148.

73. Vera, P. Canellas, E. Nerín, C. Dreolin, N. and Goshawk, J. 2022. "The migration of NIAS from ethylene-vinyl acetate corks and their identification using gas chromatography mass spectrometry and liquid chromatography ion mobility quadrupole time-of-flight mass spectrometry." *Food Chemistry*. 366 : 130592.

74. Marais, S. Hirata, Y. Langevin, D. Chappey, C. Nguyen, T.Q. and Metayer, M. 2002. "Permeation and Sorption of Water and Gases Through EVA Copolymers Films." *Materials Research Innovations*. 6 : 79-88.

75. Castaños, E. 2015. **Cromatografía de reparto.** [Online]. Available : https://cienciadelux.wordpress.com/2015/08/14/cromatografia-de-reparto/.

76. Hibshman, C. Cornelius, C.J. and Marand, E. 2003. "The gas separation effects of annealing polyimide–organosilicate hybrid membranes." *Journal of Membrane Science*. 211 : 25-40.

77. Suzuki, T. and Yamada, Y. 2005. "Physical and Gas Transport Properties of Novel Hyperbranched Polyimide – Silica Hybrid Membranes." *Polymer Bulletin*. 53 : 139-146.

78. Suzuki, T. and Yamada, Y. 2006. “Characterization of 6FDA-based hyperbranched and linear polyimide–silica hybrid membranes by gas permeation and 129Xe NMR measurements.” *Journal of Polymer Science Part B: Polymer Physics*. 44 : 291-298.
79. Kim, J.H. and Lee, Y.M. 2001. “Gas permeation properties of poly(amide-6-b-ethylene oxide)–silica hybrid membranes.” *Journal of Membrane Science*. 193 : 209-225.
80. He, Z. Pinnau, I. and Morisato, A. 2002. “Nanostructured poly(4-methyl-2-pentyne)/silica hybrid membranes for gas separation.” *Desalination*. 146 : 11-15.
81. Gomes, D. Nunes, S.P. and Peinemann, K.-V. 2005. “Membranes for gas separation based on poly(1-trimethylsilyl-1-propyne)–silica nanocomposites.” *Journal of Membrane Science*. 246 : 13-25.
82. Taheri, P. Raisi, A. and Maleh, M.S. 2021. “CO_2-selective poly (ether-block-amide)/polyethylene glycol composite blend membrane for CO_2 separation from gas mixtures.” *Environmental Science and Pollution Research*. 28 : 38274-38291.
83. Nogueira, C.d.C. de Araújo Padilha, C.E. de Souza Filho, P.F. and dos Santos, E.S. 2022. “Effects of the Addition of Poly(ethylene Glycol) and Non-ionic Surfactants on Pretreatment, Enzymatic Hydrolysis, and Ethanol Fermentation.” *BioEnergy Research*. 15 : 889-904.
84. Da Conceicao, M. Nemetz, L. Rivero, J. Hornbostel, K. and Lipscomb, G. 2023. “Gas Separation Membrane Module Modeling: A Comprehensive Review.” *Membranes*. 13070639.
85. Warsinger, D.M. Chakraborty, S. Tow, E.W. Plumlee, M.H. Bellona, C. Loutatidou, S. Karimi, L. Mikelonis, A.M. Achilli, A. Ghassemi, A. Padhye, L.P. Snyder, S.A. Curcio, S. Vecitis, C.D. Arafat, H.A. and Lienhard, J.H. 2018. “A review of polymeric membranes and processes for potable water reuse.” *Progress in Polymer Science*. 81 : 209-237.
86. Thanh, B.X. Ngo, T.-T.-M. Nguyen, T.-D.-N. Nguyen, H.-H. and Hoang, T.-K.-D. 2019. “Review on membrane module configurations used for membrane disstillation process.” *GeoScience Engineering*. 65 : 1-10.
87. Dias, A.C.S. De Sá, M.C.C. Fontoura, T.B. Menezes, D.Q. Anzai, T.K. Diehl, F.C. Thompson, P.H. and Pinto, J.C. 2020. “Modeling of spiral wound membranes for gas separations. Part I: An iterative 2D permeation model.” *Journal of Membrane Science*. 612 : 118278.

88. Sarrigani, G.V. Ding, J. Ghadi, A.E. Alam, D. Fitzgerald, P. Wiley, D.E. and Wang, D.K. 2022. "Interfacially-confined polyetherimide tubular membranes for H_2, CO_2 and N_2 separations." *Journal of Membrane Science*. 655 : 120596.

89. Adelnia, H. Bidsorkhi, H.C. Ismail, A.F. and Matsuura, T. 2015. "Gas permeability and permselectivity properties of ethylene vinyl acetate/sepiolite mixed matrix membranes." *Separation and Purification Technology*. 146 : 351-357.

90. Hassanajili, S. Masoudi, E. Karimi, G. and Khademi, M. 2013. "Mixed matrix membranes based on polyetherurethane and polyesterurethane containing silica nanoparticles for separation of CO_2/CH_4 gases." *Separation and Purification Technology*. 116 : 1-12.

91. Ghadimi, A. Mohammadi, T. and Kasiri, N. 2014. "A Novel Chemical Surface Modification for the Fabrication of PEBA/SiO_2 Nanocomposite Membranes To Separate CO_2 from Syngas and Natural Gas Streams." *Industrial & Engineering Chemistry Research*. 53 : 17476-17486.

92. Barooah, M. and Mandal, B. 2018. "Enhanced CO_2 separation performance by PVA/PEG/silica mixed matrix membrane." *Journal of Applied Polymer Science*. 135 : 46481.

93. Dilshad, M.R. Islam, A. Haider, B. Sajid, M. Ijaz, A. Khan, R.U. and Khan, W.G. 2021. "Effect of silica nanoparticles on carbon dioxide separation performances of PVA/PEG cross-linked membranes." *Chemical Papers*. 75 : 3131-3153.

94. Hou, J. Hu, L. Ren, F. Zhao, Y. Tian, W. and Qin, Y. 2023. "Building CO_2 Transport Channels in Mixed Matrix Membranes Using SiO_2 Nanosheets." *ACS Applied Nano Materials*. 6 : 17179-17186.

95. Ahmad, A.L. Jawad, Z.A. Low, S.C. and Zein, S.H.S. 2014. "A cellulose acetate/multi-walled carbon nanotube mixed matrix membrane for CO_2/N_2 separation." *Journal of Membrane Science*. 451 : 55-66.

96. Hoang, T. Truc, T.A. Thanh, D.T.M. Chinh, N.T. Tham, D.Q. Trang, N.T.T. Vu Giang, N. and Lam, V.D. 2013. "Tensile, rheological properties, thermal stability, and morphology of ethylene vinyl acetate copolymer/silica nanocomposites using EVA-g-maleic anhydride." *Journal of Composite Materials*. 48 : 505-511.

97. Marais, S. Saiter, J.M. Devallencourt, C. Nguyen, Q.T. and Métayer, M. 2002. "Study of transport of small molecules through ethylene-co-vinyl acetate copolymers films. Part B: CO_2 and O_2 gases." *Polymer Testing*. 21 : 425-431.

98. Takidis, G. Bikiaris, D.N. Papageorgiou, G.Z. Achilias, D.S. and Sideridou, I. 2003. "Compatibility of low-density polyethylene/poly(ethylene-co-vinyl acetate) binary blends prepared by melt mixing." *Journal of Applied Polymer Science*. 90 : 841-852.

99. Sefadi, J.S. and Luyt, A.S. 2011. "Morphology and properties of EVA/empty fruit bunch composites." *Journal of Thermoplastic Composite Materials*. 25 : 895-914.

100. Hakim, R.H. Cailloux, J. Santana, O.O. Bou, J. Sánchez-Soto, M. Odent, J. Raquez, J.M. Dubois, P. Carrasco, F. and Maspoch, M.L. 2017. "PLA/SiO_2 composites: Influence of the filler modifications on the morphology, crystallization behavior, and mechanical properties." *Journal of Applied Polymer Science*. 134 : 45367.

101. Xu, W. Yin, X. He, G. Zhao, J. and Wang, H. 2012. "Photografted temperature-sensitive poly(N-isopropylacrylamide) thin film with a superfast response rate and an interesting transparent–opaque–transparent change in its deswelling process." *Soft Matter*. 8 : 3105-3111.

102. Blázquez-Blázquez, E. Cerrada, M.L. Benavente, R. and Pérez, E. 2020. "Identification of Additives in Polypropylene and Their Degradation under Solar Exposure Studied by Gas Chromatography–Mass Spectrometry." *ACS Omega*. 5 : 9055-9063.

103. Alothman, O. Salahudeen, S. Elleithy, R. and Al-Zahrani, S.M. 2012. "Formation of Vinylidene in Polypropylene/Ethylene Vinyl Acetate (PP/EVA) Blends During Degradation." *Polymer-Plastics Technology and Engineering*. 51 : 540-547.

104. Kitano, H. Ichikawa, K. Fukuda, M. Mochizuki, A. and Tanaka, M. 2001. "The Structure of Water Sorbed to Polymethoxyethylacrylate Film as Examined by FT–IR Spectroscopy." *Journal of Colloid and Interface Science*. 242 : 133-140.

105. Wan, L.-S. Huang, X.-J. and Xu, Z.-K. 2007. "Diffusion and Structure of Water in Polymers Containing N-Vinyl-2-pyrrolidone." *The Journal of Physical Chemistry B*. 111 : 922-928.

106. Acik, G. Kamaci, M. and Cansoy, C.E. 2018. "Superhydrophobic EVA copolymer fibers: the impact of chemical composition on wettability and photophysical properties." *Colloid and Polymer Science*. 296 : 1759-1766.

107. Ucar, I.O. Doganci, M.D. Cansoy, C.E. Erbil, H.Y. Avramova, I. and Suzer, S. 2011. "Combined XPS and contact angle studies of ethylene vinyl acetate and polyvinyl acetate blends." *Applied Surface Science*. 257 : 9587-9594.

108. Bidsorkhi, H.C. Adelnia, H. Heidar Pour, R. and Soheilmoghaddam, M. 2015. "Preparation and characterization of ethylene-vinyl acetate/halloysite nanotube nanocomposites." *Journal of Materials Science*. 50 : 3237-3245.

109. Poisson, C. Hervais, V. Lacrampe, M.F. and Krawczak, P. 2006. "Optimization of PE/Binder/PA extrusion blow-molded films. I. Heat sealing ability improvement using PE/EVA blends." *Journal of Applied Polymer Science*. 99 : 974-985.

110. Takahashi, Y. Liang, X. and Nakajima, K. 2019. "Mechanical property and structure of a butadiene rubber composite filled with syndiotactic polybutadiene resin." *Journal of Applied Polymer Science*. 136 : 47934.

111. Liu, R. Liu, S. Yu, J. Zhang, W. Dai, J. Zhang, Y. and Zhang, G. 2020. "The Construction of a Hydrophilic Inorganic Layer Enables Mechanochemically Robust Super Antifouling UHMWPE Composite Membrane Surfaces." *Polymers*. 12030569.

112. Liu, Q. Wu, X. and Zhang, K. 2018. "Polysulfone/Polyamide-SiO_2 Composite Membrane with High Permeance for Organic Solvent Nanofiltration." *Membranes*. 8040089.

113. Mohammed, M.I. and El-Sayed, F. 2023. "PEG's impact as a plasticizer on the PVA polymer's structural, thermal, mechanical, optical, and dielectric characteristics." *Optical and Quantum Electronics*. 55 : 1141.

114. Car, A. Stropnik, C. Yave, W. and Peinemann, K.-V. 2008. "PEG modified poly(amide-b-ethylene oxide) membranes for CO_2 separation." *Journal of Membrane Science*. 307 : 88-95.

115. Yuenyao, C. Chittrakarn, T. Tirawanichakul, Y. and Sirijarukul, S. 2016. "Surface Modification of Asymmetric Polysulfone/Polyethylene Glycol Membranes by DC Ar-Glow Discharge Plasma." *International Journal of Polymer Science*. 2016 : 4759150.

116. Chieng, B.W. Ibrahim, N.A. Yunus, W.M. and Hussein, M.Z. 2014. "Poly(lactic acid)/Poly(ethylene glycol) Polymer Nanocomposites: Effects of Graphene Nanoplatelets." *Polymers*. 6010093.

117. Xu, X. He, Z. Lu, S. Guo, D. and Yu, J. 2014. "Enhanced thermal and mechanical properties of lignin/polypropylene wood-plastic composite by using flexible segment-containing reactive compatibilizer." *Macromolecular Research*. 22 : 1084-1089.

118. Sudirman, Anggaravidya, M. Budianto, E. and Gunawan, I. 2012. "Synthesis and Characterization of Polyester-Based Nanocomposite." *Procedia Chemistry*. 4 : 107-113.

119. Torre-Celeizabal, A. Casado-Coterillo, C. Gomis-Berenguer, A. Iniesta, J. and Garea, A. 2023. "Chitosan-based mixed matrix composite membranes for CO_2/CH_4 mixed gas separation. Experimental characterization and performance validation." *Separation and Purification Technology*. 325 : 124535.

120. Iulianelli, A. Russo, F. Galiano, F. Desiderio, G. Basile, A. and Figoli, A. 2019. "PLA Easy Fil – White-based membranes for CO_2 separation." *Greenhouse Gases: Science and Technology*. 9 : 360-369.

121. Aghaei, Z. Naji, L. Hadadi Asl, V. Khanbabaei, G. and Dezhagah, F. 2018. "The influence of fumed silica content and particle size in poly (amide 6-b-ethylene oxide) mixed matrix membranes for gas separation." *Separation and Purification Technology*. 199 : 47-56.

Appendix

Appendix A

FT-IR spectrum of membrane

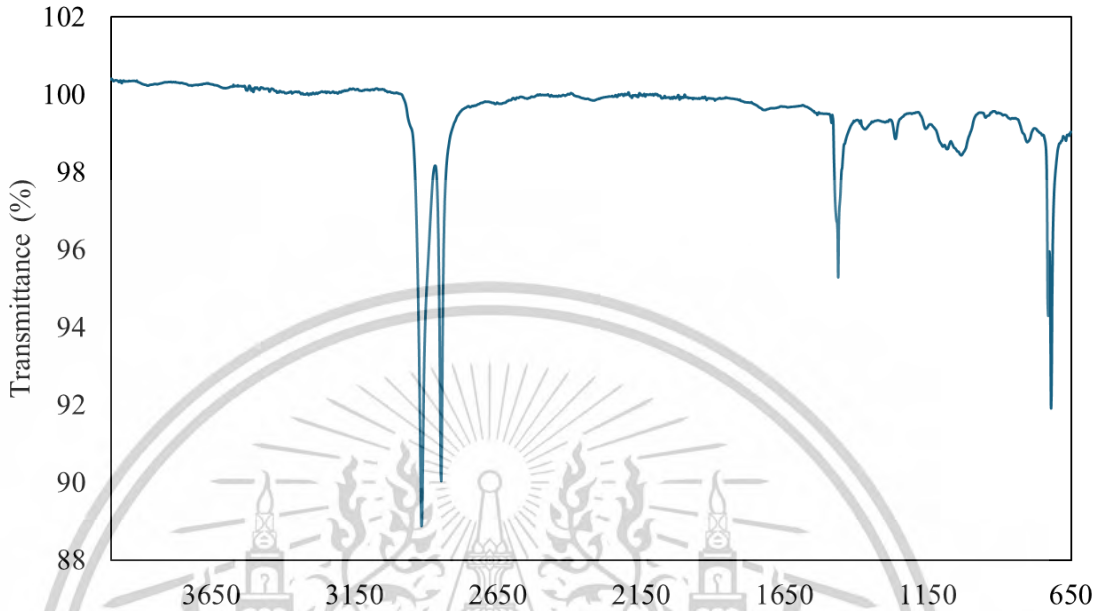

Figure A-1 FT-IR spectrum of LDPE membrane

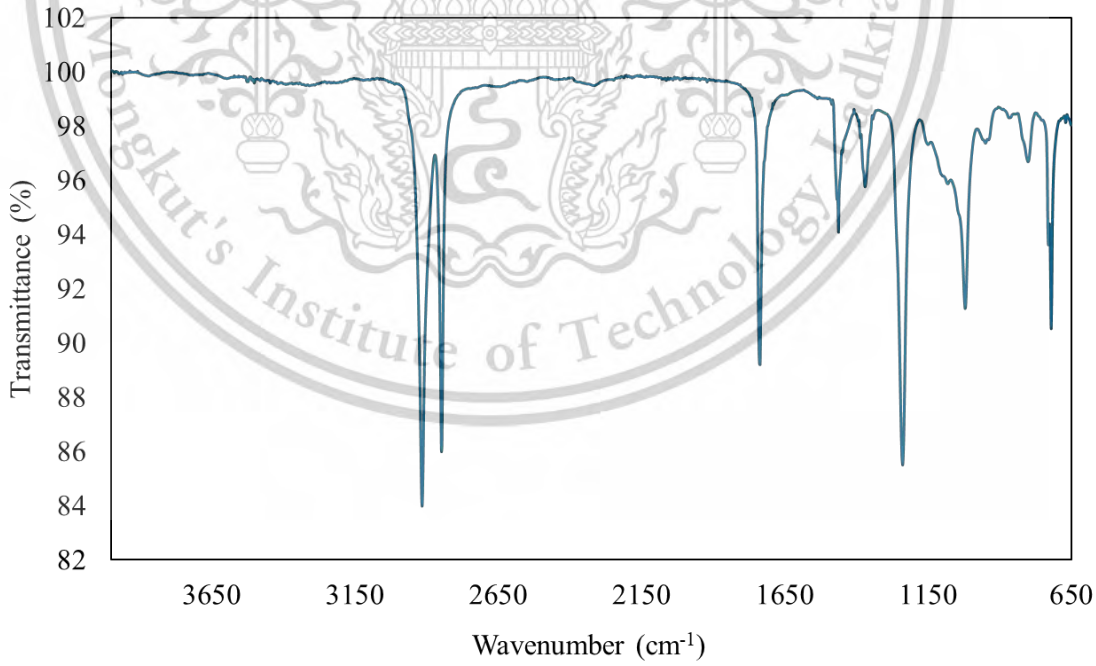

Figure A-2 FT-IR spectrum of E18 membrane

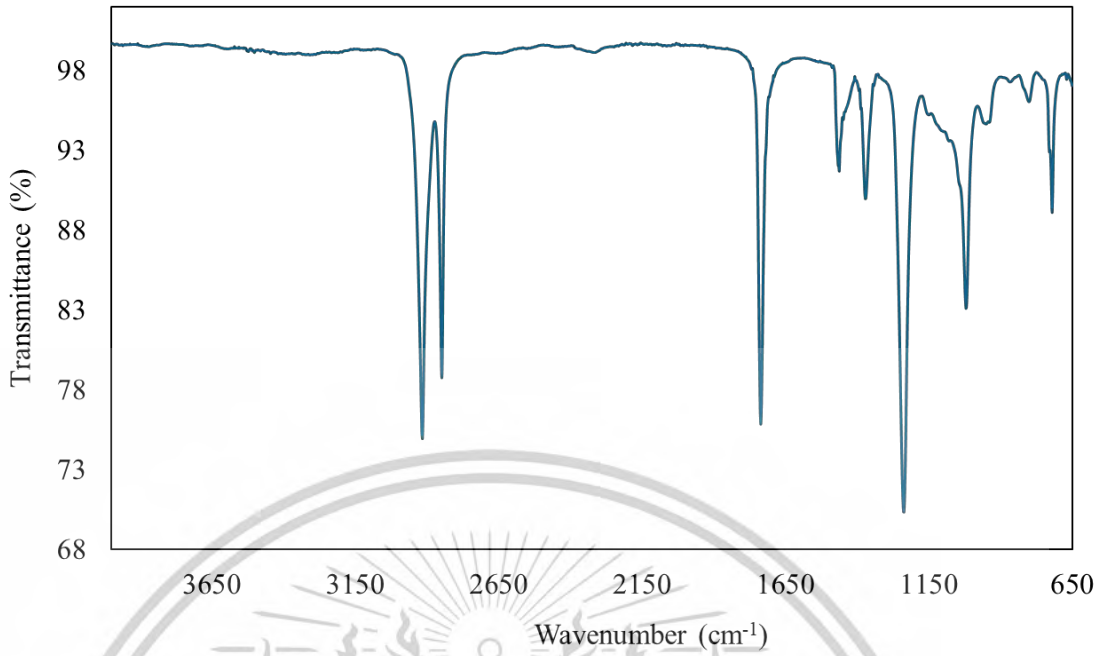

Figure A-3 FT-IR spectrum of E28 membrane

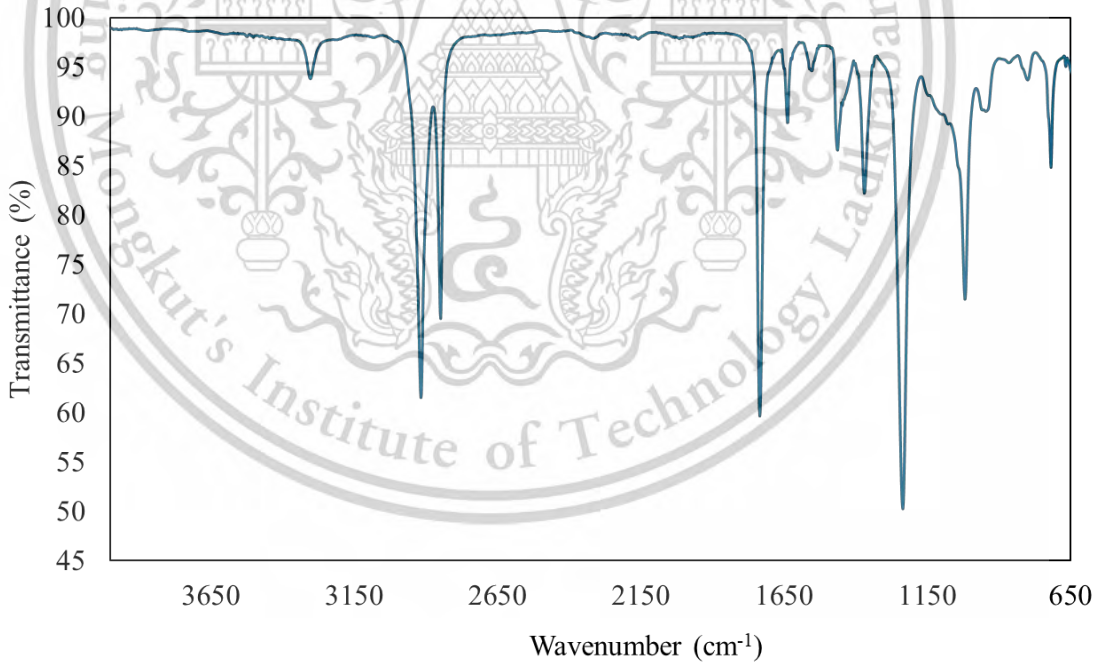

Figure A-4 FT-IR spectrum of E33 membrane

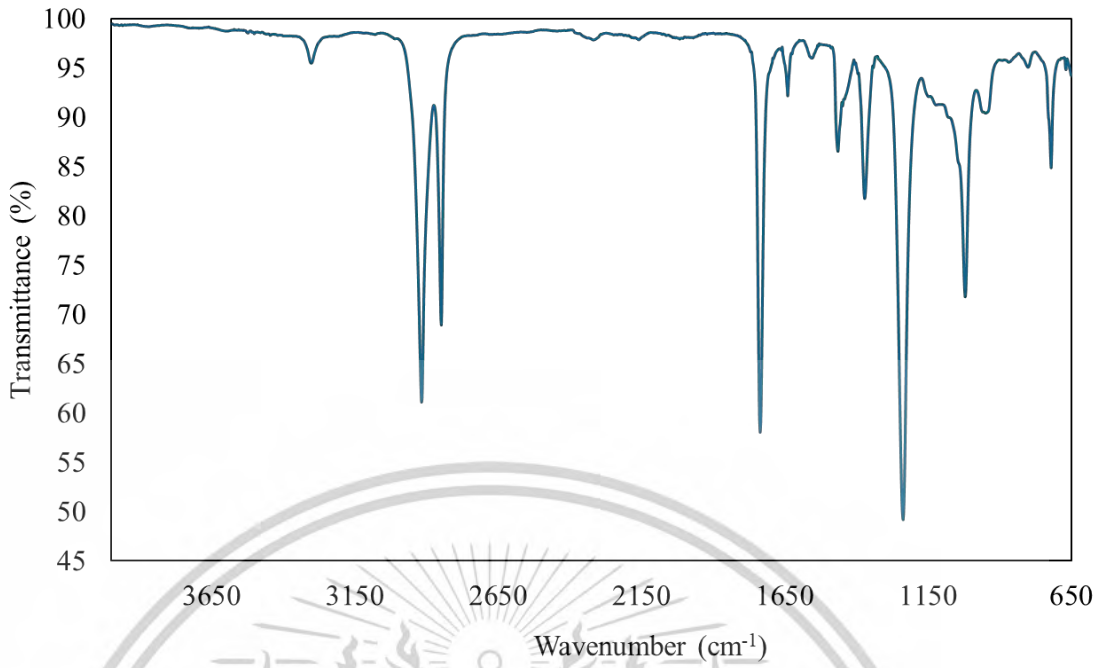

Figure A-5 FT-IR spectrum of E33S0.5 membrane

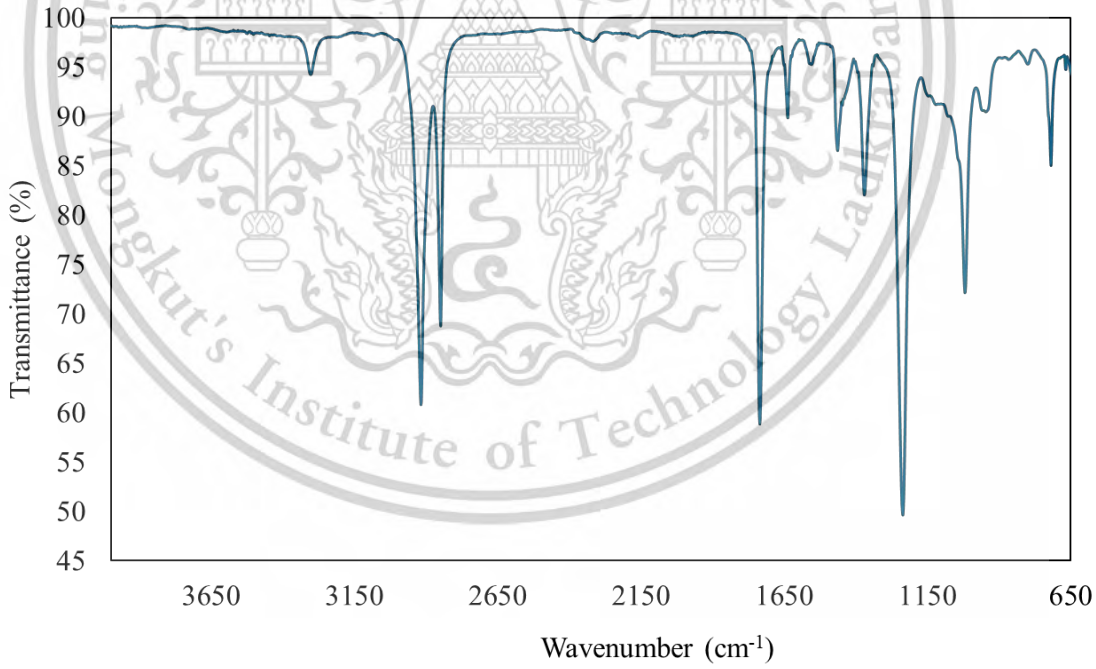

Figure A-6 FT-IR spectrum of E33S1.0 membrane

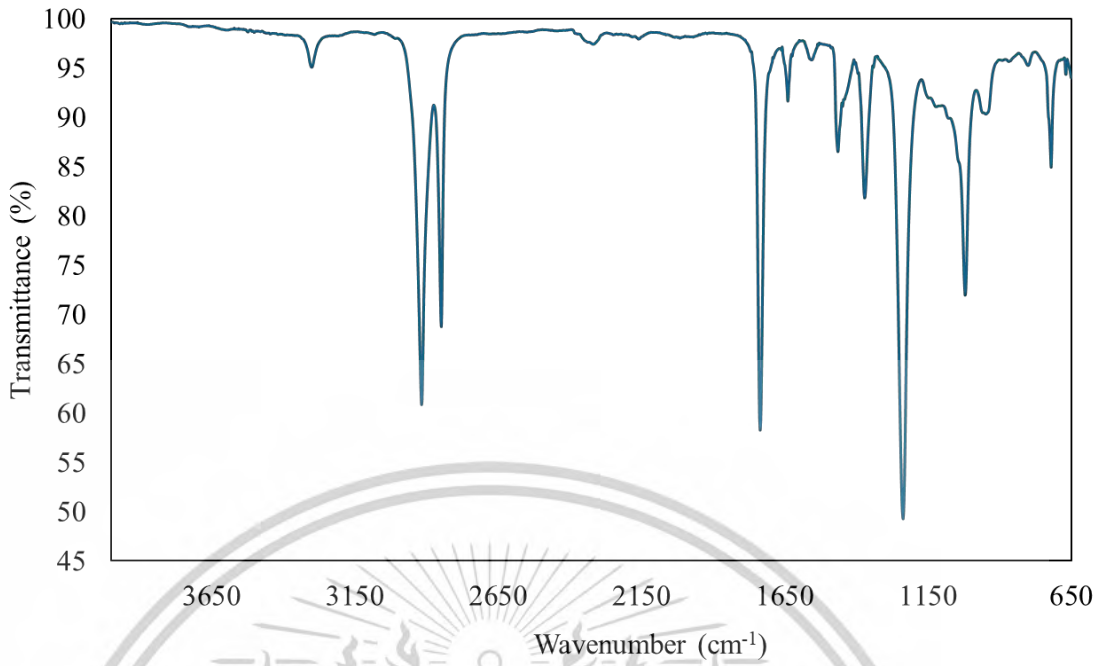

Figure A-7 FT-IR spectrum of E33S2.0 membrane

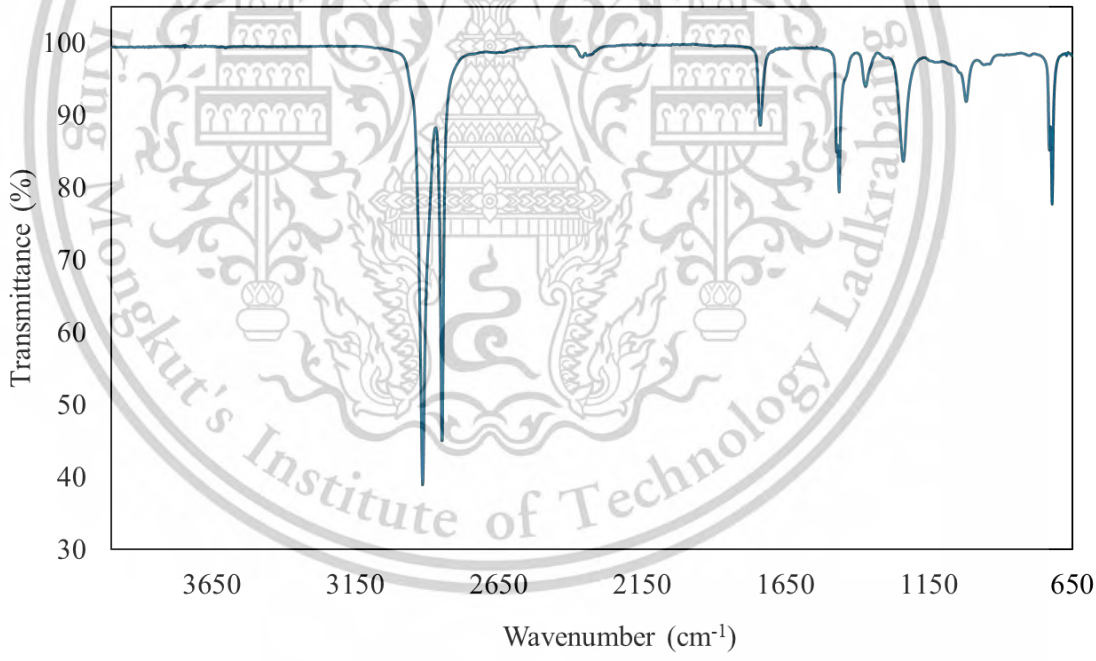

Figure A-8 FT-IR spectrum of E28-18 membrane

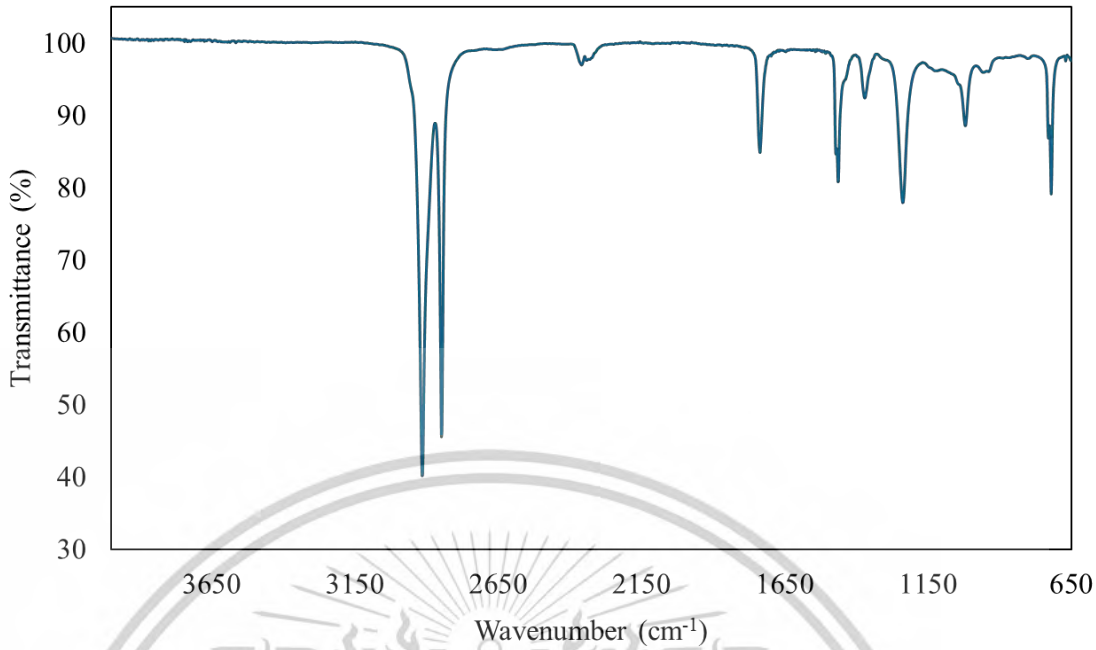

Figure A-9 FT-IR spectrum of E28-18S0.5 membrane

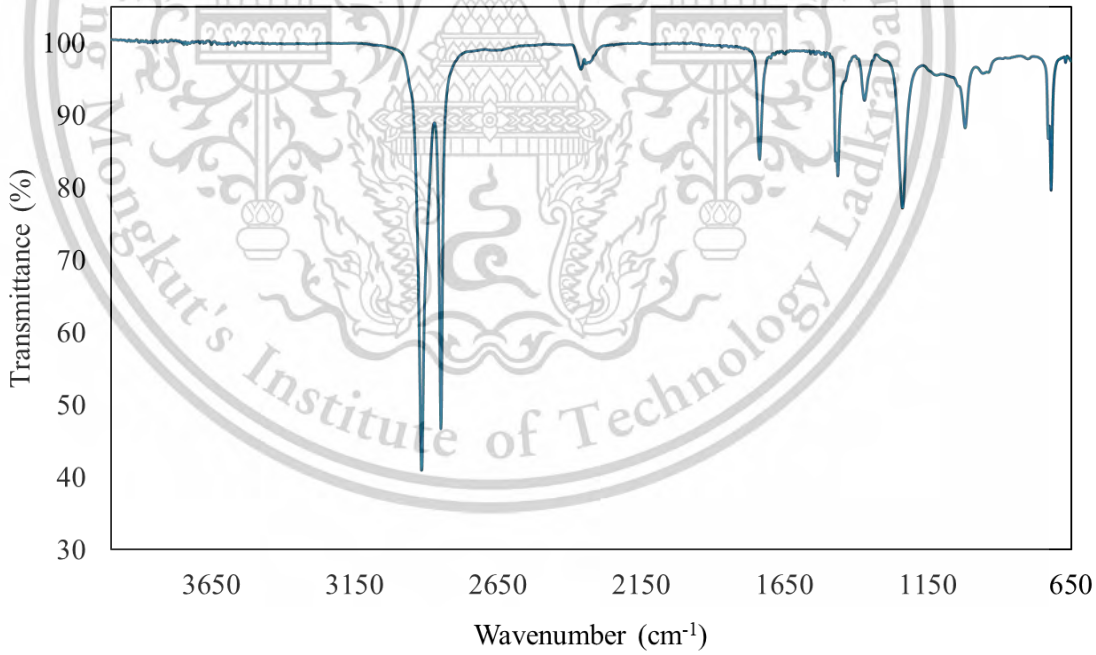

Figure A-10 FT-IR spectrum of E28-18S0.75 membrane

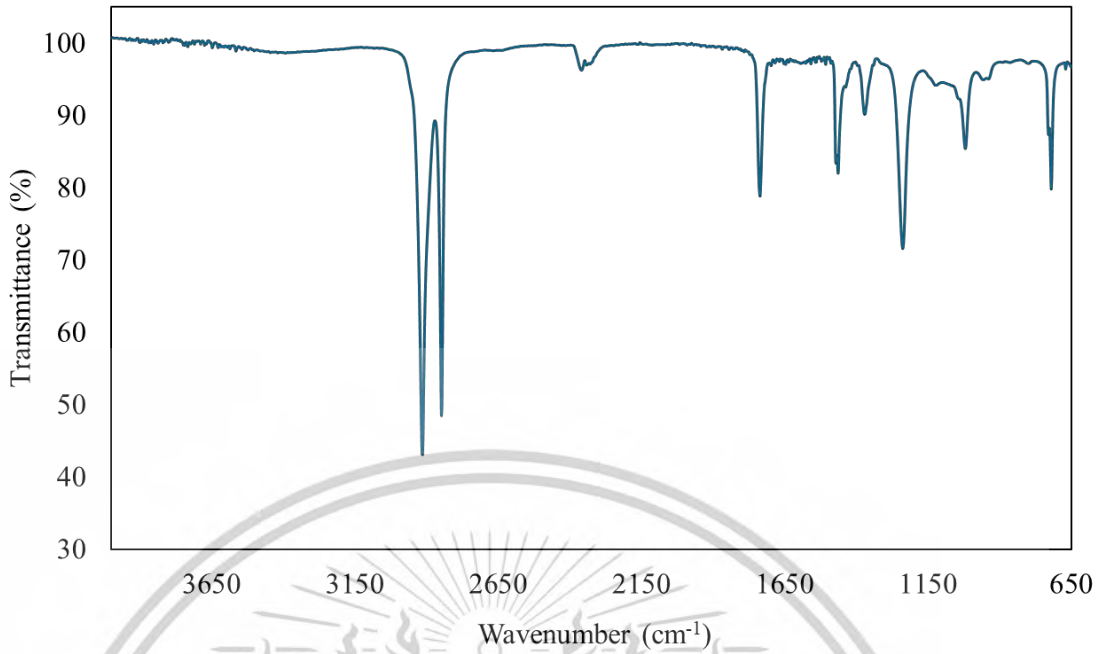

Figure A-11 FT-IR spectrum of E28-18S1.0 membrane

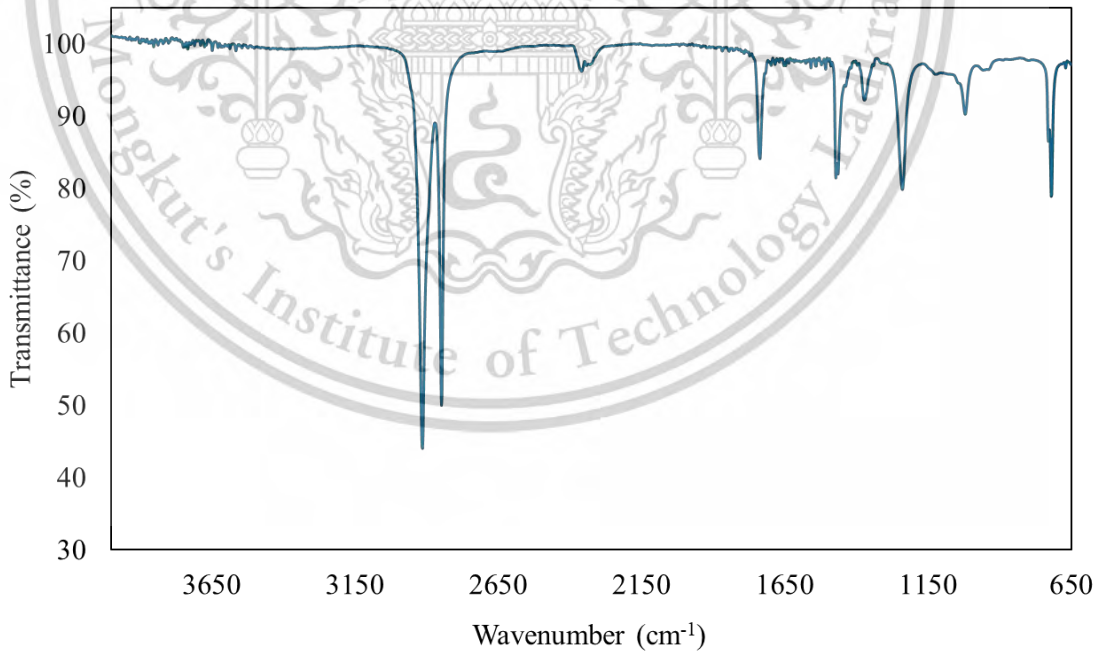

Figure A-12 FT-IR spectrum of E28-18S0.5P0.5 membrane

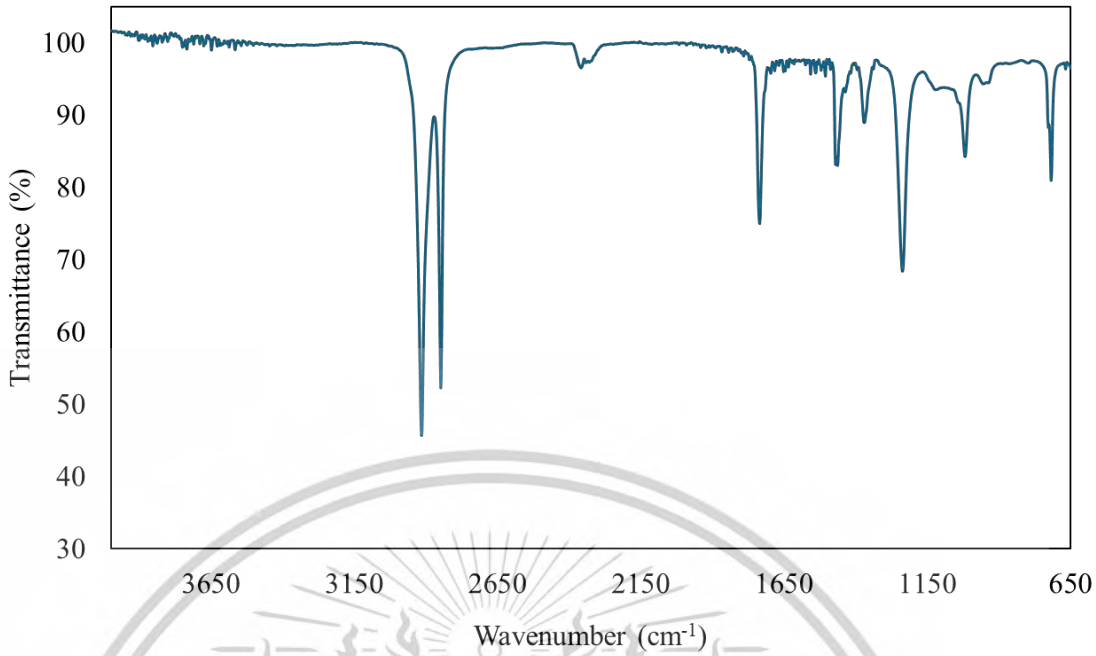

Figure A-13 FT-IR spectrum of E28-18S0.5P1.0 membrane

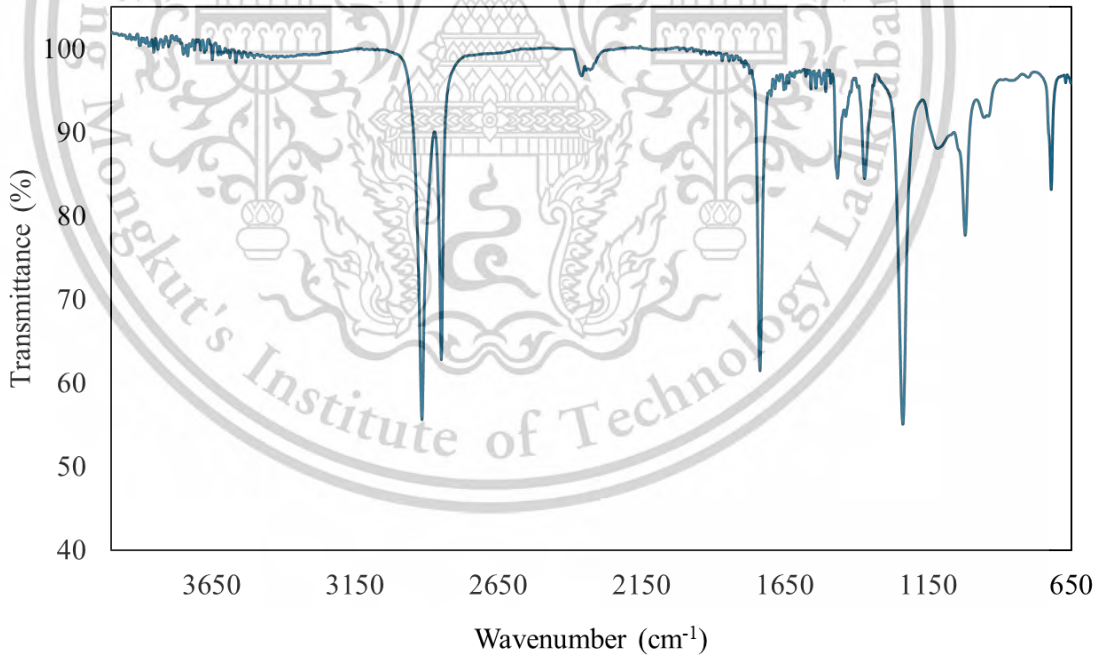

Figure A-14 FT-IR spectrum of E28-18S0.5P1.5 membrane

Appendix B

DSC thermogram of membrane

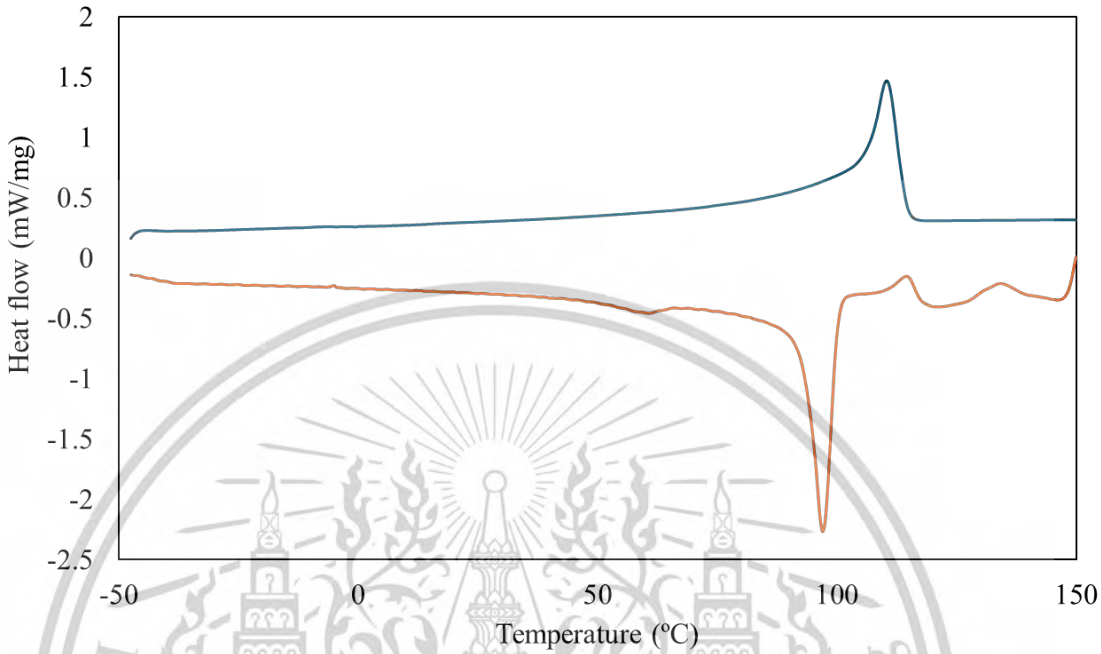

Figure B-1 DSC thermogram of LDPE membrane

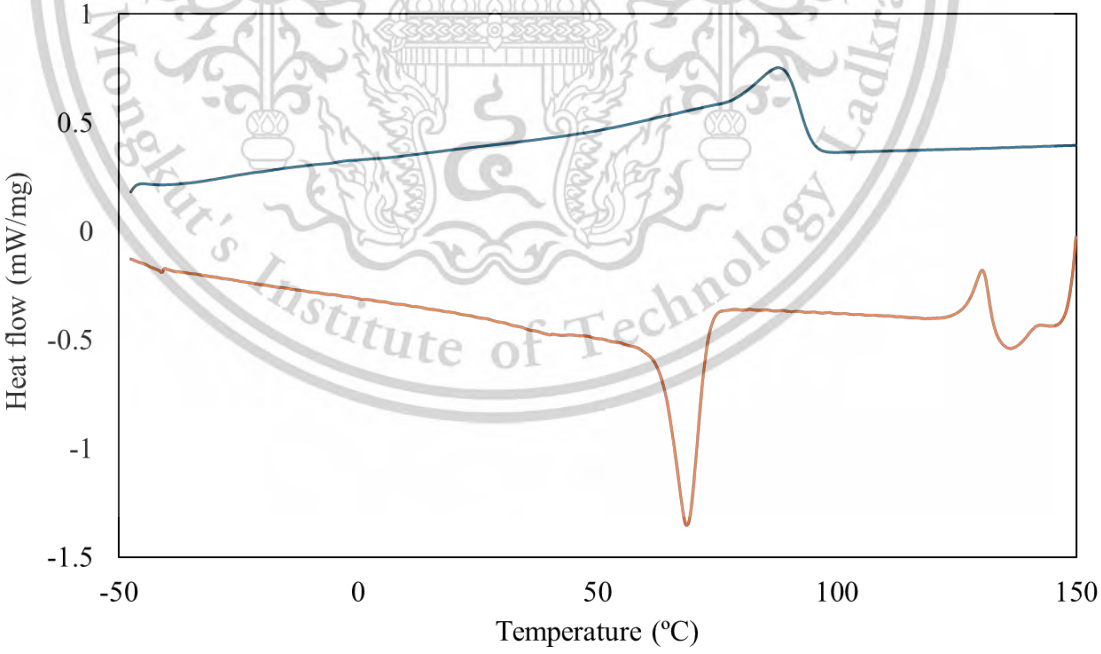

Figure B-2 DSC thermogram of E18 membrane

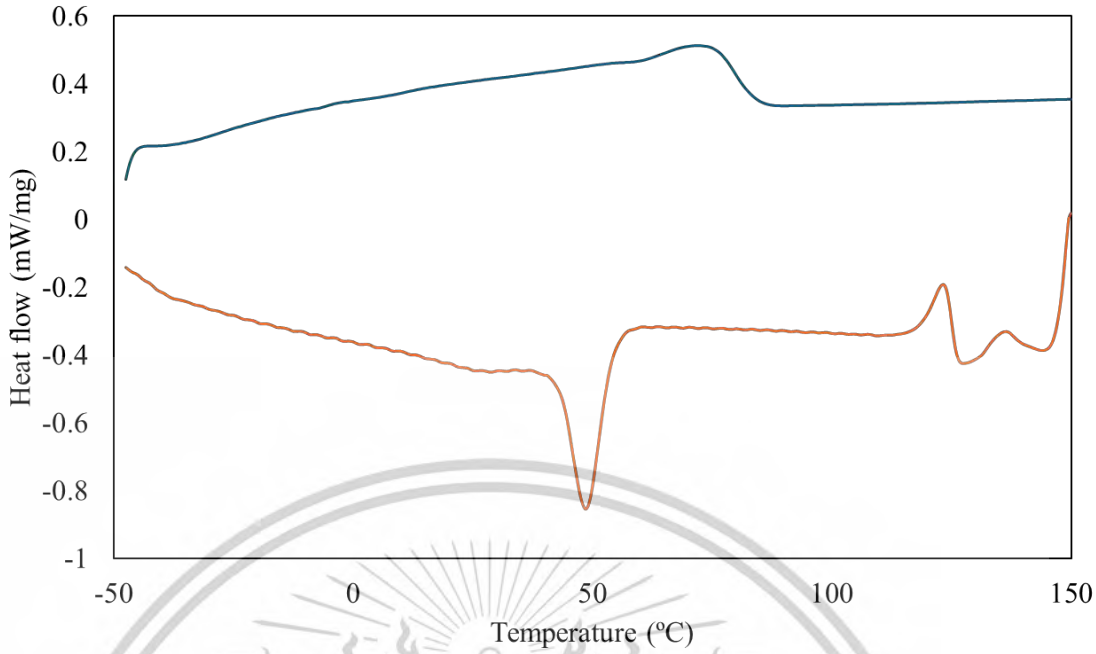

Figure B-3 DSC thermogram of E28 membrane

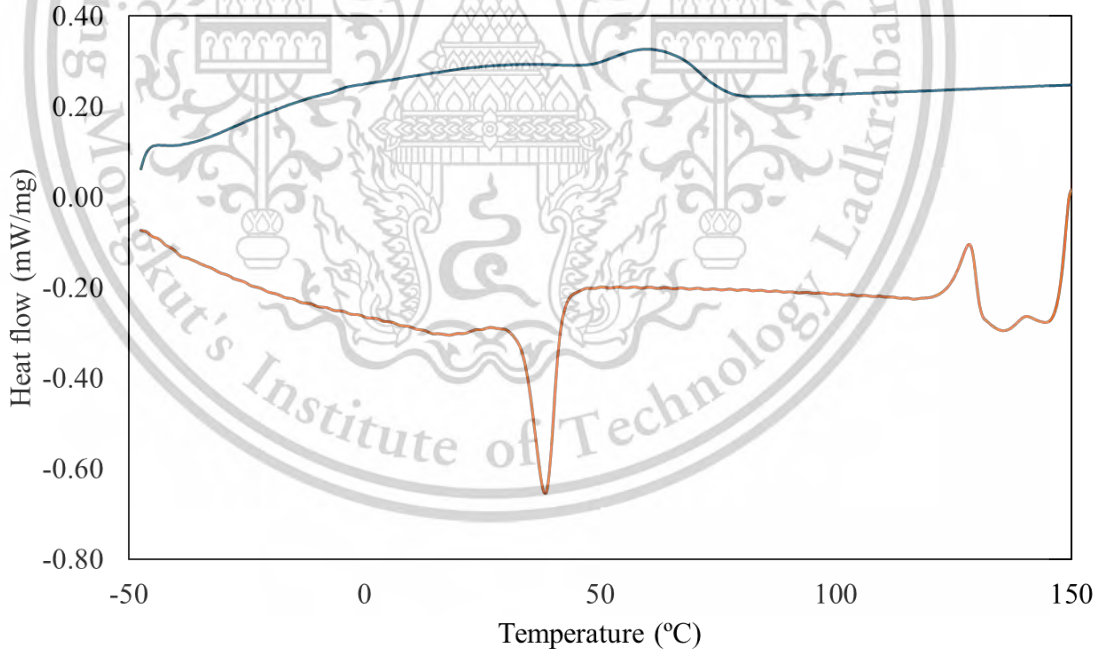

Figure B-4 DSC thermogram of E33 membrane

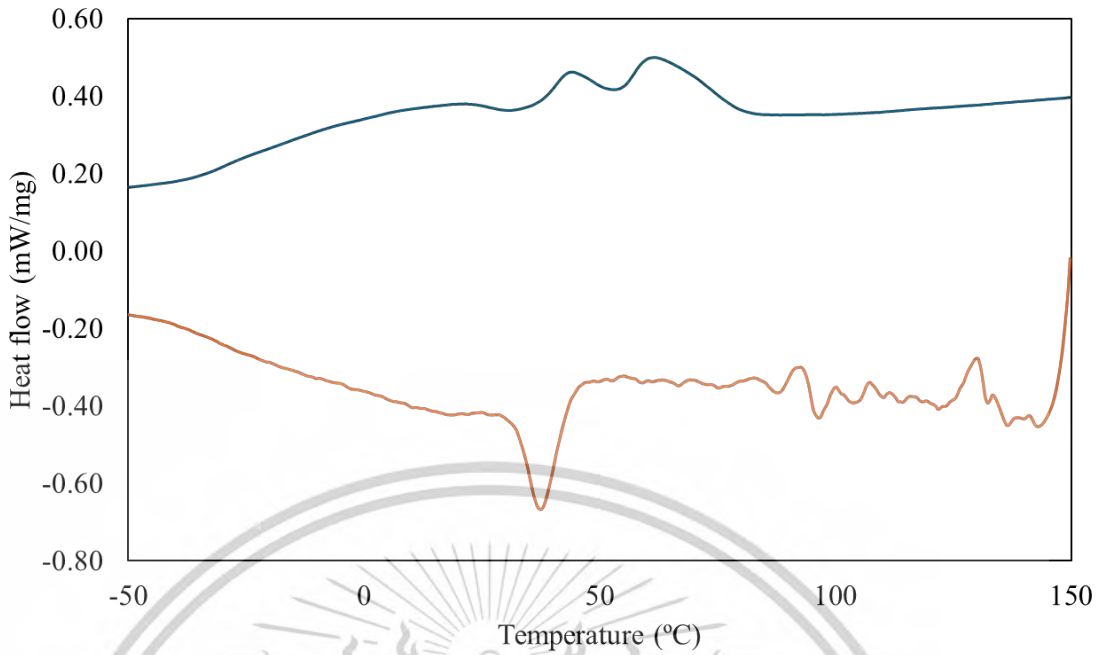

Figure B-5 DSC thermogram of E33S0.5 membrane

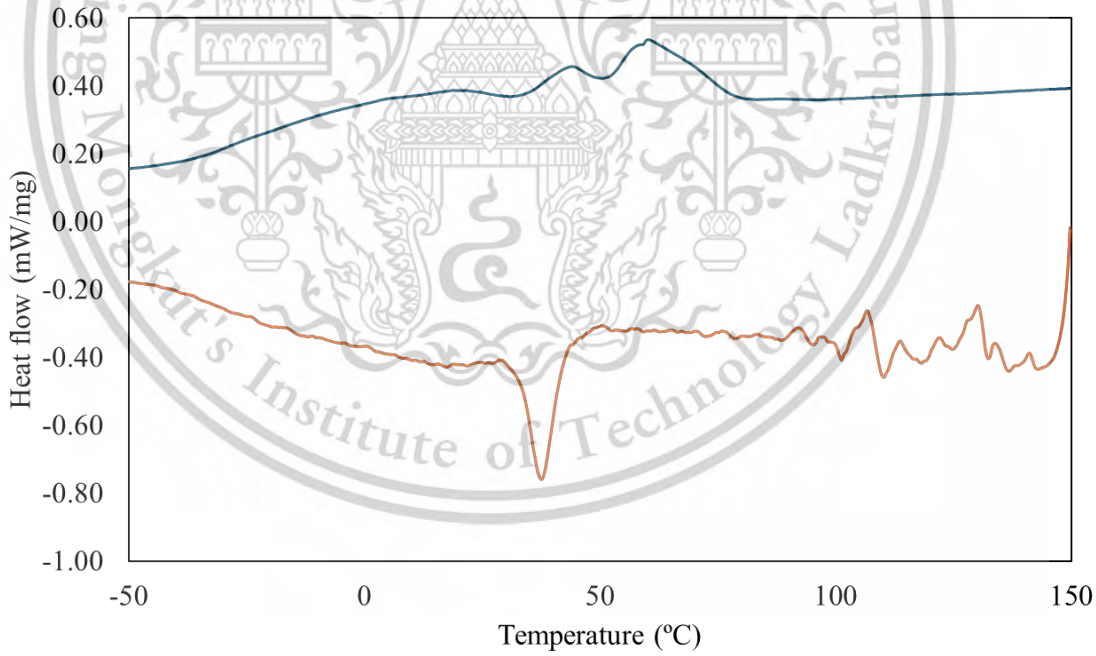

Figure B-6 DSC thermogram of E33S1.0 membrane

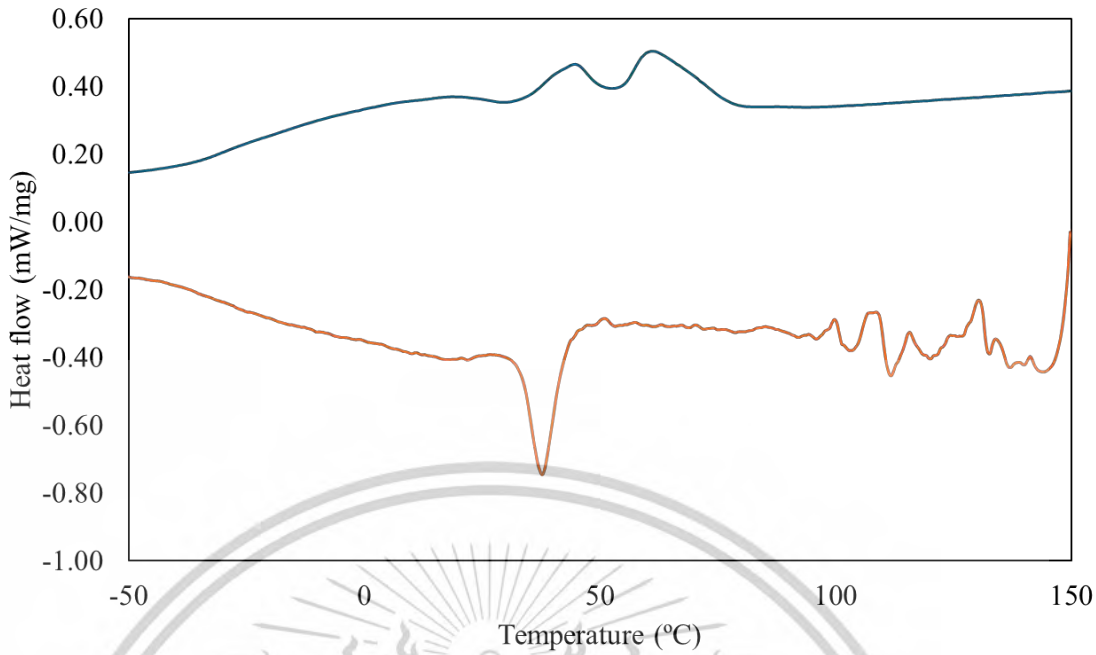

Figure B-7 DSC thermogram of E33S2.0 membrane

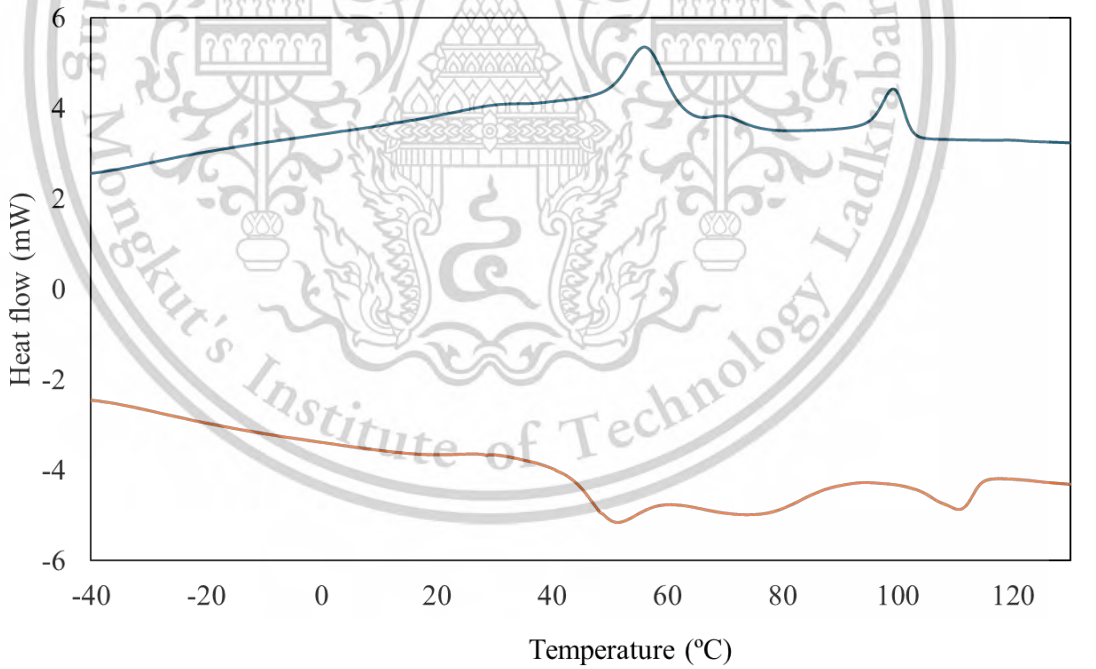

Figure B-8 DSC thermogram of E28-18 membrane

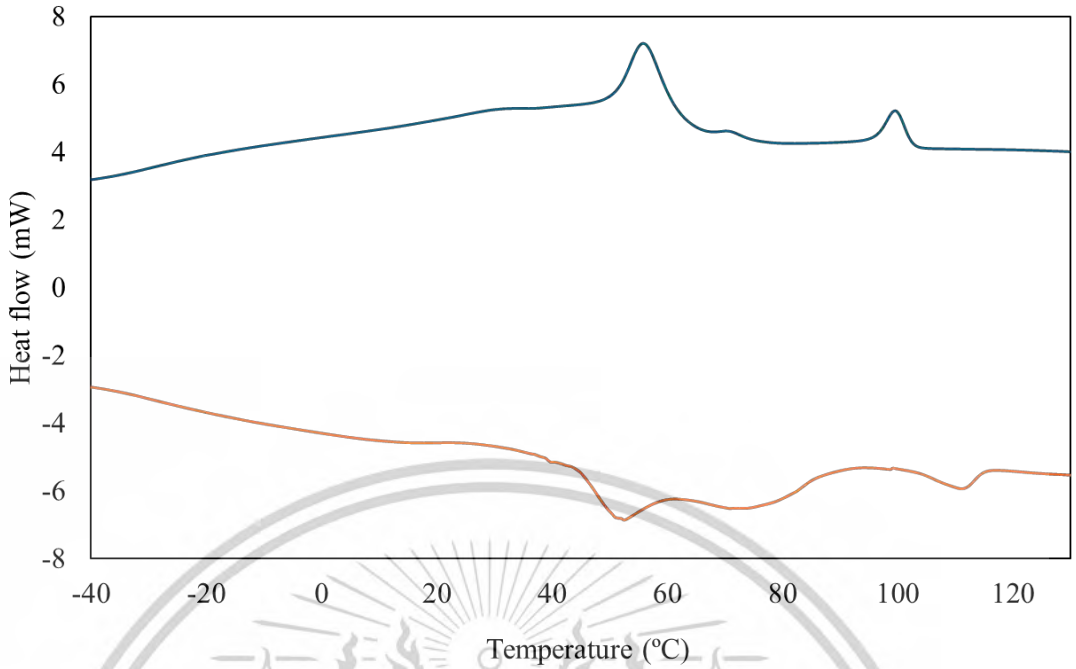

Figure B-9 DSC thermogram of E28-18S0.5 membrane

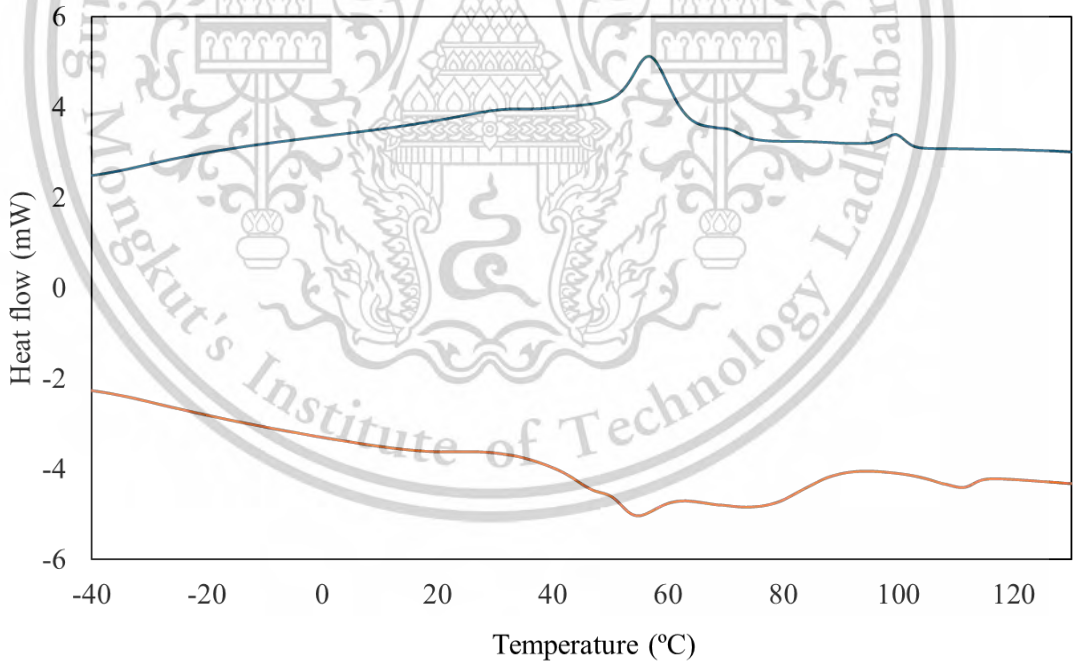

Figure B-10 DSC thermogram of E28-18S0.75 membrane

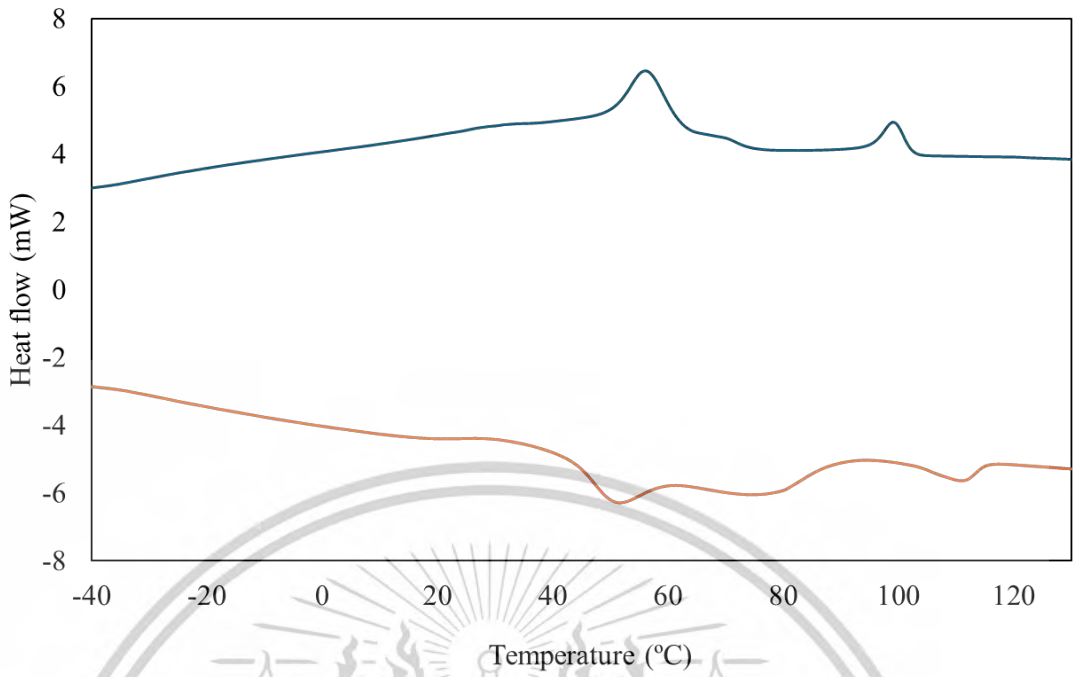

Figure B-11 DSC thermogram of E28-18S1.0 membrane

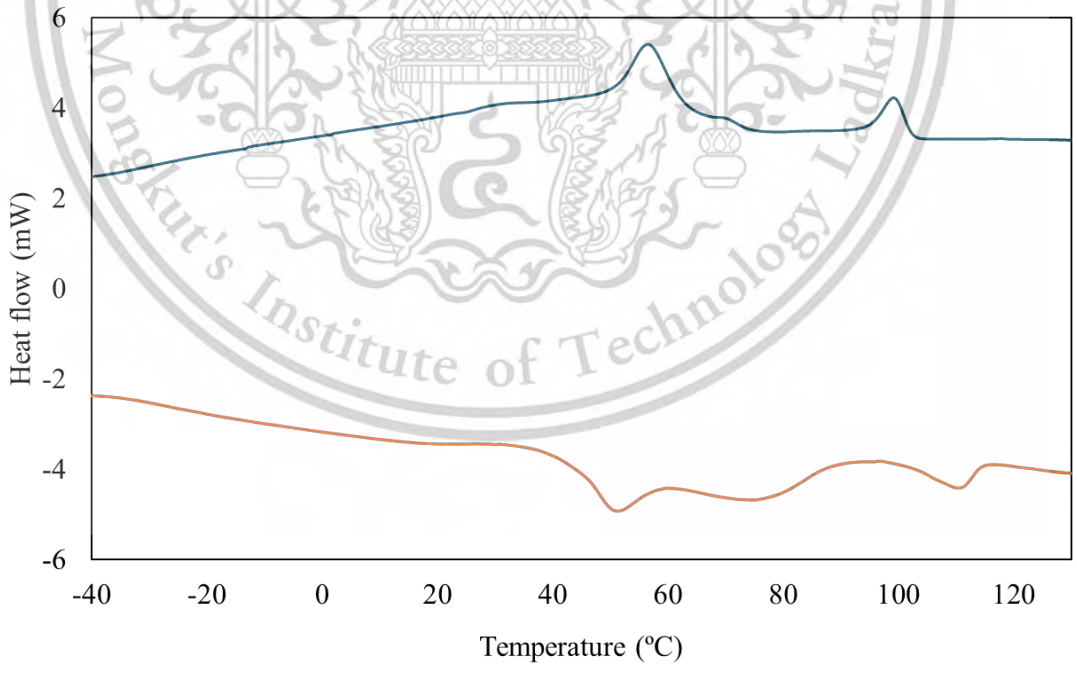

Figure B-12 DSC thermogram of E28-18S0.5P0.5 membrane

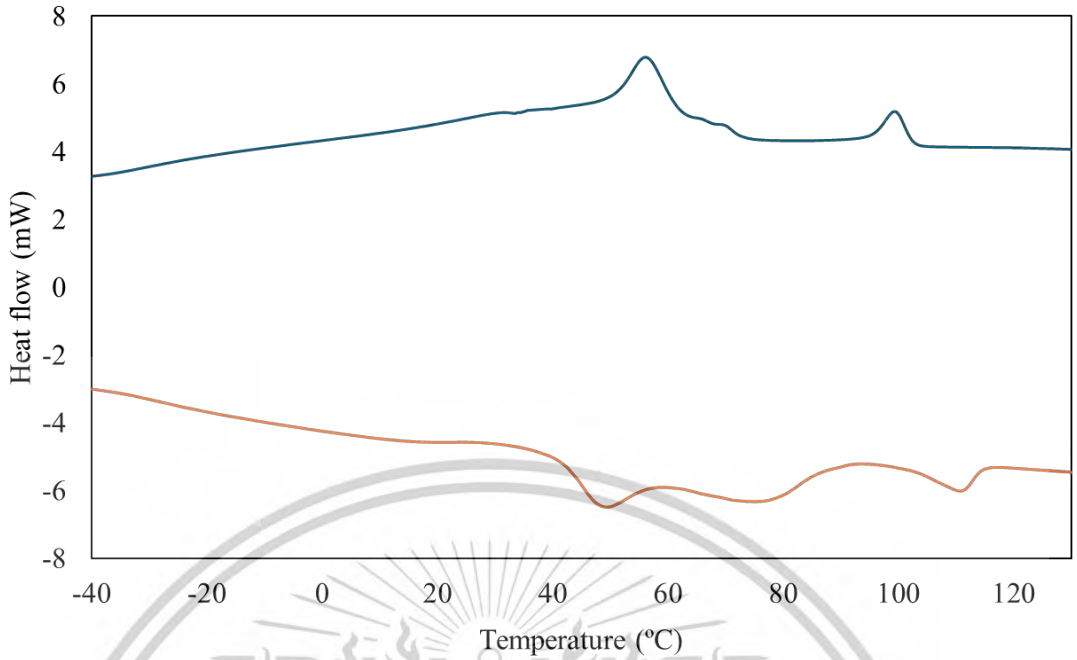

Figure B-13 DSC thermogram of E28-18S0.5P1.0 membrane

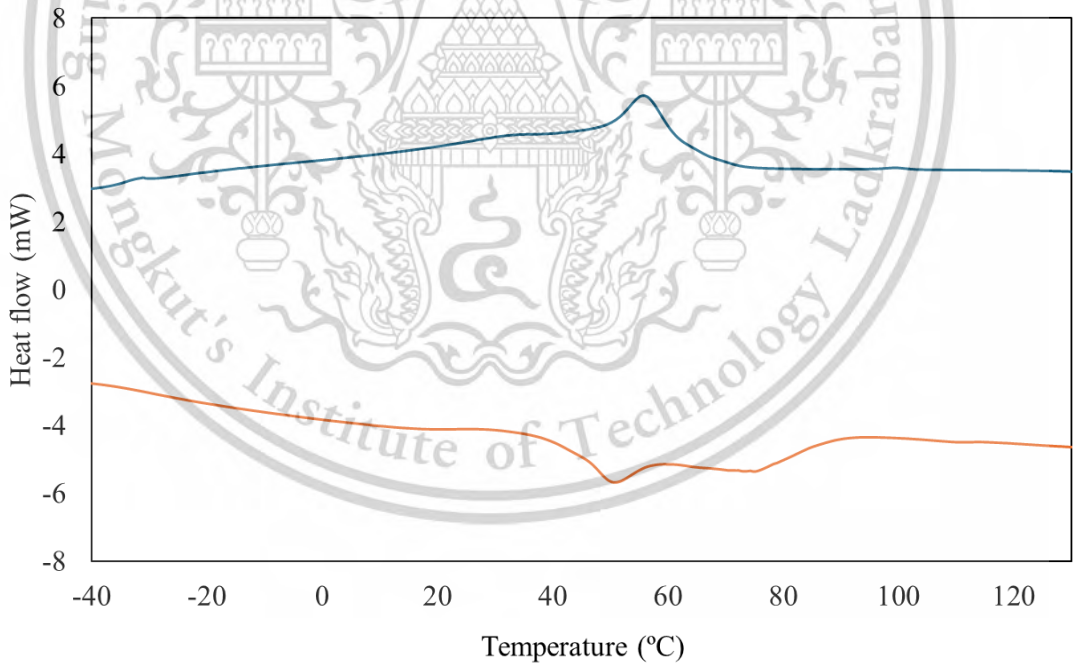

Figure B-14 DSC thermogram of E28-18S0.5P1.5 membrane

Appendix C

Contact angle of membrane

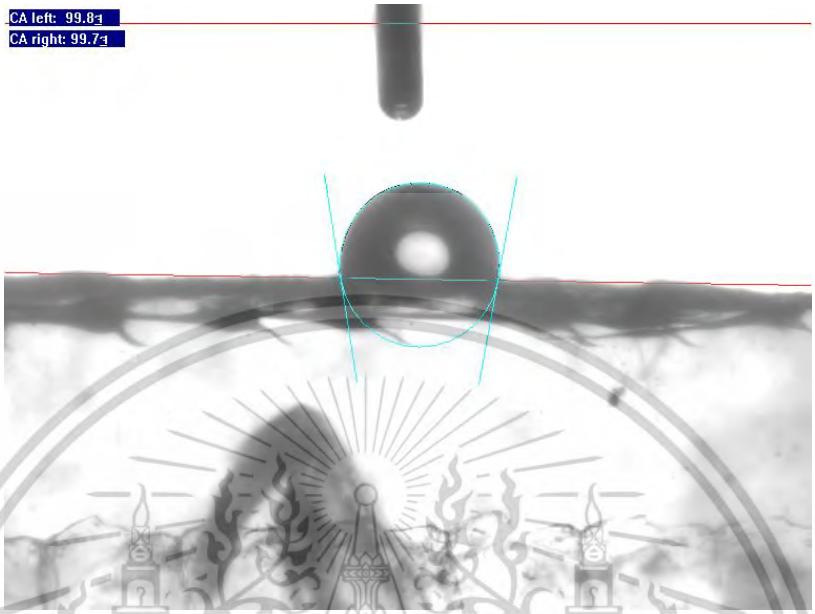

Figure C-1 Water droplet images of E33 membrane

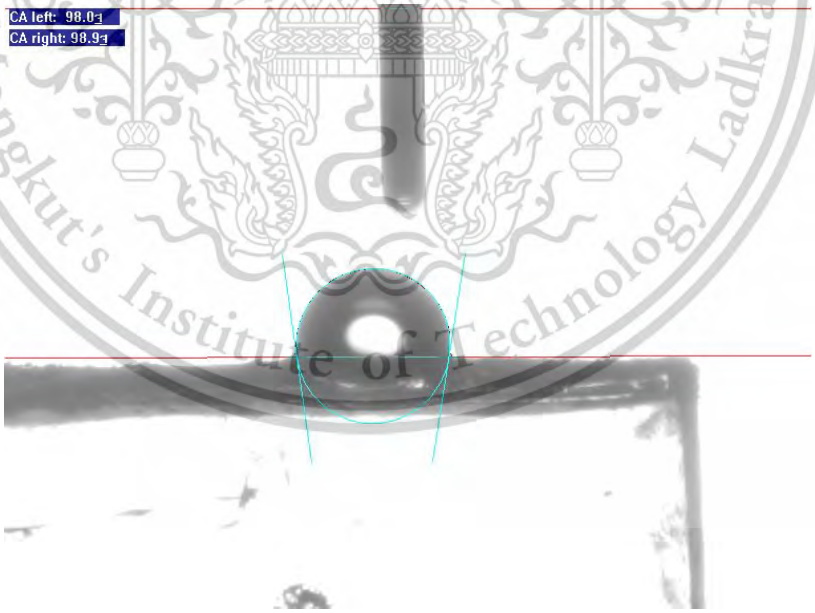

Figure C-2 Water droplet images of E33S0.5 membrane

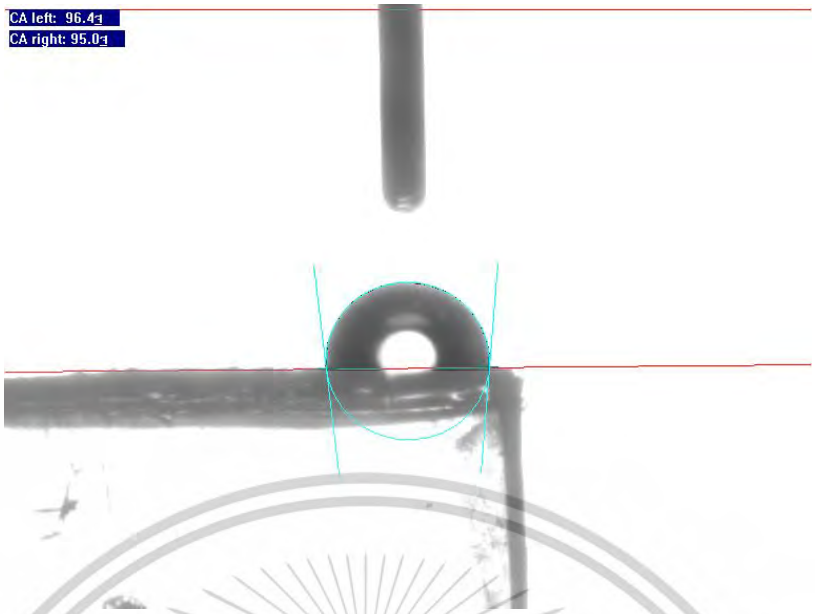

Figure C-3 Water droplet images of E33S1.0 membrane

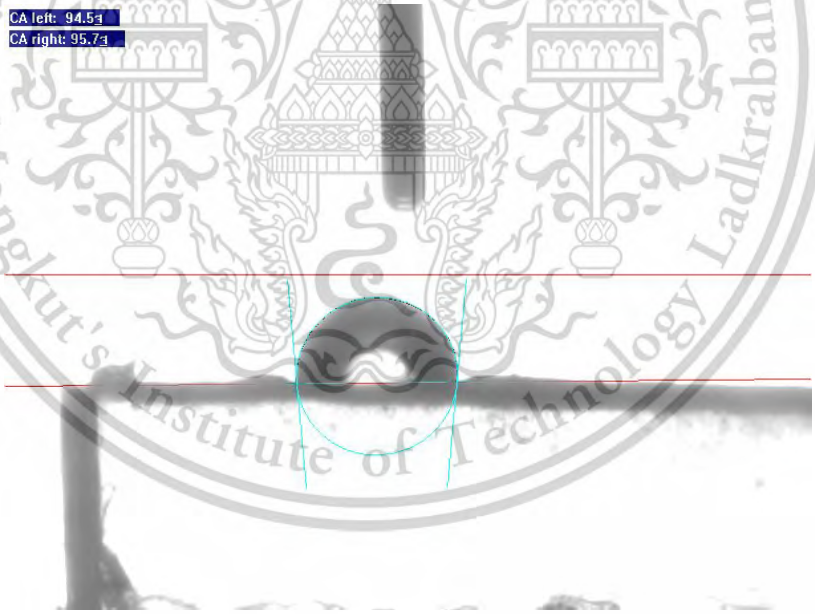

Figure C-4 Water droplet images of E33S2.0 membrane

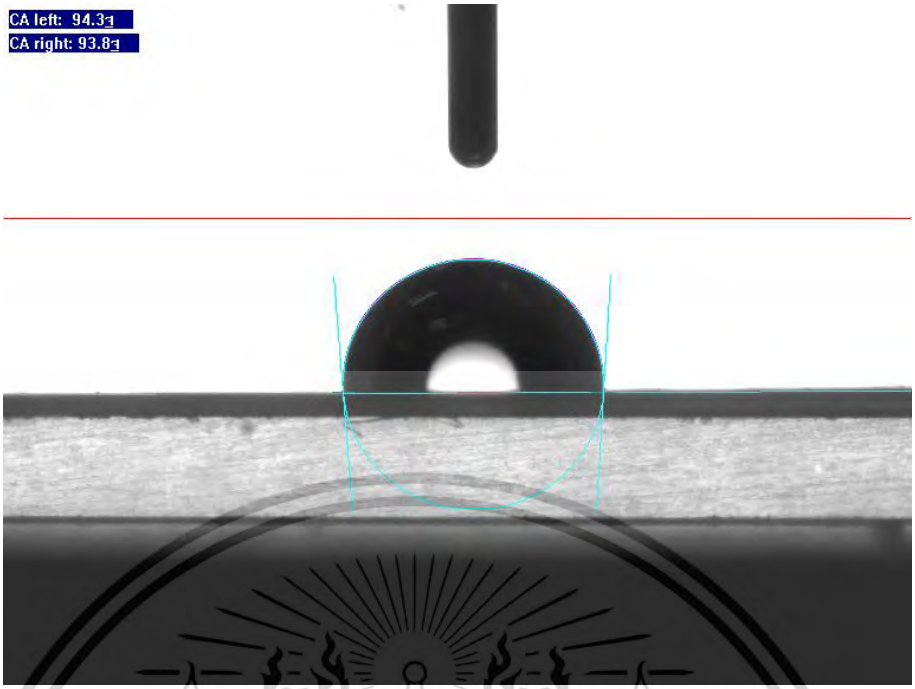

Figure C-5 Water droplet images of E28-18 membrane

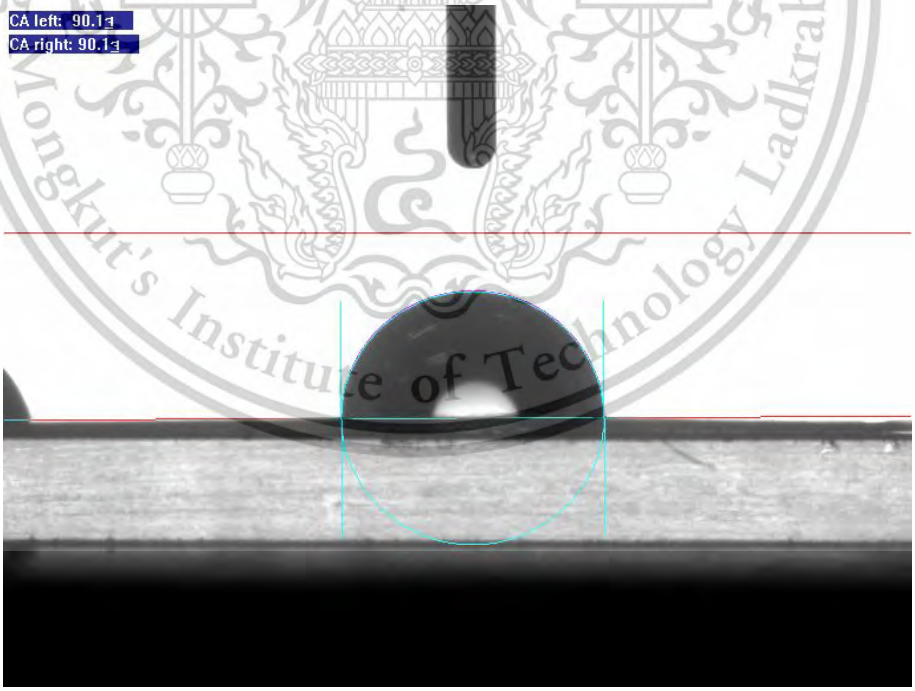

Figure C-6 Water droplet images of E28-18S0.5 membrane

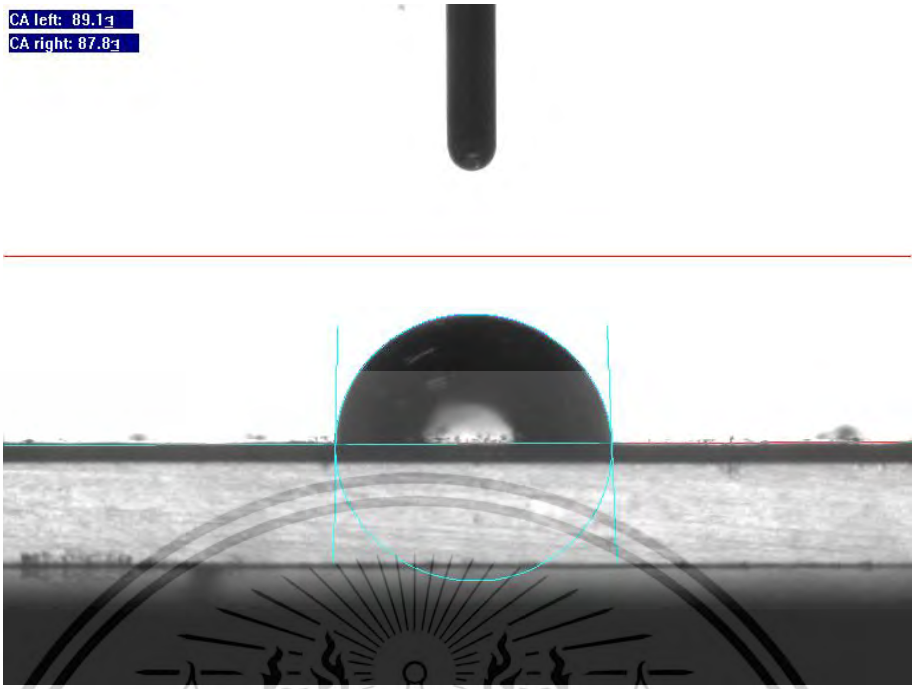

Figure C-7 Water droplet images of E28-18S0.75 membrane

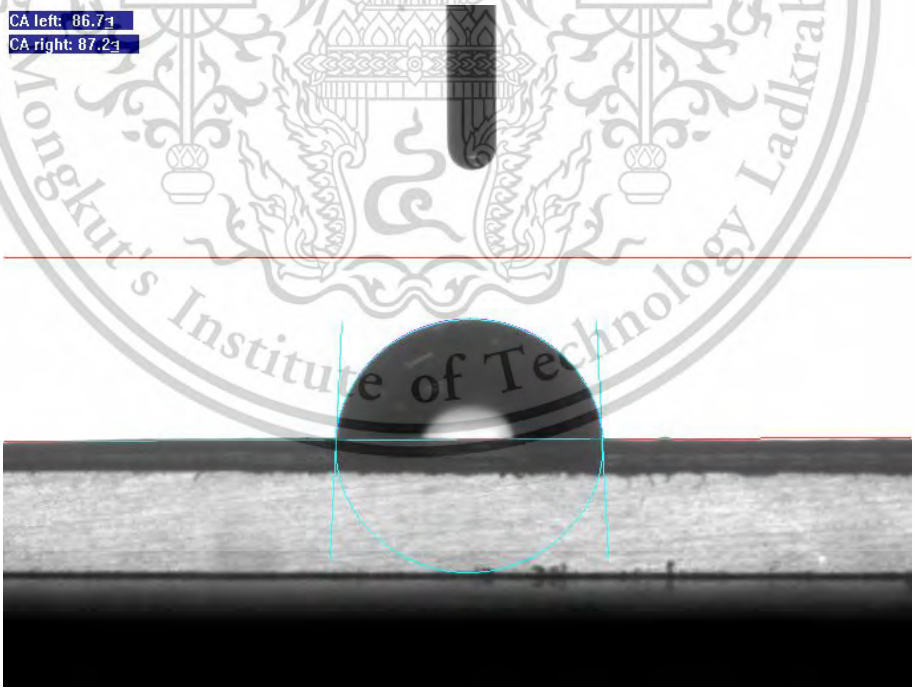

Figure C-8 Water droplet images of E28-18S1.0 membrane

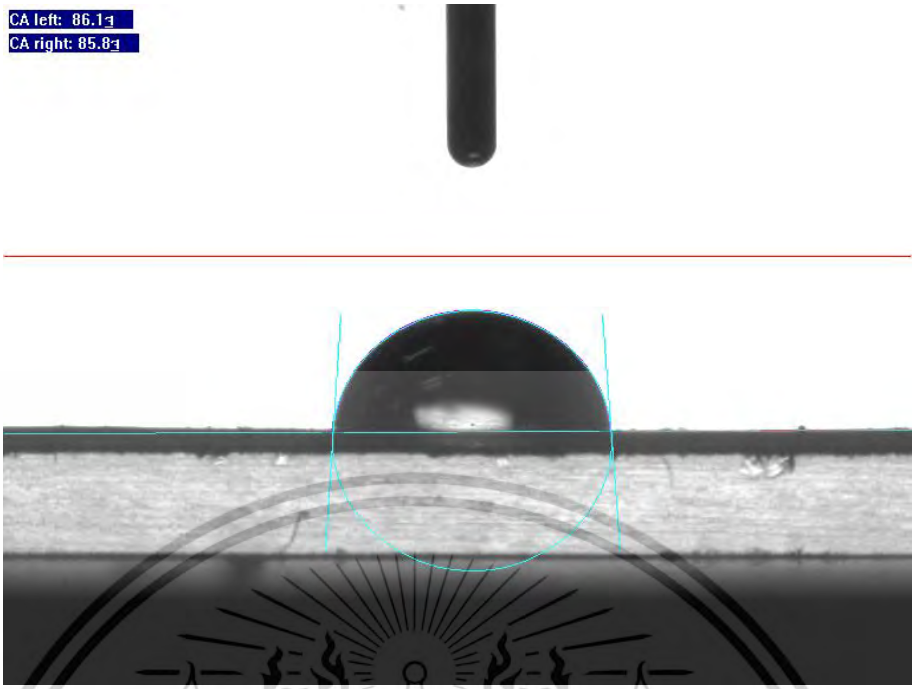

Figure C-9 Water droplet images of E28-18S0.5P0.5 membrane

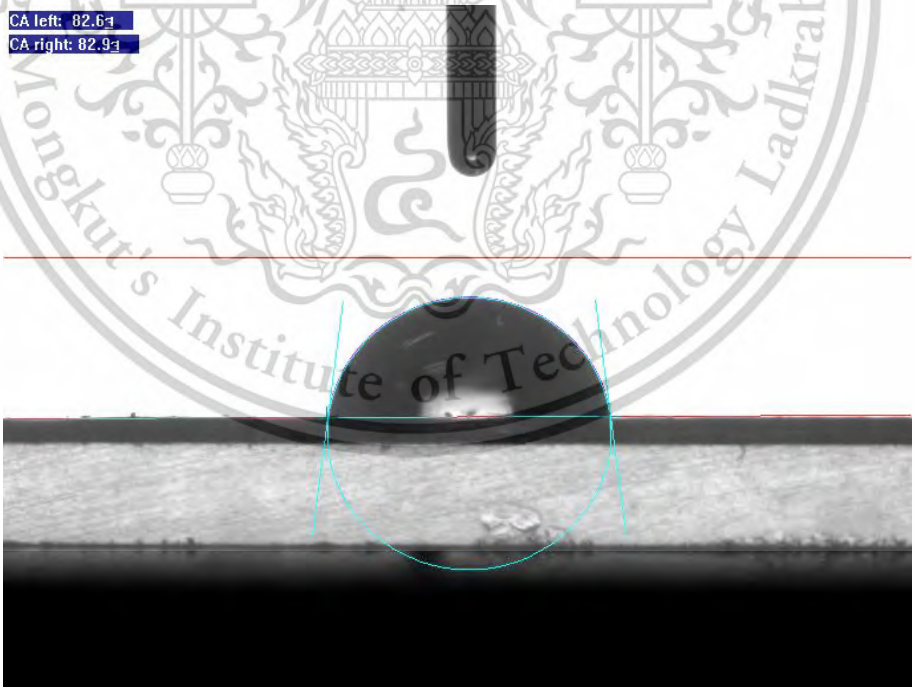

Figure C-10 Water droplet images of E28-18S0.5P1.0 membrane

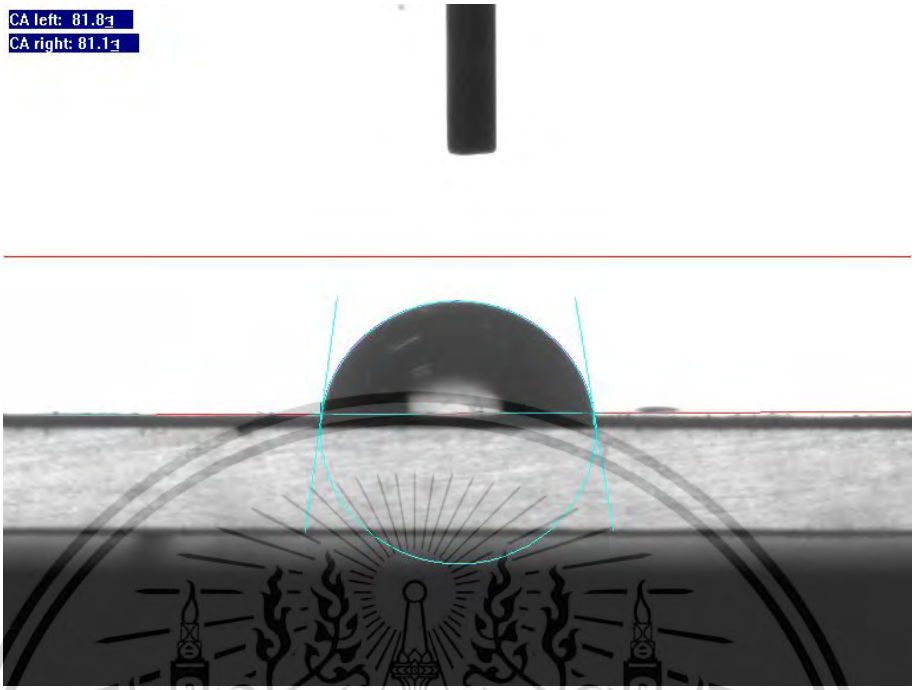

Figure C-11 Water droplet images of E28-18S0.5P1.5 membrane

Appendix D

Cross-sectional SEM/EDS elemental mapping images of membrane

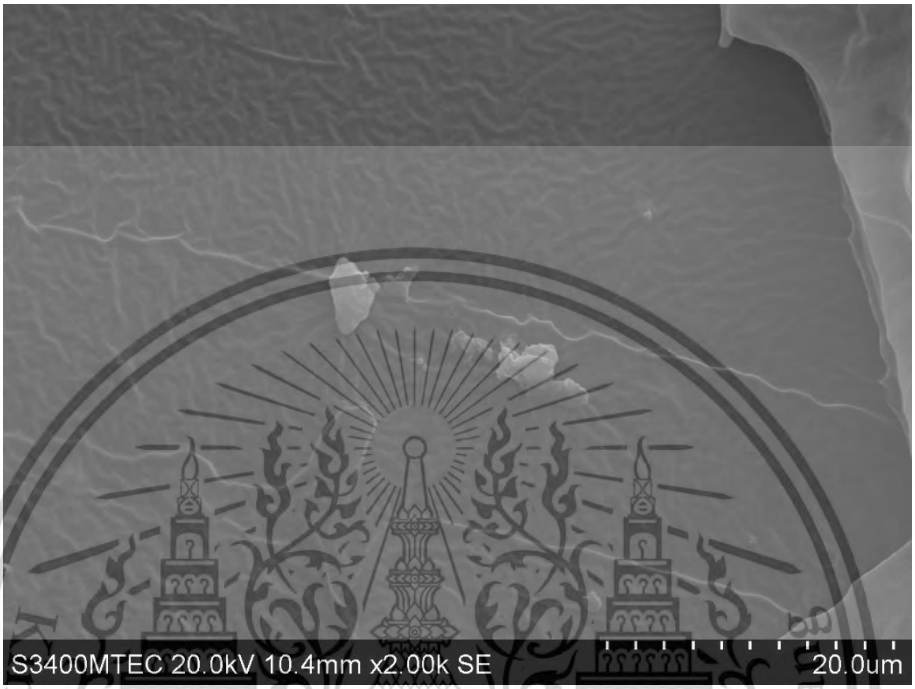

Figure D-1 Cross-sectional SEM image of E33S0.5 membrane

Figure D-2 EDS elemental mapping images of E33S0.5 membrane

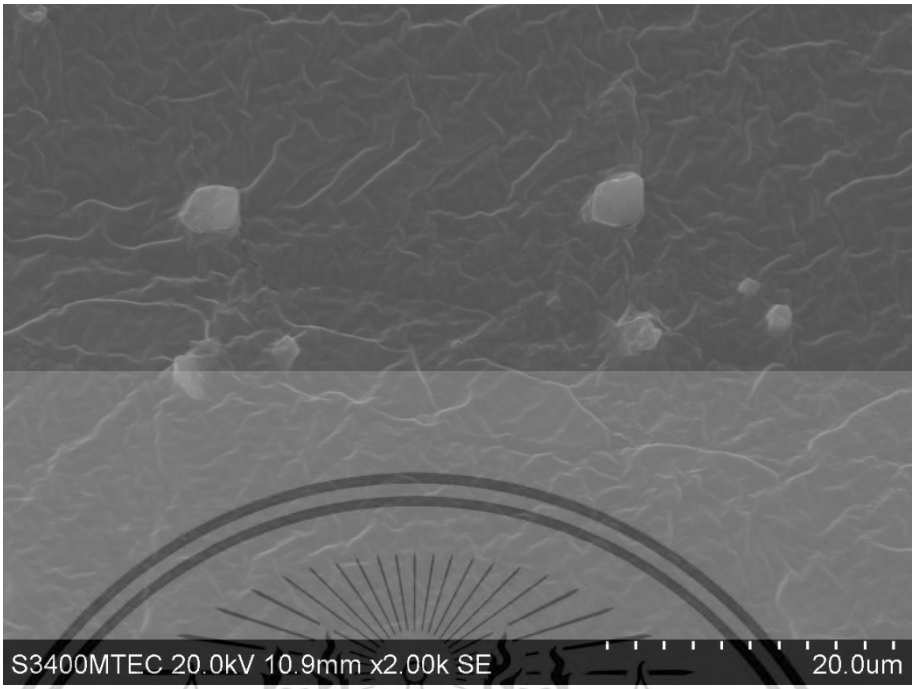

Figure D-3 Cross-sectional SEM image of E33S1.0 membrane

Figure D-4 EDS elemental mapping images of E33S1.0 membrane

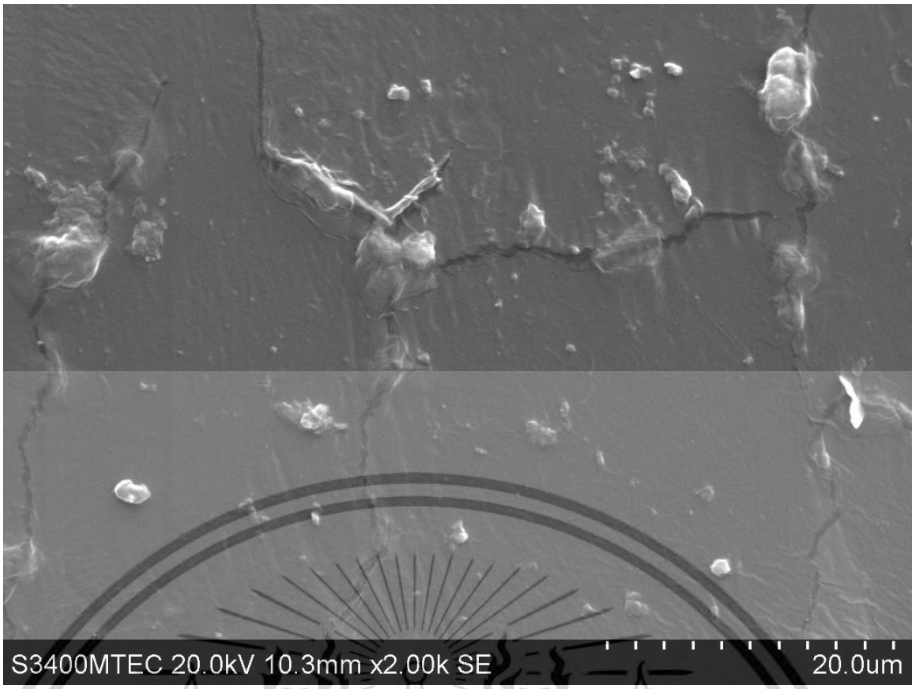

Figure D-5 Cross-sectional SEM image of E33S2.0 membrane

Figure D-6 EDS elemental mapping images of E33S2.0 membrane

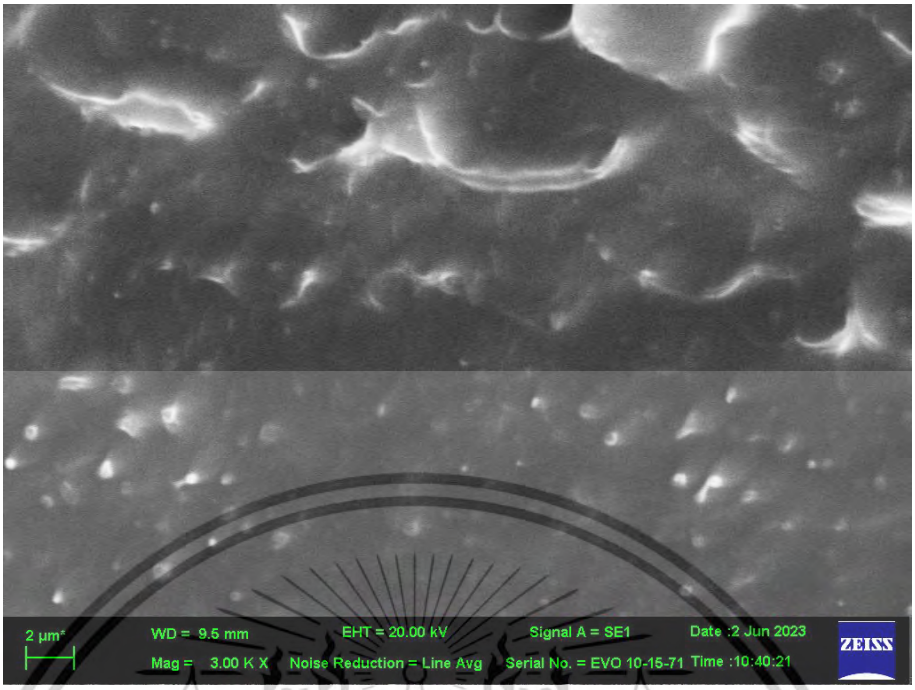

Figure D-7 Cross-sectional SEM image of E28-18S0.5 membrane

Figure D-8 EDS elemental mapping images of E28-18S0.5 membrane

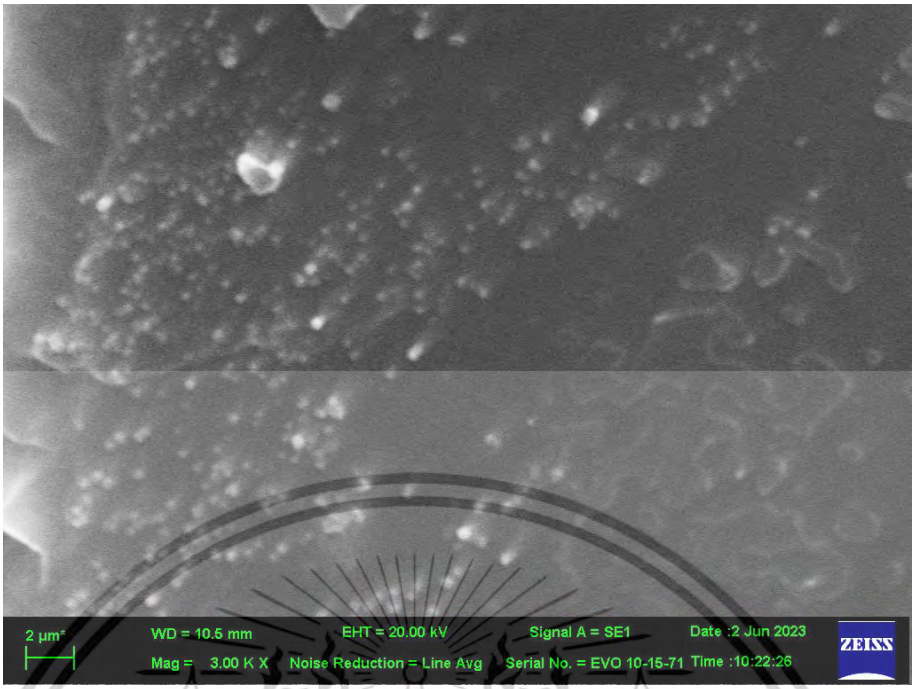

Figure D-9 Cross-sectional SEM image of E28-18S0.75 membrane

Figure D-10 EDS elemental mapping images of E28-18S0.75 membrane

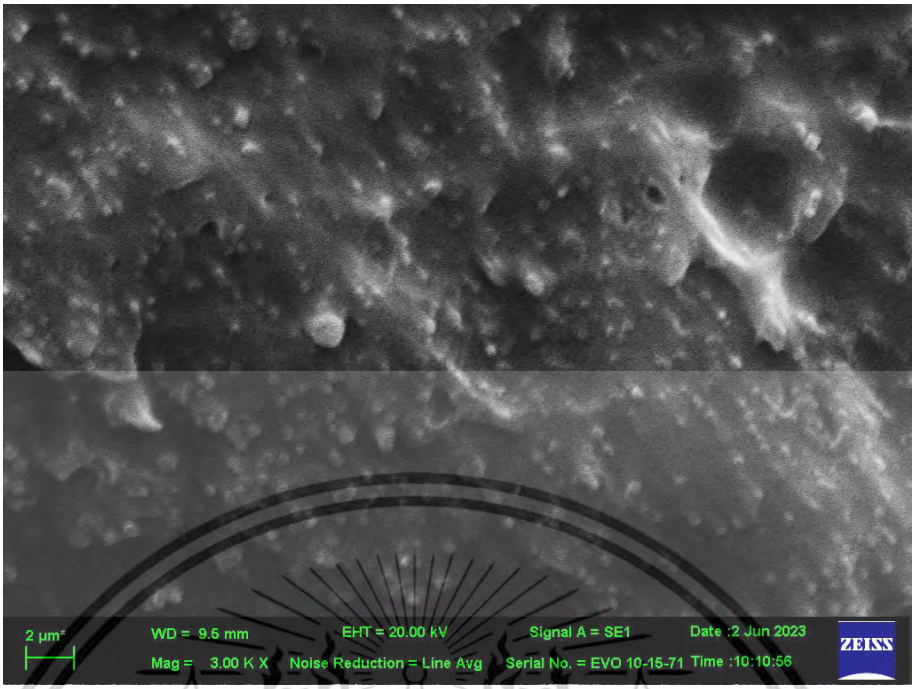

Figure D-11 Cross-sectional SEM image of E28-18S1.0 membrane

Figure D-12 EDS elemental mapping images of E28-18S1.0 membrane

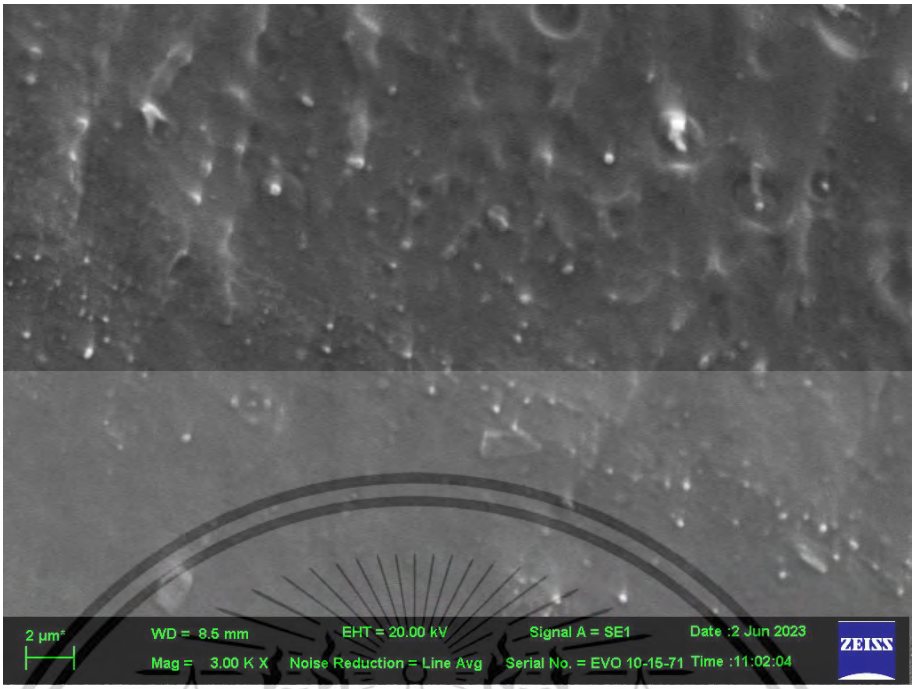

Figure D-13 Cross-sectional SEM image of E28-18S0.5P0.5 membrane

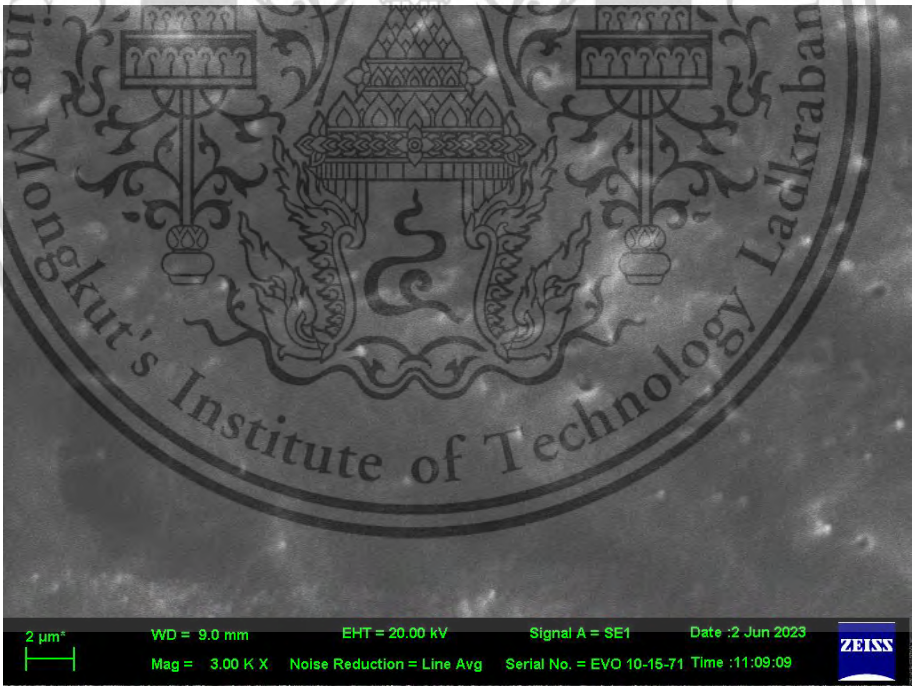

Figure D-14 Cross-sectional SEM image of E28-18S0.5P1.0 membrane

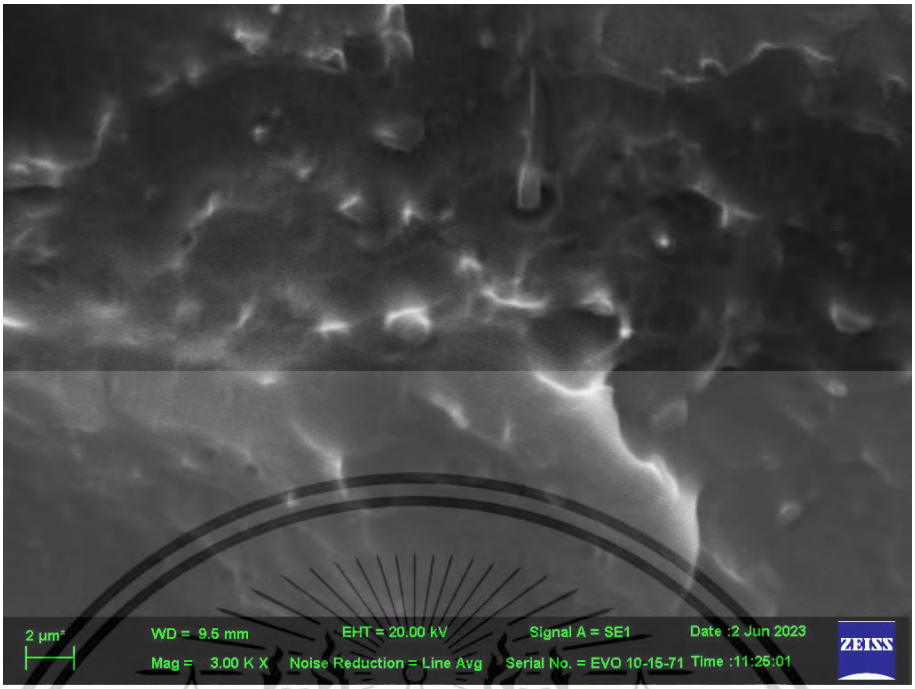

Figure D-15 Cross-sectional SEM image of E28-18S0.5P1.5 membrane

Appendix E

Mechanical properties of membrane

Table E-1 Mechanical properties of LDPE thin-flat membrane

Number	Stress (max) (MPa)	Elongation at break (%)	Young's modulus (MPa)
1	8.2	865	176.4
2	9.6	895	165.7
3	8.9	557	158.2
4	8.6	660	168.8
5	9.2	760	164.3
AVG	8.9	772	166.7
SD	0.5	105	0.7

Table E-2 Mechanical properties of E18 thin-flat membrane

Number	Stress (max) (MPa)	Elongation at break (%)	Young's modulus (MPa)
1	8.7	923	27.2
2	8.6	938	26.6
3	7.7	846	24.5
4	8.6	884	24.6
5	8.2	918	27.6
AVG	8.4	902	26.1
SD	0.4	37	1.5

Table E-3 Mechanical properties of E28 thin-flat membrane

Number	Stress (max) (MPa)	Elongation at break (%)	Young's modulus (MPa)
1	7.2	928	9.6
2	8.7	1005	8.6
3	8.8	1044	7.8
4	8.0	1020	8.9
5	8.3	961	8.5
AVG	8.2	992	8.7
SD	0.6	47	0.6

Table E-4 Mechanical properties of E33 thin-flat membrane

Number	Stress (max) (MPa)	Elongation at break (%)	Young's modulus (MPa)
1	3.3	1062	3.3
2	4.4	1045	3.4
3	4.1	1076	3.1
4	3.7	1081	3.4
5	4.1	1043	3.2
AVG	3.9	1061	3.3
SD	0.4	17	0.1

Table E-5 Mechanical properties of E33S0.5 thin-flat membrane

Number	Stress (max) (MPa)	Elongation at break (%)	Young's modulus (MPa)
1	3.1	1154	3.4
2	5.5	1342	3.3
3	4.2	1434	3.5
4	4.4	1335	3.4
5	4.1	1284	3.6
AVG	4.2	1310	3.4
SD	0.8	102	0.1

Table E-6 Mechanical properties of E33S1.0 thin-flat membrane

Number	Stress (max) (MPa)	Elongation at break (%)	Young's modulus (MPa)
1	5.4	1283	2.9
2	3.3	1190	2.7
3	6.2	1303	3.4
4	5.2	1236	3.3
5	4.5	1278	2.7
AVG	4.9	1258	3.0
SD	1.1	45	0.3

Table E-7 Mechanical properties of E33S2.0 thin-flat membrane

Number	Stress (max) (MPa)	Elongation at break (%)	Young's modulus (MPa)
1	3.9	1068	3.4
2	3.6	1049	2.9
3	3.8	1065	3.6
4	3.9	1028	3.1
5	3.7	1091	3.5
AVG	3.8	1060	3.3
SD	0.1	23	0.3

Table E-8 Mechanical properties of E18 membrane

Number	Stress (max) (MPa)	Elongation at break (%)	Young's modulus (MPa)
1	10.3	863	27.7
2	10.9	887	27.2
3	11.0	874	28.3
4	11.1	929	28.6
5	12.8	929	28.9
6	6.9	653	26.7
7	12.4	900	30.0
AVG	10.8	863	28.2
SD	1.9	95	1.1

Table E-9 Mechanical properties of E28 membrane

Number	Stress (max) (MPa)	Elongation at break (%)	Young's modulus (MPa)
1	6.3	661	13.8
2	4.9	523	14.2
3	5.6	633	14.0
4	6.7	660	14.2
5	6.8	646	13.9
6	8.8	788	13.4
7	6.5	681	14.7
AVG	6.5	656	14.0
SD	1.2	78	0.4

Table E-10 Mechanical properties of E28-18 membrane

Number	Stress (max) (MPa)	Elongation at break (%)	Young's modulus (MPa)
1	11.6	1055	18.9
2	10.4	1019	18.8
3	9.4	1000	20.1
4	8.1	879	20.0
5	12.5	1132	19.1
AVG	10.4	1017	19.4
SD	1.7	92	0.6

Table E-11 Mechanical properties of E28-18S0.5 membrane

Number	Stress (max) (MPa)	Elongation at break (%)	Young's modulus (MPa)
1	11.7	870	36.5
2	13.6	955	27.5
3	11.6	905	30.1
4	11.1	873	30.4
5	10.5	910	29.2
AVG	11.7	902	30.8
SD	1.2	34	3.4

Table E-12 Mechanical properties of E28-18S0.75 membrane

Number	Stress (max) (MPa)	Elongation at break (%)	Young's modulus (MPa)
1	9.2	906	25.8
2	11.7	1005	24.7
3	8.5	878	21.7
4	10.2	931	26.4
5	11.2	997	27.1
AVG	10.1	944	25.1
SD	1.3	56	2.1

Table E-13 Mechanical properties of E28-18S1.0 membrane

Number	Stress (max) (MPa)	Elongation at break (%)	Young's modulus (MPa)
1	10.0	919	19.7
2	11.2	948	20.2
3	10.2	877	21.4
4	10.9	885	21.8
5	10.7	890	20.1
AVG	10.6	904	20.6
SD	0.5	29	0.9

Table E-14 Mechanical properties of E28-18S0.5P0.5 membrane

Number	Stress (max) (MPa)	Elongation at break (%)	Young's modulus (MPa)
1	13.2	1003	21.6
2	12.1	988	18.9
3	12.3	1003	18.7
4	10.1	927	21.6
5	11.7	1063	19.7
AVG	11.9	997	20.1
SD	1.1	49	1.4

Table E-15 Mechanical properties of E28-18S0.5P1.0 membrane

Number	Stress (max) (MPa)	Elongation at break (%)	Young's modulus (MPa)
1	12.0	925	17.7
2	9.8	873	18.6
3	11.1	868	18.2
4	12.5	949	18.2
5	10.8	934	16.7
AVG	11.2	910	17.9
SD	1.1	37	0.7

Table E-16 Mechanical properties of E28-18S0.5P1.5 membrane

Number	Stress (max) (MPa)	Elongation at break (%)	Young's modulus (MPa)
1	12.5	841	13.8
2	14.5	910	19.0
3	10.9	824	16.0
4	13.3	853	17.8
5	9.7	771	17.0
AVG	12.2	840	16.7
SD	1.9	50	2.0

Appendix F

Storage modulus, loss modulus and tan delta of membrane

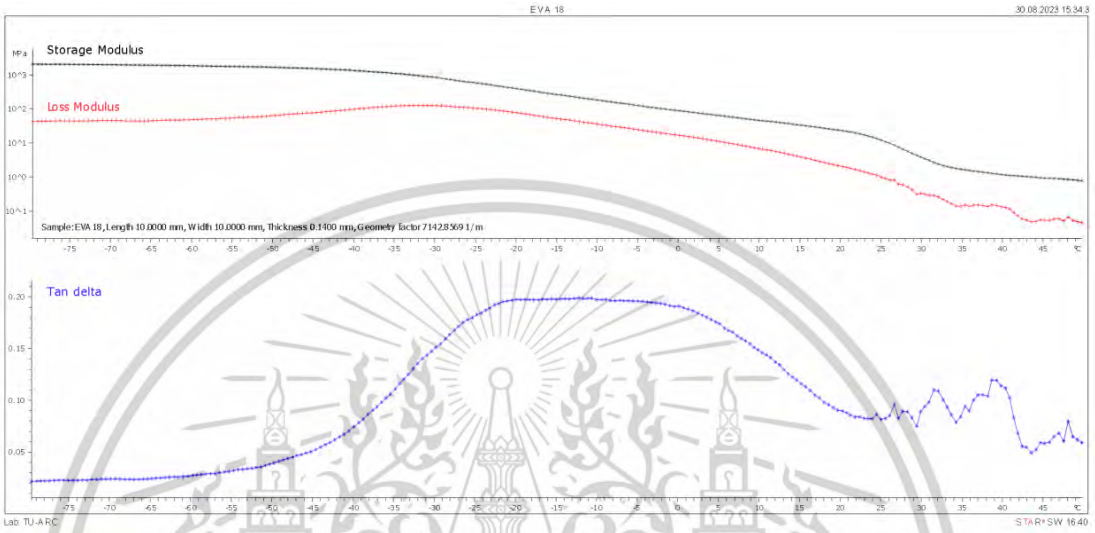

Figure F-1 Storage modulus, loss modulus and tan delta of E18 membrane

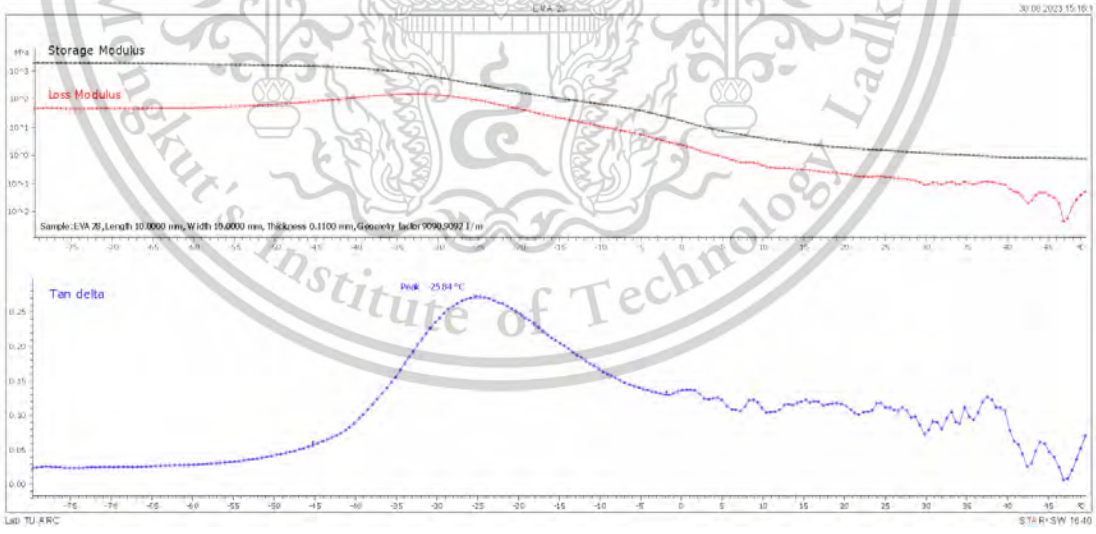

Figure F-2 Storage modulus, loss modulus and tan delta of E28 membrane

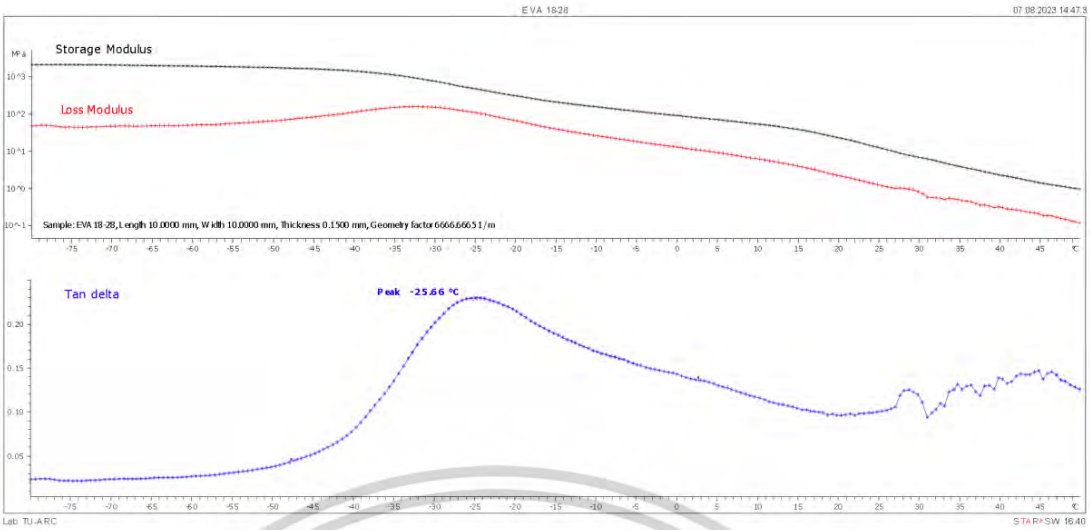

Figure F-3 Storage modulus, loss modulus and tan delta of E28-18 membrane

Appendix G

Peel strength of thin-tubular membrane

Table G-1 Peel strength of E18, E28 and E28-18 membranes

Number	Peel strength (N/m^2)		
	E18	E28	E28-18
1	0.18	0.31	0.22
2	0.18	0.31	0.18
3	0.18	0.31	0.22
4	0.17	0.31	0.18
5	0.13	0.35	0.21
AVG	0.17	0.32	0.20
SD	0.02	0.02	0.02

Appendix H

Gas permeation of membrane

Table H-1 CO_2 flux of LDPE thin-flat membrane

Number	Area sample	Area standard	Flow rate (mL/min)	Membrane area (m^2)	CO_2 permeation (mL/min)	CO_2 flux (mL/m^2.s)
1	0.36	99.25	30	0.0025	0.11	0.73
2	0.36	98.88	30	0.0025	0.11	0.73
3	0.34	98.7	30	0.0025	0.10	0.69
Average					0.11	0.71
SD					0.01	0.02

Table H-2 CH_4 flux of LDPE thin-flat membrane

Number	Area sample	Area standard	Flow rate (mL/min)	Membrane area (m^2)	CH_4 permeation (mL/min)	CH_4 flux (mL/m^2.s)
1	0.32	85.89	30	0.0025	0.11	0.75
2	0.31	88.26	30	0.0025	0.11	0.70
3	0.28	89.58	30	0.0025	0.09	0.63
Average					0.10	0.69
SD					0.01	0.06

Table H-3 CO_2 flux of E18 thin-flat membrane

Number	Area sample	Area standard	Flow rate (mL/min)	Membrane area (m^2)	CO_2 permeation (mL/min)	CO_2 flux (mL/m^2.s)
1	0.77	99.16	30	0.0025	0.23	1.55
2	0.76	99.16	30	0.0025	0.23	1.53
3	0.76	99.07	30	0.0025	0.23	1.53
Average					0.23	1.54
SD					0.00	0.01

Table H-4 CH_4 flux of E18 thin-flat membrane

Number	Area sample	Area standard	Flow rate (mL/min)	Membrane area (m^2)	CH_4 permeation (mL/min)	CH_4 flux (mL/m^2.s)
1	0.19	84.74	30	0.0025	0.07	0.45
2	0.17	84.98	30	0.0025	0.06	0.40
3	0.18	84	30	0.0025	0.06	0.43
Average					0.06	0.43
SD					0.01	0.03

Table H-5 CO_2 flux of E28 thin-flat membrane

Number	Area sample	Area standard	Flow rate (mL/min)	Membrane area (m^2)	CO_2 permeation (mL/min)	CO_2 flux (mL/m^2.s)
1	1.01	101.48	30	0.0025	0.29	1.99
2	0.97	102.96	30	0.0025	0.28	1.88
3	0.94	102.41	30	0.0025	0.27	1.83
Average					0.28	1.90
SD					0.01	0.08

Table H-6 CH_4 flux of E28 thin-flat membrane

Number	Area sample	Area standard	Flow rate (mL/min)	Membrane area (m^2)	CH_4 permeation (mL/min)	CH_4 flux (mL/m^2.s)
1	0.18	83.59	30	0.0025	0.06	0.43
2	0.18	83.92	30	0.0025	0.06	0.43
3	0.18	84.08	30	0.0025	0.06	0.43
Average					0.06	0.43
SD					0.00	0.00

Table H-7 CO_2 flux of E33 thin-flat membrane

Number	Area sample	Area standard	Flow rate (mL/min)	Membrane area (m^2)	CO_2 permeation (mL/min)	CO_2 flux ($mL/m^2.s$)
1	1.08	103.8	30	0.0025	0.31	2.08
2	1.07	105.46	30	0.0025	0.30	2.03
3	1.03	104.91	30	0.0025	0.29	1.96
Average					0.30	2.02
SD					0.01	0.06

Table H-8 CH_4 flux of E33 thin-flat membrane

Number	Area sample	Area standard	Flow rate (mL/min)	Membrane area (m^2)	CH_4 permeation (mL/min)	CH_4 flux ($mL/m^2.s$)
1	0.19	85.39	30	0.0025	0.07	0.45
2	0.18	86.21	30	0.0025	0.06	0.42
3	0.17	86.79	30	0.0025	0.06	0.39
Average					0.06	0.42
SD					0.01	0.03

Table H-9 CO_2 flux of E33S0.5 thin-flat membrane

Number	Area sample	Area standard	Flow rate (mL/min)	Membrane area (m^2)	CO_2 permeation (mL/min)	CO_2 flux ($mL/m^2.s$)
1	0.96	85.17	30	0.0025	0.34	2.25
2	0.97	85.17	30	0.0025	0.34	2.28
3	0.94	85.17	30	0.0025	0.33	2.21
Average					0.34	2.25
SD					0.01	0.04

Table H-10 CH_4 flux of E33S0.5 thin-flat membrane

Number	Area sample	Area standard	Flow rate (mL/min)	Membrane area (m^2)	CH_4 permeation (mL/min)	CH_4 flux (mL/m^2.s)
1	0.18	69.89	30	0.0025	0.08	0.52
2	0.18	69.89	30	0.0025	0.08	0.52
3	0.16	69.89	30	0.0025	0.07	0.46
Average					0.07	0.50
SD					0.01	0.03

Table H-11 CO_2 flux of E33S1.0 thin-flat membrane

Number	Area sample	Area standard	Flow rate (mL/min)	Membrane area (m^2)	CO_2 permeation (mL/min)	CO_2 flux (mL/m^2.s)
1	1.9	87.17	30	0.0025	0.65	4.36
2	1.81	87.17	30	0.0025	0.62	4.15
3	1.9	87.17	30	0.0025	0.65	4.36
Average					0.64	4.29
SD					0.02	0.12

Table H-12 CH_4 flux of E33S1.0 thin-flat membrane

Number	Area sample	Area standard	Flow rate (mL/min)	Membrane area (m^2)	CH_4 permeation (mL/min)	CH_4 flux (mL/m^2.s)
1	0.18	71.5	30	0.0025	0.08	0.50
2	0.19	71.5	30	0.0025	0.08	0.53
3	0.18	71.5	30	0.0025	0.08	0.50
Average					0.08	0.51
SD					0.00	0.02

Table H-13 CO_2 flux of E33S2.0 thin-flat membrane

Number	Area sample	Area standard	Flow rate (mL/min)	Membrane area (m^2)	CO_2 permeation (mL/min)	CO_2 flux (mL/m^2.s)
1	2.46	82.48	30	0.0025	0.89	5.97
2	2.5	82.48	30	0.0025	0.91	6.06
3	2.44	82.48	30	0.0025	0.89	5.92
Average					0.90	5.98
SD					0.01	0.07

Table H-14 CH_4 flux of E33S2.0 thin-flat membrane

Number	Area sample	Area standard	Flow rate (mL/min)	Membrane area (m^2)	CH_4 permeation (mL/min)	CH_4 flux (mL/m^2.s)
1	0.19	72.27	30	0.0025	0.08	0.53
2	0.19	72.27	30	0.0025	0.08	0.53
3	0.18	72.27	30	0.0025	0.07	0.50
Average					0.08	0.52
SD					0.01	0.02

Table H-15 Gas separation of E18 membrane

Before connecting module

Feed gas (mL/min)	Membrane area (m^2)	ΔP (atm)	Gas ratio (%)					Normalize (%)		Feed gas (mL/min)	
			CH_4	CO_2	O_2	H_2S	Bal.	CH_4	CO_2	CH_4	CO_2
202.38	1.20	0.0020	62.4	38.1	0.2	1 ppm	0	62.1	37.9	125.65	76.72

After connecting module

Time (min)	Vent gas (mL/min)	ΔP (atm)	Gas ratio (%)					Normalize (%)		Retentate (mL/min)		Permeate (mL/min)		Total (mL/min)	Permeate ($mL/m^2.s$)		CO_2/CH_4 Selectivity	CH_4 purity (%)
			CH_4	CO_2	O_2	H_2S	Bal.	CH_4	CO_2	CH_4	CO_2	CH_4	CO_2		CH_4	CO_2		
20	178.73	0.0023	64.4	33.6	0	1 ppm	2.1	65.7	34.3	117.45	61.27	8.20	15.44	23.64	0.11	0.21	2.82	65.71
40	178.25	0.0023	63.5	33.6	0	1 ppm	2.9	65.3	34.6	116.56	61.68	9.08	15.04	24.13	0.13	0.20	2.48	65.39
60	178.10	0.0023	63.3	33.4	0	1 ppm	3.3	65.4	34.5	116.58	61.51	9.07	15.20	24.28	0.13	0.21	2.51	65.46
80	178.02	0.0023	63.3	33.4	0	1 ppm	3.3	65.4	34.5	116.53	61.48	9.12	15.23	24.36	0.13	0.21	2.50	65.46
100	177.90	0.0023	63.2	33.3	0	1 ppm	3.4	65.4	34.5	116.51	61.38	9.14	15.33	24.48	0.13	0.21	2.51	65.49
120	178.20	0.0023	63.3	33.5	0	1 ppm	3.3	65.3	34.6	116.52	61.67	9.12	15.05	24.18	0.13	0.20	2.47	65.39
Avg (40-120 min)										116.54	61.54	9.11	15.17	24.28	0.13	0.21	2.42	65.44
SD										0.03	0.13	0.03	0.12	0.14	0.00	0.01	0.02	0.05

Table H-16 Gas separation of E28 membrane

Before connecting module

Feed gas (mL/min)	Membrane area (m^2)	ΔP (atm)	Gas ratio (%)					Normalize (%)		Feed gas (mL/min)	
			CH_4	CO_2	O_2	H_2S	Bal.	CH_4	CO_2	CH_4	CO_2
207.53	1.20	0.0020	61.0	38.3	2.0	0 ppm	0	61.43	38.56	127.48	80.04

After connecting module

Time (min)	Vent gas (mL/min)	ΔP (atm)	Gas ratio (%)					Normalize (%)		Retentate (mL/min)		Permeate (mL/min)		Total (mL/min)	Permeate ($mL/m^2.s$)		CO_2/CH_4 Selectivity	CH_4 purity (%)
			CH_4	CO_2	O_2	H_2S	Bal.	CH_4	CO_2	CH_4	CO_2	CH_4	CO_2		CH_4	CO_2		
20	171.09	0.0064	63.0	32.7	1.7	0 ppm	2.6	65.83	34.16	112.63	58.46	14.85	21.58	36.44	0.20	0.29	2.17	65.83
40	169.15	0.0054	63.8	32.5	1.4	0 ppm	2.2	66.25	33.74	112.06	57.08	15.42	22.95	38.38	0.21	0.31	2.23	66.25
60	168.10	0.0053	63.8	32.8	1.3	0 ppm	2.2	66.04	33.95	111.02	57.07	16.46	22.96	39.42	0.22	0.31	2.09	66.04
80	171.72	0.0055	63.6	32.8	1.6	0 ppm	2.0	65.97	34.02	113.29	58.42	14.19	21.61	35.80	0.19	0.30	2.28	65.97
100	172.56	0.0052	63.6	32.7	1.6	0 ppm	2.0	66.04	33.95	113.96	58.59	13.52	21.44	34.97	0.18	0.29	2.37	66.04
120	172.88	0.0052	63.3	32.7	1.5	0 ppm	2.2	65.93	34.06	113.99	58.89	13.48	21.15	34.64	0.18	0.29	2.35	65.93
Avg (20-120 min)										112.82	58.10	14.65	21.94	36.60	0.20	0.30	2.25	66.00
SD										1.16	0.80	1.63	0.80	1.91	0.02	0.01	0.11	0.14

Table H-17 Gas separation of E28-18 membrane

Before connecting module

Feed gas (mL/min)	Membrane area (m^2)	ΔP (atm)	Gas ratio (%)					Normalize (%)		Feed gas (mL/min)	
			CH_4	CO_2	O_2	H_2S	Bal.	CH_4	CO_2	CH_4	CO_2
195.57	1.20	0.0020	62.1	38.0	0.9	0	0	62.05	37.95	121.35	74.22

After connecting module

Time (min)	Vent gas (mL/min)	ΔP (atm)	Gas ratio (%)					Normalize (%)		Retentate (mL/min)		Permeate (mL/min)		Total (mL/min)	Permeate ($mL/m^2.s$)		CO_2/CH_4 Selectivity	CH_4 purity (%)
			CH_4	CO_2	O_2	H_2S	Bal.	CH_4	CO_2	CH_4	CO_2	CH_4	CO_2		CH_4	CO_2		
20	177.94	0.0025	65.2	34.7	0	0	1.9	65.24	34.76	116.08	61.85	5.26	12.36	17.63	0.07	0.17	3.52	65.24
40	175.75	0.0025	64.0	33.6	0.1	0	1.0	65.59	34.40	115.28	60.46	6.06	13.75	19.82	0.08	0.19	3.39	65.59
60	172.12	0.0025	65.8	34.2	0	1 ppm	1.6	65.85	34.15	113.34	58.77	8.01	15.43	23.45	0.11	0.21	2.89	65.85
80	171.14	0.0025	65.9	34.1	0	0	2.2	65.95	34.05	112.86	58.27	8.48	15.94	24.43	0.12	0.22	2.81	65.95
100	169.20	0.0025	66.0	34.0	0	0	2.6	66.02	33.98	111.70	57.49	9.64	16.72	26.37	0.13	0.23	2.60	66.02
120	168.73	0.0025	66.3	33.7	0	0	2.8	66.26	33.73	111.81	56.91	9.53	17.30	26.84	0.13	0.24	2.72	66.26
Avg (60-120 min)										112.43	57.86	8.91	16.35	25.27	0.12	0.23	2.88	66.02
SD										0.80	0.82	0.80	0.83	1.60	0.01	0.01	0.12	0.17

Table H-18 Gas separation of E28-18S0.5 membrane

Before connecting module

Feed gas (mL/min)	Membrane area (m^2)	ΔP (atm)	Gas ratio (%)					Normalize (%)		Feed gas (mL/min)	
			CH_4	CO_2	O_2	H_2S	Bal.	CH_4	CO_2	CH_4	CO_2
200.49	1.20	0.0020	60.7	37.2	1	1 ppm	1.1	62.00	37.99	124.30	76.18

After connecting module

Time (min)	Vent gas (mL/min)	ΔP (atm)	Gas ratio (%)					Normalize (%)		Retentate (mL/min)		Permeate (mL/min)		Total (mL/min)	Permeate ($mL/m^2.s$)		CO_2/CH_4 Selectivity	CH_4 purity (%)
			CH_4	CO_2	O_2	H_2S	Bal.	CH_4	CO_2	CH_4	CO_2	CH_4	CO_2		CH_4	CO_2		
20	176.99	0.0025	62.3	31.3	3.3	2 ppm	3	66.55	33.44	117.80	59.18	6.50	16.99	23.50	0.09	0.23	3.92	66.55
40	179.42	0.0025	61.5	31.6	3.3	1 ppm	3.6	66.05	33.94	118.52	60.89	5.78	15.28	21.07	0.08	0.21	3.96	66.05
60	179.67	0.0025	61.4	31.7	3.3	0	3.6	65.95	34.04	118.49	61.17	5.81	15.00	20.82	0.08	0.20	3.87	65.95
80	179.23	0.0025	61.5	31.6	3.3	1 ppm	3.6	66.05	33.94	118.39	60.83	5.91	15.34	21.26	0.08	0.21	3.89	66.05
100	179.42	0.0025	61.4	31.7	3.3	0	3.6	65.95	34.04	118.32	61.09	5.97	15.09	21.07	0.08	0.20	3.78	65.95
120	179.42	0.0025	61.5	31.6	3.3	1 ppm	3.6	66.05	33.94	118.52	60.89	5.78	15.28	21.07	0.08	0.21	3.96	66.05
Avg (40-120 min)										118.45	60.97	5.85	15.20	21.05	0.08	0.21	3.89	66.01
SD										0.09	0.15	0.09	0.15	0.16	0.00	0.01	0.07	0.05

Table H-19 Gas separation of E28-18S0.75 membrane

Before connecting module

Feed gas (mL/min)	Membrane area (m^2)	ΔP (atm)	Gas ratio (%)					Normalize (%)		Feed gas (mL/min)	
			CH_4	CO_2	O_2	H_2S	Bal.	CH_4	CO_2	CH_4	CO_2
201.02	1.20	0.0020	59.7	37.8	1.3	1 ppm	1.3	61.23	38.76	123.08	77.93

After connecting module

Time (min)	Vent gas (mL/min)	ΔP (atm)	Gas ratio (%)					Normalize (%)		Retentate (mL/min)		Permeate (mL/min)		Total (mL/min)	Permeate ($mL/m^2.s$)		CO_2/CH_4 Selectivity	CH_4 purity (%)
			CH_4	CO_2	O_2	H_2S	Bal.	CH_4	CO_2	CH_4	CO_2	CH_4	CO_2		CH_4	CO_2		
20	-	-	-	-	-	-	-	-	-	-	-	-	-	-	-	-	-	-
40	171.56	0.0022	63.4	31.9	0.4	0	5.4	66.52	33.47	114.13	57.42	8.95	20.50	29.46	0.12	0.28	3.43	66.52
60	169.53	0.0022	63.3	31.6	0.4	1 ppm	5.6	66.70	33.29	113.07	56.45	10.00	21.48	31.49	0.13	0.29	3.22	66.70
80	169.72	0.0022	63.3	31.6	0.4	1 ppm	5.7	66.70	33.29	113.20	56.51	9.87	21.42	31.30	0.13	0.29	3.25	66.70
100	169.53	0.0022	63.3	31.6	0.4	1 ppm	5.6	66.70	33.29	113.07	56.45	10.00	21.48	31.49	0.13	0.29	3.22	66.70
120	169.72	0.0022	63.3	31.6	0.4	1 ppm	5.7	66.70	33.29	113.20	56.51	9.87	21.42	31.30	0.13	0.29	3.25	66.70
Avg (60-120 min)										113.14	56.48	9.94	21.45	31.40	0.13	0.29	3.23	66.70
SD										0.08	0.03	0.08	0.03	0.11	0.00	0.00	0.02	0.00

Table H-20 Gas separation of E28-18S1.0 membrane

Before connecting module

Feed gas (mL/min)	Membrane area (m^2)	ΔP (atm)	Gas ratio (%)					Normalize (%)		Feed gas (mL/min)	
			CH_4	CO_2	O_2	H_2S	Bal.	CH_4	CO_2	CH_4	CO_2
200.8	1.20	0.0020	61.9	38	0.3	3 ppm	0	61.96	38.04	124.42	76.38

After connecting module

Time (min)	Vent gas (mL/min)	ΔP (atm)	Gas ratio (%)					Normalize (%)		Retentate (mL/min)		Permeate (mL/min)		Total (mL/min)	Permeate ($mL/m^2.s$)		CO_2/CH_4 Selectivity	CH_4 purity (%)
			CH_4	CO_2	O_2	H_2S	Bal.	CH_4	CO_2	CH_4	CO_2	CH_4	CO_2		CH_4	CO_2		
20	171.40	0.0022	64.1	32.8	0	1 ppm	3.1	66.15	33.84	113.38	58.01	11.03	18.36	29.40	0.15	0.25	2.49	66.15
40	168.94	0.0022	64.0	32.4	0	2 ppm	3.6	66.39	33.60	112.15	56.78	12.26	19.59	31.86	0.17	0.27	2.39	66.39
60	167.22	0.0022	64.0	32.4	0	2 ppm	3.6	66.39	33.60	111.01	56.20	13.40	20.17	33.58	0.18	0.28	2.25	66.39
80	167.22	0.0022	65.4	32.3	0	4 ppm	2.9	66.93	33.060	111.93	55.28	12.48	21.09	33.58	0.17	0.29	2.53	66.93
100	167.22	0.0022	65.5	32.4	0	2 ppm	3.6	66.90	33.09	111.87	55.34	12.54	21.03	33.58	0.17	0.29	2.51	66.90
120	167.22	0.0022	65.6	32.2	0	2 ppm	3.6	67.07	32.92	112.16	55.05	12.25	21.32	33.58	0.17	0.29	2.60	67.07
Avg (60-120 min)										111.74	55.47	12.67	20.90	33.58	0.17	0.29	2.48	66.82
SD										0.50	0.50	0.50	0.50	0.00	0.01	0.01	0.15	0.30

Table H-21 Gas separation of E28-18S0.5P0.5 membrane

Before connecting module

Feed gas (mL/min)	Membrane area (m^2)	ΔP (atm)	Gas ratio (%)					Normalize (%)		Feed gas (mL/min)	
			CH_4	CO_2	O_2	H_2S	Bal.	CH_4	CO_2	CH_4	CO_2
199.60	1.20	0.0020	61.3	38.6	0.8	0	0	61.36	38.64	122.47	77.123

After connecting module

Time (min)	Vent gas (mL/min)	ΔP (atm)	Gas ratio (%)					Normalize (%)		Retentate (mL/min)		Permeate (mL/min)		Total (mL/min)	Permeate ($mL/m^2.s$)		CO_2/CH_4 Selectivity	CH_4 purity (%)
			CH_4	CO_2	O_2	H_2S	Bal.	CH_4	CO_2	CH_4	CO_2	CH_4	CO_2		CH_4	CO_2		
20	174.82	0.0025	64.3	32.8	0.1	1 ppm	1.8	66.22	33.77	115.76	59.05	6.71	18.06	24.78	0.09	0.25	4.03	66.22
40	173.91	0.0025	64.6	32.5	0.1	0	2.8	66.52	33.47	115.70	58.20	6.77	18.91	25.69	0.09	0.26	4.18	66.52
60	174.82	0.0025	64.6	32.4	0.1	0	2.9	66.59	33.40	116.42	58.39	6.05	18.72	24.78	0.08	0.26	4.64	66.59
80	174.21	0.0025	64.5	32.1	0	1 ppm	3.3	66.77	33.22	116.32	57.88	6.15	19.23	25.39	0.08	0.27	4.68	66.77
100	172.01	0.0025	64.5	32.1	0	1 ppm	3.3	66.77	33.22	114.85	57.15	7.62	19.96	27.59	0.10	0.28	3.92	66.77
120	173.95	0.0025	64.0	32.1	0	1 ppm	3.3	66.59	33.40	115.84	58.10	6.62	19.01	25.64	0.09	0.26	4.30	66.59
Avg (20-120 min)										115.81	58.13	6.65	18.98	25.64	0.09	0.26	4.30	66.58
SD										0.56	0.62	0.56	0.62	1.03	0.01	0.01	0.31	0.20

Table H-22 Gas separation of E28-18S0.5P1.0 membrane

Before connecting module

Feed gas (mL/min)	Membrane area (m^2)	ΔP (atm)	Gas ratio (%)					Normalize (%)		Feed gas (mL/min)	
			CH_4	CO_2	O_2	H_2S	Bal.	CH_4	CO_2	CH_4	CO_2
199.20	1.20	0.0020	60.2	37.8	1.0	0	1.0	61.43	38.57	122.37	76.83

After connecting module

Time (min)	Vent gas (mL/min)	ΔP (atm)	Gas ratio (%)					Normalize (%)		Retentate (mL/min)		Permeate (mL/min)		Total (mL/min)	Permeate ($mL/m^2.s$)		CO_2/CH_4 Selectivity	CH_4 purity (%)
			CH_4	CO_2	O_2	H_2S	Bal.	CH_4	CO_2	CH_4	CO_2	CH_4	CO_2		CH_4	CO_2		
20	172.51	0.0024	62.9	30.2	2.6	0	4.2	67.56	32.43	116.55	55.95	5.81	20.87	26.69	0.08	0.29	5.38	67.56
40	171.21	0.0024	62.9	30.3	2.6	0	4.1	67.48	32.51	115.54	55.66	6.81	21.17	27.99	0.09	0.29	4.65	67.48
60	171.03	0.0024	63.8	30.0	2.0	2 ppm	4.2	68.01	31.98	116.32	54.70	6.03	22.13	28.17	0.08	0.31	5.50	68.01
80	171.03	0.0024	63.2	30.0	2.8	0	4.0	67.81	32.18	115.97	55.05	6.38	21.78	28.17	0.09	0.30	5.11	67.81
100	171.03	0.0024	63.5	30.0	2.0	0	4.0	67.91	32.08	116.15	54.87	6.21	21.95	28.17	0.08	0.30	5.30	67.91
120	171.03	0.0024	63.5	30.0	2.0	0	4.0	67.91	32.08	116.15	54.87	6.21	21.95	28.17	0.08	0.30	5.30	67.91
Avg (60-120 min)										116.15	54.87	6.21	21.95	28.17	0.08	0.30	5.30	67.91
SD										0.14	0.14	0.14	0.14	0.00	0.01	0.01	0.16	0.08

Table H-23 Gas separation of E28-18S0.5P1.5 membrane

Before connecting module

Feed gas (mL/min)	Membrane area (m^2)	ΔP (atm)	Gas ratio (%)					Normalize (%)		Feed gas (mL/min)	
			CH_4	CO_2	O_2	H_2S	Bal.	CH_4	CO_2	CH_4	CO_2
202.15	1.20	0.0020	60.9	38.6	0.2	0	0.3	61.20	38.80	123.72	78.42

After connecting module

Time (min)	Vent gas (mL/min)	ΔP (atm)	Gas ratio (%)					Normalize (%)		Retentate (mL/min)		Permeate (mL/min)		Total (mL/min)	Permeate ($mL/m^2.s$)		CO_2/CH_4 Selectivity	CH_4 purity (%)
			CH_4	CO_2	O_2	H_2S	Bal.	CH_4	CO_2	CH_4	CO_2	CH_4	CO_2		CH_4	CO_2		
20	149.37	0.0024	66.0	29.9	0	1 ppm	4.2	68.82	31.17	102.79	46.57	20.92	31.85	52.78	0.29	0.44	2.28	68.82
40	153.57	0.0024	65.7	30.2	0	1 ppm	4.2	68.50	31.49	105.20	48.36	18.51	30.06	48.58	0.25	0.41	2.43	68.50
60	154.21	0.0024	65.4	30.0	0	1 ppm	4.6	68.55	31.44	105.71	48.49	18.01	29.92	47.94	0.25	0.41	2.49	68.55
80	154.03	0.0024	65.5	30.0	0	1 ppm	4.5	68.58	31.41	105.64	48.38	18.08	30.03	48.12	0.25	0.41	2.49	68.58
100	154.12	0.0024	65.4	30.0	0	1 ppm	4.5	68.55	31.44	105.65	48.46	18.07	29.95	48.03	0.25	0.41	2.48	68.55
120	154.12	0.0024	65.5	30.0	0	1 ppm	4.5	68.58	31.41	105.70	48.41	18.02	30.00	48.03	0.25	0.41	2.49	68.58
Avg (60-120 min)										105.68	48.44	18.04	29.98	48.03	0.25	0.41	2.49	68.57
SD										0.04	0.05	0.04	0.05	0.07	0.00	0.00	0.01	0.02

Appendix I

Thickness of the membranes

Table I-1 Membrane thickness of thin-flat membrane

Number	Membrane thickness (μm)						
	LDPE	E18	E28	E33	E33S0.5	E33S1.0	E33S2.0
1	37	38	33	30	36	36	32
2	41	32	36	33	38	39	35
3	39	38	38	37	39	37	33
4	38	33	42	35	38	37	36
5	40	35	35	30	37	35	34
6	39	33	40	36	40	34	34
7	42	39	38	32	38	32	33
8	37	36	41	33	36	38	34
9	38	34	39	34	39	35	36
10	39	37	36	35	38	36	32
AVG	39.00	35.50	37.80	33.50	37.90	35.90	33.90
SD	1.63	2.46	2.82	2.37	1.29	2.02	1.45

Table I-2 Membrane thickness of thin-tubular membrane

Number	Membrane thickness (μm)								
	E18	E28	E28-18	E28-18S0.5	E28-18S0.75	E28-18S1.0	E28-18S0.5P0.5	E28-18S0.5P1.0	E28-18S0.5P1.5
1	70	68	70	70	68	68	70	65	60
2	80	73	78	75	70	75	70	70	68
3	68	75	73	80	75	82	88	82	80
4	77	83	75	85	75	78	85	77	70
5	75	78	80	80	70	70	75	68	83
6	80	82	75	72	70	80	82	80	65
7	75	75	75	77	75	75	77	75	75
8	75	83	73	82	70	75	72	75	70
9	80	80	77	75	73	80	80	73	75
10	73	75	70	78	73	70	80	73	73
AVG	75.30	77.20	74.60	77.40	71.90	75.30	77.90	73.80	71.90
SD	4.16	4.89	3.23	4.58	2.60	4.79	6.21	5.22	6.83

Researcher Biography

Name Mr. Prachya Watasit

Education B. Sci (Chemistry), Kasetsart University

M. Sci (Petrochemistry and Polymer science), Chulalongkorn University

Ph.D. (Applied Chemistry) King Mongkut's Institute of Technology Ladkrabang

Work Lecturer at Rajabhat Rajanagarindra University

Research Atmospheric CO_2/CH_4 permeability of EVA copolymer/SiO_2 composite membrane for biogas purification, 2021, *Journal of Applied Polymer Science*. 138 : 51229.

Tubular EVA copolymer/SiO_2/PEG composite membrane for CO_2 removal from household biogas, 2024, *Polymer Engineering and Science*. 65 : 1123-1135.